University of Zurich[UZH]

Modelling basin scale sediment dynamics of the Red River basin in Vietnam with TOPKAPI-ETH: reconstructing the past and predicting future changes

ESS 511 Master's Thesis

Author
Yixuan Zhou
21-739-354

Supervised by
Dr. Ilja van Meerveld
Prof. Dr. Paolo Burlando (paolo.burlando@ifu.baug.ethz.ch)
Dr. Anna Costa (acosta@ethz.ch)
Dr. Scott Sinclair (sinclair@ifu.baug.ethz.ch)

Faculty representative
Dr. Ilja van Meerveld

30.09.2023
Department of Geography, University of Zurich

Acknowledgements

I would like to express my deepest appreciation to all the people who help me with this thesis.

First and foremost, I would like to thank my supervisors: Prof. Dr. Paolo Burlando, Dr. Anna Costa, Dr. Scott Sinclair, and Dr. Ilja van Meerveld. I begin by acknowledging Prof. Dr. Paolo Burlando who gave me the chance to work on a very interesting topic and develop my experience at Institute of Environmental Engineering of ETH. A huge thanks goes to Dr. Anna Costa for her patience, support, and guidance in every little step of my master thesis project. She makes every goal of my thesis achievable and exciting. I would also like to thank Dr. Scott Sinclair for his assistance with the modeling aspects of my research. I am very grateful for the chance to discuss with you. Thank you for all your guidance in the past one year. Many thanks to Dr. Ilja van Meerveld for her support from the very beginning of my thesis. Thank you for your dedicated feedback towards my proposal, presentation and thesis.

Special recognition goes to Prof. Dr. Paolo Burlando and Dr. Anna Costa for affording me the opportunity to travel to Hanoi, where I participated in a workshop and presented some of my research findings. I am also appreciative of the support provided by the REBECCA project and HUNRE. To the audience at the master's thesis colloquium, I offer my sincere thanks for your questions and feedback. These experiences have prompted me to reevaluate my project and have proven to be invaluable in shaping my skills.

Thank you all for making this experience one of the best memories of my master study in Zurich.

I would like to warmly thank my family and friends for their support throughout my study, despite the physical distance. Many thanks to the colleagues and friends that I met in Zurich. Thank you for always being so supportive, which has made my master's study a truly joyful and enriching experience.

CONTENT

Acknowledgements 1
List of figures 4
List of tables 6
Abstract 7
1. Introduction 8
2. Literature review 9
2.1 Sediment transport simulation 9
2.2 Impact of land use changes 10
2.3 Impact of the reservoir construction 11
3. Study area 13
3.1 Basin description 13
3.2 Climate 14
3.3 Hydrological regimes and the sediment transport 15
3.4 Land use 16
3.5 Reservoir constructions 17
4. Data and methods 19
4.1 Data description 19
4.2 Time series analysis 21
4.3 Trapping efficiency calculation 21
4.4 Sediment flux modelling 22
4.4.1 Soil erosion 22
4.4.2 Suspended sediment transport 25
4.4.3 Reservoir operation 26
4.5 Calibration and validation 27
4.6 Sensitivity analysis 28
4.7 Simulating the impact of anthropogenic activities 29
4.8 Future scenarios 30
4.8.1 Land use 30
4.8.2 Operating policies of the reservoirs 32
5. Time series analysis 33

5.1 Streamflow....33
5.2 Suspended sediment concentration....35
6. Basin-scale sediment dynamics simulation....38
6.1 Model performance evaluation....38
6.1.1 Model calibration and validation....38
6.1.2 Model performance in simulating high SSC events....40
6.2 Sensitivity analysis....42
6.3 Simulated basin-scale sediment regime....43
7. Scenario analysis of the basin-scale sediment dynamic....47
7.1 Land use changes scenarios....47
7.1.1 Sediment flux at Hanoi....47
7.1.2 Intra-annual variability of sediment load....50
7.1.3 Spatial pattern of changes in erosion....51
7.2 Reservoir operations....58
7.2.1 Trapping effect of the reservoir....58
7.2.2 Influence on the sediment load at Hanoi....61
8. Future changes in the sediment regime....63
8.1 Future land use changes scenarios....63
8.2 Future reservoir operation policies....65
9. Discussion....68
9.1 Impacts of land use changes....68
9.2 Impacts of reservoir constructions....69
9.3 Challenges and limitations of the current model....70
10. Conclusion....73
References....75
Appendix....80
Appendix 1: K-factor map, C-factor map, and alpha maps....80
Appendix 2: Maps of land use changes in scenarios analysis....83
Personal Declaration....86

List of figures

Figure 1 The location of the Red River Bain and the main tributes (Kmusser, 2009). 13
Figure 2 The DEM of the Red River Basin and main reservoirs in the basin. 14
Figure 3 Monthly averages of rainfall, temperature and discharge at Son Tay (1960 –2008; data from the Institute of Meteorology, Hydrology and Environment (IMHE, Hanoi, Vietnam) (Dang et al., 2010). 15
Figure 4 Monthly discharge at Hanoi station (1956 - 2019). 15
Figure 5 Land use map of the Red River Basin of the year 2015. 17
Figure 6 Locations of hydrological stations and hydropower plants in the Red River Basin. 20
Figure 7 Land use predictions for the year 2050 under different SSP-RCP scenarios. 31
Figure 8 Annual mean streamflow and the year of changing point for Hanoi, SonTay, Hoa Binh and Lao Cai station. 33
Figure 9 Monthly mean streamflow before and after the changing points. 35
Figure 10 Annual mean SSC for stations with significant decreasing trends and the timing of the changing points. 36
Figure 11 Monthly mean suspended sediment concentration (SSC) before and after changing points. 37
Figure 12 The simulated and observed monthly mean SSC at the calibration station (Lai Chau). The input alpha map was obtained using Torri et al. (1997)'s method. 39
Figure 13 The simulated and observed monthly mean SSC at the validation station (Ham Yen). The input alpha map was obtained using Torri et al. (1997)'s method. 39
Figure 14 Annual sediment load at Lai Chau station and the sediment load in high SSC events. The numbers of high SSC days in each year were presented above purple bars. 40
Figure 15 Scatter plots of suspended sediment concentration (SSC), streamflow (Q), and the corresponding precipitation (P) in high SSC events at Lai Chau station. 41
Figure 16 Mean monthly simulated SSC at Lai Chau station from 2005 to 2010 using two methods (namely Torri et al. (1997) and Sharpley and William (1990)) to calculate the K-factor. 42
Figure 17 Monthly mean simulated SSC at Lai Chau from 2005 to 2010 with different alpha1 values. Input alph1 value is 0.3 and 0.05 for Torri et al. 's and Sharpley and Williams 's method, respectively. 43
Figure 18 Mean annual cumulative erosion mass of the red river basin (2005 - 2010). 44
Figure 19 Mean monthly cumulative erosion mass of the red river basin (2005 - 2010) 45
Figure 20 Averaged annual mean SSC (2005 - 2010) of red river basin. 46
Figure 21 Annual mean Q and SSC at Hanoi station from 2005 to 2019 under different forest expansion scenarios. 47
Figure 22 Annual mean Q and SSC at Hanoi station from 2005 – 2019 under different cropland expansion scenario. 48
Figure 23 Annual mean Q and SSC at Hanoi station from 2005 – 2019 under different cropland expansion scenarios. 49
Figure 24 Mean annual sediment load at Hanoi station under different land use changes scenarios. 50
Figure 25 Mean monthly sediment load for different land use changes scenarios. 51
Figure 26 Changes in mean annual cumulative erosion mass (2005 - 2010) when the entire

basin is covered with forest. LU = Land use. 52
Figure 27 Changes in mean annual cumulative erosion mass (2005 - 2010) when the entire basin is covered by cropland. LU = Land use. 53
Figure 28 Changes in the mean annual cumulative erosion mass under different forest expansion scenarios. LU = Land use. 54
Figure 29 Changes in the mean annual cumulative erosion mass under different cropland expansion scenarios. LU = Land use. 56
Figure 30 Changes in the mean annual cumulative erosion mass under different urban expansion scenarios. LU = Land use. 57
Figure 31 Monthly mean observed and simulated trapping efficiency (TE) for the four main reservoirs. 59
Figure 32 Simulated monthly mean streamflow (Q) under the reservoir operation scenario for four stations locating downstream of four main reservoirs. 60
Figure 33 Simulated monthly mean suspended sediment concentration (SSC) under the reservoir operation scenario for four stations locating downstream of the four main reservoirs. 60
Figure 34 Annual sediment load at Hanoi from 2005 to 2019. TE = Trapping efficiency. 61
Figure 35 Simulated monthly sediment load at Hanoi (2005 - 2019) under scenarios with and without reservoir. 62
Figure 36 Annual cumulative erosion mass under different SSP scenarios. The input meteorological data was from 2005 to 2010. 63
Figure 37 Simulated mean annual sediment load (2005 - 2019) at Hanoi using the land use maps of 2050 under different SSP scenarios. 64
Figure 38 Simulated monthly suspended sediment load (SL) at Hanoi using future land use maps under different SSP scenarios. 65
Figure 39 Mean annual sediment load (2011 - 2019) under different reservoir operation scenarios. Subbasin Da, Thao, and Lo is represented by the simulation at Hoa Binh, Yen Bai and Vu Quang station, respectively. 66
Figure 40 The monthly sediment load at Hanoi (2011 - 2019) under different reservoir operation scenarios. 67

List of tables

Table 1 Information of main reservoirs in the Red River Basin. 18
Table 2 The available time period of the observed data 19
Table 3 Source and the original resolution of the spatial data 21
Table 4 The crop management index (C-Factor value) for different land cover types. 23
Table 5 Descriptions of anthropogenic activities' scenarios. 29
Table 6 Mann-Kendall's test outputs for the monthly mean streamflow 34
Table 7 Mann-Kendall's test outputs for the monthly mean suspended sediment concentration (SSC). 37
Table 8 Goodness of fit for the calibration (Lai Chau) and the validation (Ham Yen) station. 40
Table 9 Annul mean trapping efficiency (TE) of the four main reservoirs within red river basin. 58

Abstract

Sediment transport in large river system is of great significance for the global sediment budget. Nowadays, the sediment transport of most large river basins is experiencing the impacts from multiple human activities. The Red River Basin (RRB) is the second large Vietnamese rice production area, and belongs to the most densely populated region in the world. Understanding anthropogenic activities' impact on the sediment regime of the basin would provide a reference for future water and sediment management work. The main objectives of this thesis are detecting the changes in the observed suspended sediment concentration (SSC) and streamflow (Q) within the basin during past decades, and exploring the impacts of land use changes and reservoir construction on the sediment regime changes using TOPKAPI-ETH model. The results present a decreasing trend from 2000 to 2020 for both SSC and Q. The timing of such changes mainly concentrated in the reservoir construction period. The simulations under different scenarios show that reservoir could significantly reduce the sediment load through sediment trapping. Such a reduction is more than 90% for large reservoirs regardless of different reservoir operation policies. Regarding the impact of land use changes, the changes in sediment transport is more sensitive to the location rather than the proportion of land use changes. Under the future land use scenarios, about 40% decrease of cropland could result in 14% of sediment load reduction at Hanoi. Though the impact of land use change on annual sediment load is not as large as that of reservoir construction, multiple consequent changes (e.g., streamflow, soil erodibility) due to land use changes and their combined impacts would bring high uncertainty to the sediment regime. The results indicate the importance of considering the location of the land use change when evaluating its impact on sediment regime. Besides, the construction of reservoir needs to carefully considered due to its tremendous and irreversible impacts on sediment transport and further consequences.

1. Introduction

River transport is the dominant material transport process on the Earth's surface (Rhoads, 2020). Fine sediment, produced by upland erosion and transported by rivers as suspended load, represent an important contribution to the global sediment budget. This is particularly true in large river systems, which deliver sediment to densely populated and highly productive river deltas. Most of the world's largest deltas are experiencing significant subsidence due to reduced sediment fluxes from upstream areas (Schmitt et al., 2021). Multiple anthropogenic factors, such as land use changes and reservoir construction, are influencing the sediment delivery to deltas. Understanding how sediment transport is influenced by these activities is of great significance for predicting the development of coastal geomorphology and improving water and sediment management.

The Red River Basin (RRB) is the second large Vietnamese rice production area, and plays an integral role in the local economy (Yu et al., 2010). In the past decades, the RRB has experienced multiple anthropogenic activities, e.g., forest restoration, urban expansion, reservoir construction. These factors have a strong impact on sediment dynamics by influencing the soil erodibility, trapping sediment, and altering the transport capacity of the Red River. Reconstructing spatial and temporal suspended sediment transport, and exploring how it has been influenced by anthropogenic activities would provide a reference for water and sediment management of the basin.

This thesis has three main objectives. The first one is to understand how did the suspended sediment concentration (SSC) in the RRB change since 1990s. The second one is to use a physically-based model to simulate the impacts of various land use changes and reservoir construction on the sediment regime. This would help to understand what could be the possible influencing factors on the sediment load changes in the past decades. The last objective is to evaluating the possible changes in sediment flux due to human activities in the future, aiming to provide some suggestions for the future sediment management work in large basins.

2. Literature review

2.1 Sediment transport simulation

Basin scale sediment transport is a product of sediment erosion and deposition processes within a basin. Many different models have been proposed to describe and predict these processes. These models could be classified into three groups, namely empirical models, conceptual models, and physically-based models (de Vente and Poesen, 2005). Though these models do not always fall into one category strictly, as physically-based models still retain some empirical descriptions.

Empirical models build an empirical relationship between the sediment yield and the contributing variables. Most empirical models build a regression relationship between rainfall (or runoff) and sediment yield, such as Fournier model (Fournier, 1960) and Dendy and Boltan model (Dendy and Bolton, 1976). Some models, such as RUSLE model (Renard et al., 1997), also consider the relationship between sediment yield and other environmental factors (e.g., rainfall, soil erodibility, slope length and steepness, crop cover and management factor, conservation practice).

Conceptual models further conceptualize the soil detachment and deposition processes that would influence the sediment transport simulation. For example, in SWAT model (Arnold et al., 1998), the basin was firstly divided into sub-basins. The hydrological responses are similar inside each sub-basin. The soil loss and deposition are simulated inside each sub-basin according to the lumped conceptualized processes that are related to runoff, soil erodibility, land cover, etc. Other conceptual models, such as AGNPS (Young et al., 1989) and MMF (Morgan, 2001), also have similar conceptualized schemes.

The above-mentioned simple models are very useful in describing the large-scale patterns that do not possess large spatial variance. However, there are many cases in which the complex and heterogeneous conditions inside a watershed are necessary to understand how natural and human systems function and interact (Fatichi et al., 2016). Especially when the interest lies in specific variables and their spatial variances,

such as assessing the spatial variance that is caused by land management impacts (Ewen et al., 2000; Pierini et al., 2014). Under this condition, the advantage of the distributed physically-based model is evident.

Physically-based models are built on physical laws. The hydrologic state variables and fluxes are theoretically observable, and obey the laws of conservation of mass, energy, and momentum (Fatichi et al., 2016). When a physically-based model is applied spatially, it could present the space-time variability at a sub-hillslope scale. Since we live in an era that human impacts at the watershed scale are not negligible, a physically-based model could better reflect the localized human activities and integrate these changes into the sediment transport processes. For example, WEPP (Flanagan et al., 2001) and EUROSEM (Morgan et al., 1998) could incorporate the variance of crop types and road constructions inside the model, though these models are only applicable in small catchment scale (< 100 km^2). For the sediment transportation simulation in large river systems, some physically-based models have been developed in recent decades, such as MOSART-sediment at the global scale (Li et al., 2021), and TOPKAPI-ETH model that could be applied in the basin that is larger than 100,000 km^2 (Fatichi et al., 2015). These models could simulate the sediment transport for large basins, and integrate human activities that could exert larger scale impact (e.g., reservoir construction module in TOPKAPI-ETH model) inside the model.

Nevertheless, it has to be mentioned that even the physically-based models have not been able to describe all the sediment production and transport processes so far due to the insufficient system knowledge and unfeasible data requirements (de Vente and Poesen, 2005; Fatichi et al., 2016). Even though, the understandings about the natural sediment transport processes and their interactions with human activities could be benefited from these distributed physically-based simulations.

2.2 Impact of land use changes

Land use can affect both the flowing water and the rate of sediment erosion (Milliman and Farnsworth, 2011). In the short term, land use changes can influence rainfall erosion intensity through alterations in land cover and its effect on the interception

process (Meng et al., 2021). Additionally, changes in surface flow, including the amount, velocity, and roughness, can influence flow erosion intensity. Looking ahead in the long term, land use changes have the potential to impact regional precipitation and runoff patterns, further affecting soil erosion processes. Moreover, land use changes can modify soil properties and structure, influencing undersurface hydraulic conditions and, consequently, soil erosion processes.

Over the past decades, human-caused land use changes have been demonstrated to significantly influence water erosion in basins worldwide (Panagos et al., 2015b; Garcia-Ruiz, 2010; Smith et al., 2016), potentially resulting in changes in river sediment loads. However, in many regions, intensified land use changes occurred before the establishment of river sediment monitoring programs (Walling and Fang, 2003), making it challenging to assess their impact on river sediment load. In such cases, a basin-scale hydrological model that integrates soil erosion and river sediment transportation could be valuable in understanding and assessing the impact of land use changes.

Besides the size and area of different land use types, the spatial pattern of the land use also plays a significant role in soil erosion processes (Szilassi et al., 2006; Ouyang et al., 2010). Research by Szilassi et al. (2006) revealed that increasing landscape fragmentation opens corridors for sediment transport to the receiving drainage network. Similarly, Ouyang et al. (2010) highlighted that increasing sediment transportation is more influenced by the increasing patch edge than patch area. Therefore, the distribution of land use changes is supposed to be a non-negligible factor when assessing their impact on soil erosion.

2.3 Impact of the reservoir construction

Reservoir constructions have emerged as one of the most significant influencing factors on land-ocean sediment fluxes in recent decades (Li et al., 2020). Reservoirs could directly trap sediments transported from upstream areas. Moreover, reservoir operations alter natural discharge, further influencing the stream's sediment transport capacity, leading to potential changes in the amount and spatial-temporal variability of

sediment transport (Yang et al., 2018).

Walling and Fang (2003) analyzed the annual suspended sediment load and discharge for 145 major rivers worldwide. They found that about 50% of the rivers exhibited a statistically significant decreasing trend in suspended sediment load over the long term (> 25 years), while over 60% showed no decreasing trend in the annual discharge. Similarly, Li et al. (2020) reported that the sediment flux of 20.8% of rivers (896 out of 4307 rivers) globally has decreased in recent years, while the annual water flux from rivers to the sea remained stable. In many basins worldwide, despite the increased precipitation, runoff, deforestation, and soil degradation, which normally associated with an increasing sediment load, observed sediment load has been detected to decrease by more than 50% (e.g., Amsler and Drago, 2009; Yang et al., 2018). These findings suggest that reservoir operations have a more significant impact on controlling sediment flux than changes in water fluxes or even land use changes in intensively managed catchments.

While the direct influences of reservoir constructions are evident in many basins, the long-term indirect impacts of reservoirs remain uncertain or unknown. Large dams may potentially alter local precipitation patterns through changes in evaporation, surface temperature, and other factors (Milliman and Farnsworth, 2011). Additionally, the construction of new reservoirs often leads to consequent land use changes due to land inundation and changes in the availability of water for irrigation. Predicting and explaining these changes with observed data or models can be challenging.

3. Study area

3.1 Basin description

The Red River Basin (RRB) is located in the south-east of the Indochinese peninsula of the southeast Asia (from 20°00' to 25°30' N; from 100° 00' to 107° 10' E). The total area of the basin is about 169,000 km^2, with 51.35% in Vietnam's territory, 48% in China, and 0.65% in Laos (Figure 1). It is the second largest basin of Vietnam, hosting more than 20 million people.

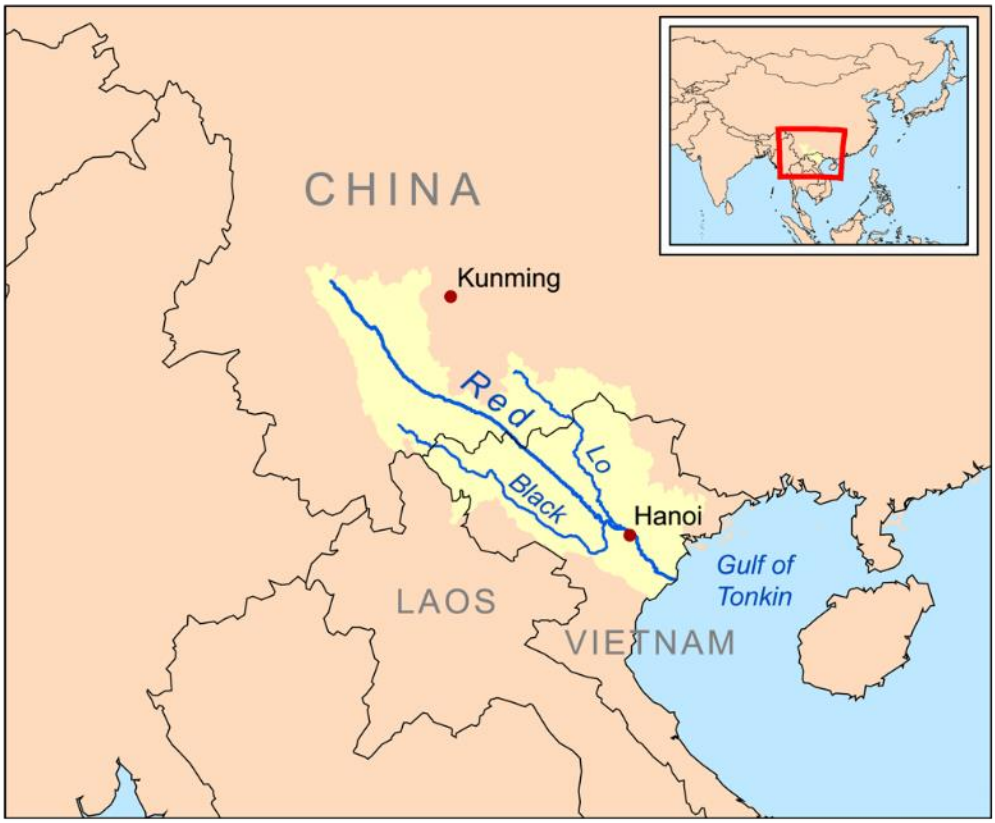

Figure 1 The location of the Red River Bain and the main tributes (Kmusser, 2009).

The elevation of the RRB ranges from 0 to 3103 m (Figure 2). The basin spreads across the mountainous area in the northwestern part, the midlands, and the lowland in the southeastern part. The general slope direction is northwest-southeast. More than 90% of the basin presents a hilly topography. Only the red river delta has a relative flat terrain. The delta region is one of the most densely populated regions in Vietnam with about 20% of the national population. Hanoi, the capital of Vietnam, is also located in the red river delta (Figure 1).

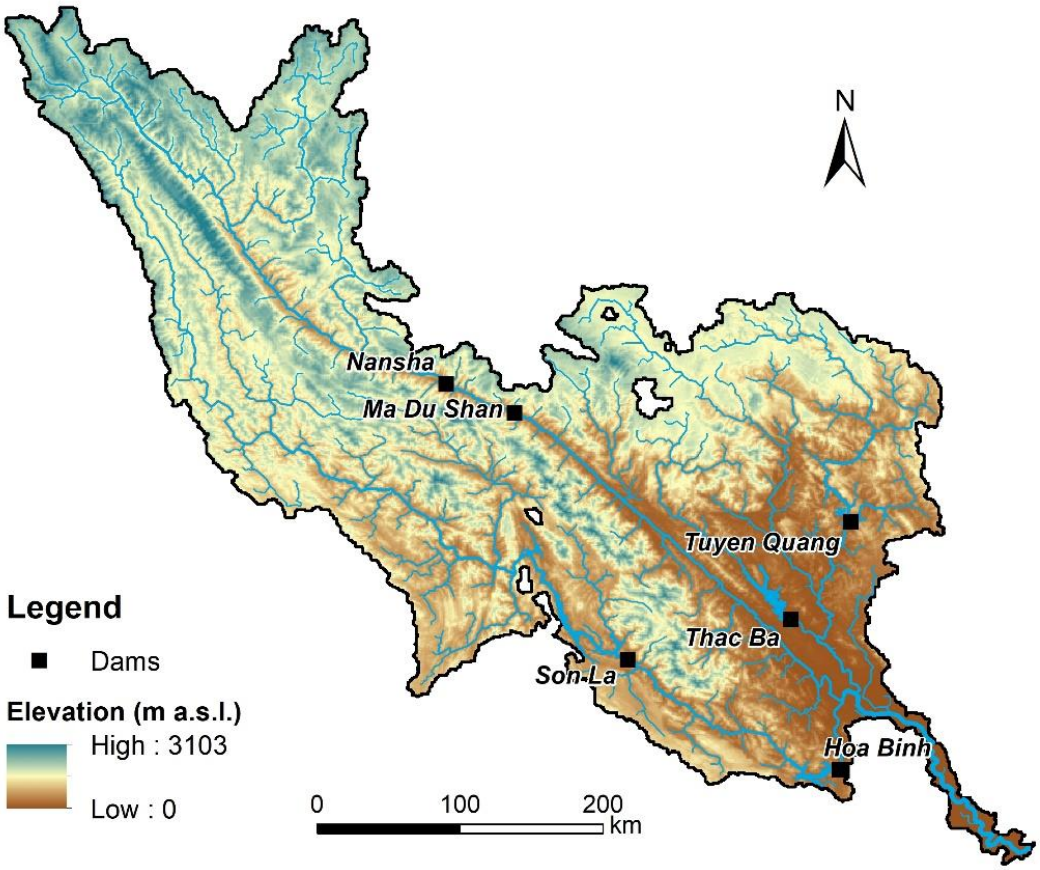

Figure 2 The DEM of the Red River Basin and main reservoirs in the basin.

3.2 Climate

The RRB is characterized by a subtropical and tropical monsoon climate. The annual mean precipitation is 1590 mm for the whole basin (Le et al., 2007), and varies from about 840 to 4000 mm/year in space (Bui et al., 2022). There are two distinguished seasons for the RRB: wet season (from May to October) and dry season (from November to April). Figure 3 shows the monthly averages of rainfall and temperature. During the wet season, winds from south-southeast bring warm and humid air to the basin. About 80% of the annual precipitation concentrates in the wet season, and the monthly mean temperature (above 25 °C) in this season is the highest in a year (Figure 3). During the dry season, the winds from the northeast bring cool and dry air masses. The averaged monthly precipitation is generally lower than 50 mm, and the monthly temperature ranges from 16 to 21 °C (World Data, 2023).

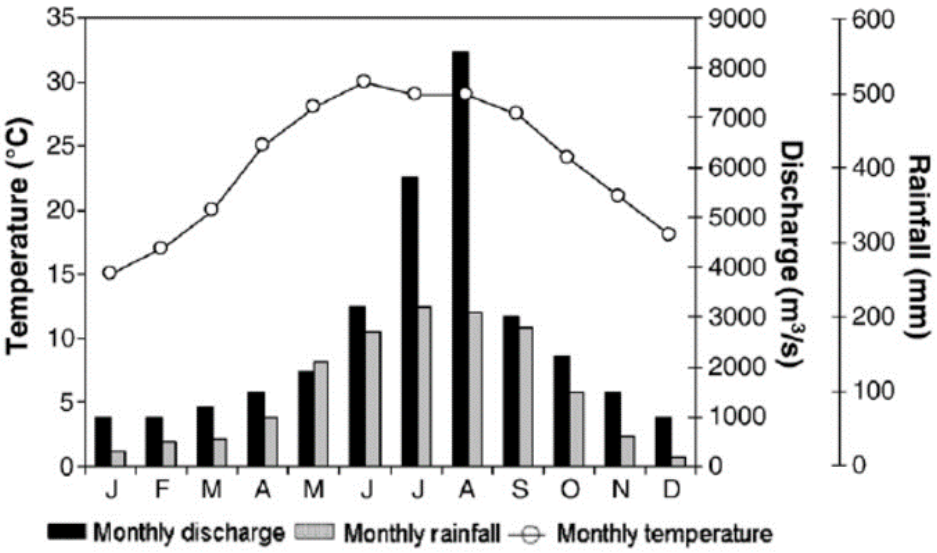

Figure 3 Monthly averages of rainfall, temperature and discharge at Son Tay (1960 –2008; data from the Institute of Meteorology, Hydrology and Environment (IMHE, Hanoi, Vietnam) (Dang et al., 2010).

3.3 Hydrological regimes and the sediment transport

The name of the Red River comes from its reddish-brown silt-laden water. The Red River has three main tributaries: Lo, Thao (Red) and Da (Black) River (Figure 1). All of the three tributaries originate in the southeastern China at the elevation of over 2000 m (Figure 2). Da river flows into the Thao River, and then Thao and Lo Rivers flow into the Red River at Viet Tri (about 80 km upstream from Hanoi). Then the Red River flows eastward into the Tonkin Bay with the total length of about 1140 km (Hiep et al., 2023).

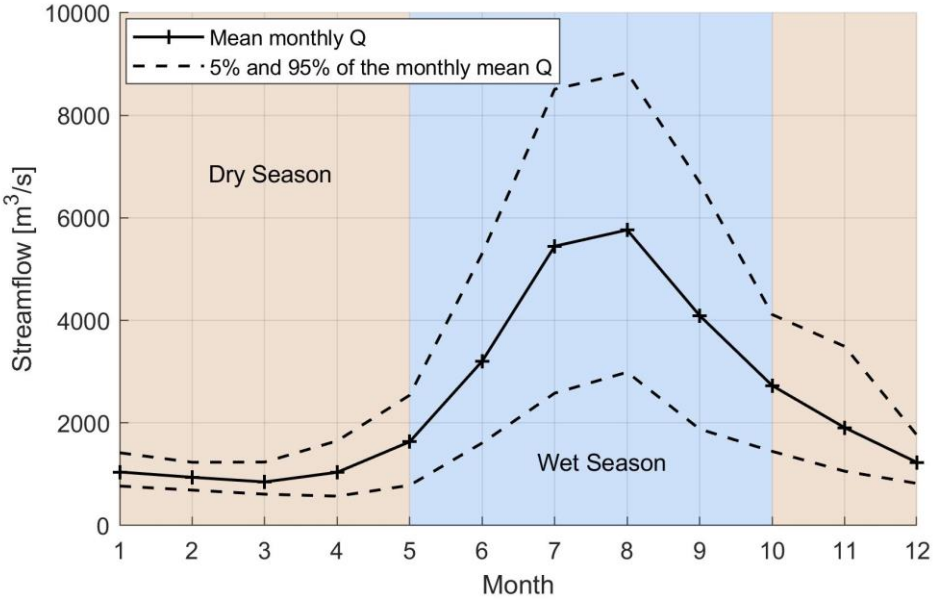

Figure 4 Monthly discharge at Hanoi station (1956 - 2019).

The mean annual discharge at Hanoi (1956 - 2010) is 2,500 m^3/s. The wet and dry seasons can be well distinguished in streamflow (Figure 3 & 4). The highest monthly mean discharge (over 5000 m^3/s) usually occurs in July or August. The highest daily discharge in past decades was 22,000 m^3/s, which was observed in August 20th 1971. The low flow season goes from November to April. And the average monthly discharge is generally lower than 3000 m^3/s at Hanoi during the low flow season.

The sediment transport in RRB is extremely high. Before the impoundment of the Hoa Binh reservoir (the largest reservoir in RRB), the reported sediment load could reach 116 to 166 $\times$ 10^6 t yr^{-1} (Le et al., 2007). These three sub-basins show large differences in sediment load: Lo River possesses the lowest suspended sediment load with lower than 500 t $km^{-2}y^{-1}$, while Thao River Basin and Da River Basin are main sediment sources with the sediment load of 55 – 1060 t km^{-2} y^{-1} and 228 – 1193 t km^{-2} y^{-1}, respectively (Le et al., 2007).

3.4 Land use

Forests accounted for the largest proportion of land use in the RRB, occupying 39.2% (in the year 2015) of the total land area (ESA, 2022). It is mainly located in the upstream region and the midland area (Figure 2 & 4). The RRB has experienced severe deforestation in last century due to the economic growth. Since 1995, the forest area started to increase with the forest rehabilitation and plantation (Phan et al., 2021). From 1995 to 2015, the forest area in RRB has increased by about 5% (ESA, 2022).

Agriculture land is the second largest land use type in RRB, covering 18.49% of the total land area (ESA, 2022). It is mainly located along the river and concentrated in the delta region. Rice is the main agriculture product in Red River Delta, and is planted biannually (first from February to June and a second time from July to October) (Yuen et al., 2021). The Red River Delta is the second largest rice production area in Vietnam. In past two decades, the proportion of agriculture has experienced a slight increase (about 2%). Due to the limitation of the expansion of arable land, irrigation was developed to increase the cropping intensity (Tuan and François, 2000).

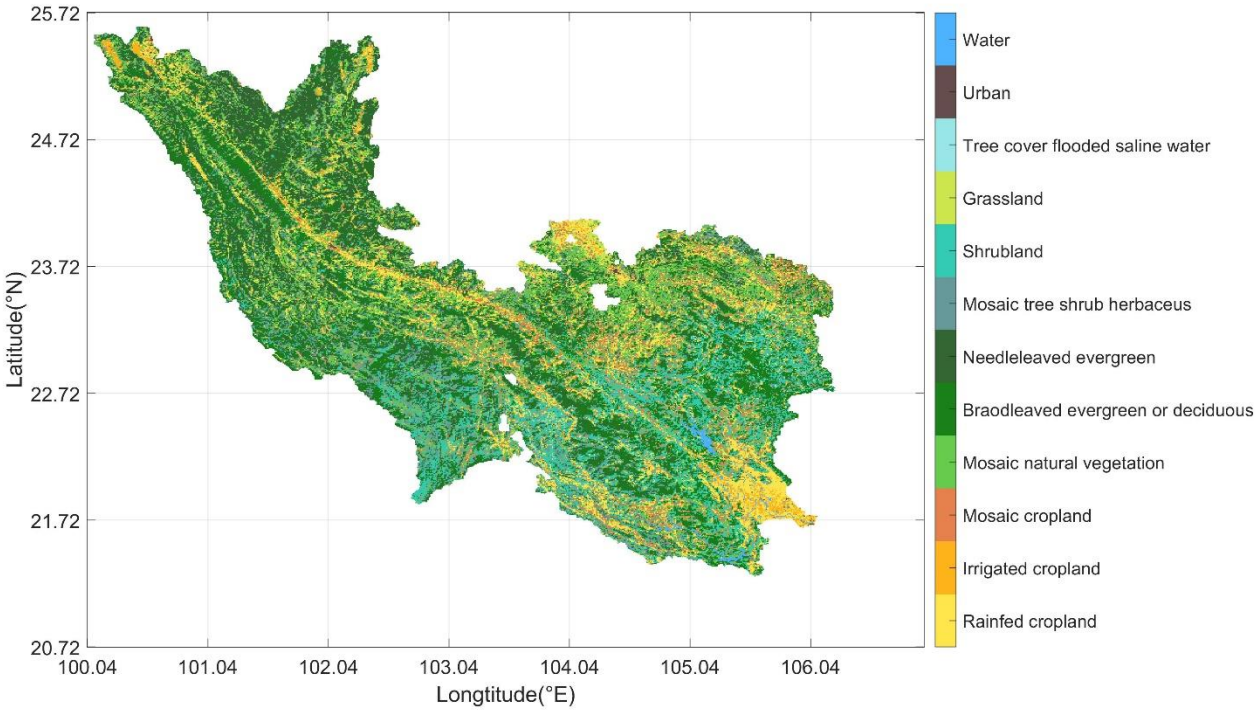

Figure 5 Land use map of the Red River Basin of the year 2015.

The rapid population and economic growth in past decades have accelerated the urbanization in RRB. The urban land consists of 0.11% of the whole basin, and is mainly concentrated in the delta region (ESA, 2022). The population density of the inhabitants could reach over 1000 inhabitants/km^2 in the delta region, while the population density is less than 150 inhabitants/km^2 in other sub-basins (CEIC, 2021).

Requirements on the ecological restoration, agricultural products, and urbanization have resulted in continuous land use changes in RRB. These changes have also changed the hydrological and sediment transport regime of the basin.

3.5 Reservoir constructions

The RRB is exposed to high risk of flood due to the large amount of concentrated precipitation that is brought by the monsoon. In order to protect the population and the property from floods, dozens of reservoirs with large or small size were constructed in past decades. Nowadays, these reservoirs also play a key role for energy production and water supply for irrigation. In Vietnam, more than 30% of the electricity is generated by hydropower (Ritchie, 2022). In RRB, there are six main large reservoirs located along different tributaries: Son La and Hoa Binh on Da River; Ma Du Shan

(Chinese reservoir), Nan Sha (Chinese reservoir), and Thac Ba on Thao River, and Tuyen Quang on Lo River (Table 1, Figure 2).

Table 1 Information of main reservoirs in the Red River Basin.

Name	Start of the Construction	Commission	Tributes	Active Storage (million m^3)
Hoa Binh	1979	1994	Da River (Black river in Figure 1)	6054
Son La	2005	2012		6504
Tuyen Quang	2002	2008	Lo River	2300
Thac Ba	1960	1971		2490
Nansha	2005	2009	Thao River (Red river in Figure 1)	265
Ma Du Shan	2007	2011		482

* The time for the start of the construction and commission are from Reservoir Mapping Tool (http://damtool-servir.adpc.net/), and the active storages are from IMRR project report (2015).

4. Data and methods

4.1 Data description

This thesis mainly used two types of the data:

- Observed time series data at hydrological stations and reservoirs
- Spatial-distributed meteorological and environmental data for modelling

The available observed data at hydrological stations include the daily scale streamflow (m^3/s) and the suspended sediment concentration (SSC, g/m^3) from 1988 to 2019 (Table 2). There are 14 available hydrological stations in RRB (Figure 5). The observed water level and release are available for 4 main reservoirs in Vietnam's territory from 2011 to 2020 (Table 1, Figure 6).

Table 2 The available time period of the observed data

Station	1990	1995	2000	2005	2010	2015	2019
Bao Yen							
Ghenh Ga							
Chiem Hoa							
Ham Yen							
Hoa Binh							
Hanoi							
Lai Chau							
Lao Cai							
Son Tay							
Ta Bu							
Thanh Son							
Thuong Cat							
Vu Quang							
Yen Bai							

SSC Streamflow

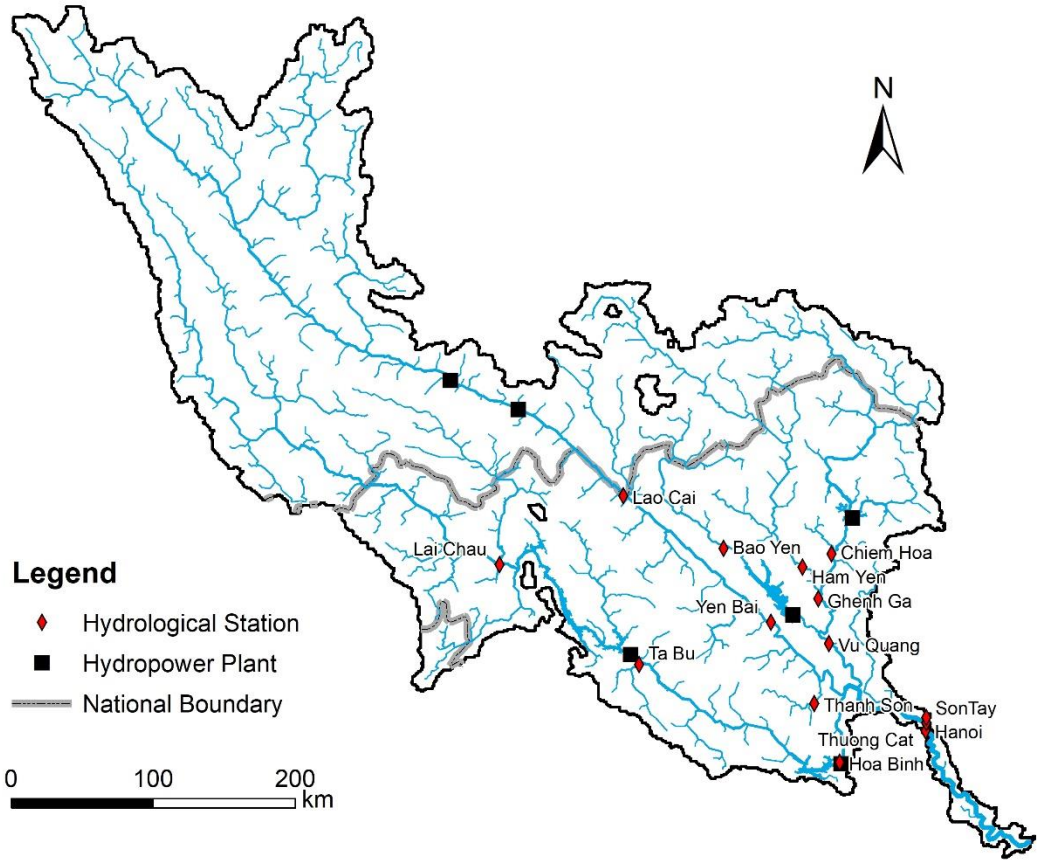

Figure 6 Locations of hydrological stations and hydropower plants in the Red River Basin.

Table 3 shows the spatial data that were used in this thesis. The meteorological data includes daily scale cloud cover transmissivity, precipitation, and temperature. The cloud cover transmissivity and the temperature were derived from ERA5 (at roughly 25 x 25 km resolution), and the precipitation data is from GPM-IMERG (at roughly 10 x 10 km resolution). The digital elevation model (DEM) at roughly 1 x 1 km resolution was extracted from HydroSHEDS. River network was derived from the DEM using D8 method, which assumes the flow direction from each cell to its steepest downslope 8 neighbor cells. The land use map is from the European Space Agency (ESA) Climate Change Initiative (resolution 250 x 250 m). Soil properties were extracted from World Soil Information Database at a resolution of 300 x 300 m, and include soil bulk density, the content of clay, silt, sand and organic matter of three layers (0 – 5 cm, 5 – 15 cm, 15 – 30 cm). Soil and land use maps were upscaled to 1 × 1 km resolution to match the modelling requirement. Climate inputs at selected pixels were fed into the hydrological model as virtual stations.

Table 3 Source and the original resolution of the spatial data

Data	Source and Resolution
DEM	HydroSHEDS (1 x 1 km)
Soil Properties	World Soil Information Database (3 layers from 0 to 30cm, 250 x 250 m)
Land use	European Space Agency (ESA) Climate Change Initiative (300 x 300 m)
River network	Derived with GIS using D4 method
Cloud Cover Transmissivity	ERA5 (25 x 25 km)
Precipitation	GPM-IMERG (10 x 10 km)
Temperature	ERA5 (25 x 25 km)

4.2 Time series analysis

This thesis used Mann-Kendall test and Pettitt test to analyze the temporal variation of the observed SSC and streamflow. Before the time series analysis, the daily-scale data was transformed to monthly and annual mean, respectively.

Mann-Kendall test (Mann, 1945; Kendall, 1975) is used to find trends in the data. It is a non-parametric test and does not require the normality of the data. The null hypothesis (H_0) is that there is no change in the mean of a series. The H_0 will be rejected if a significant decreasing or increasing trend is detected. This test was applied to both the monthly mean and the annual mean data using MATLAB (Fatichi, 2023).

Pettitt test (1979) is a non-parametric test for detecting the abrupt change in a time series. It uses the Mann-Whitney statistic to test if sample sets before and after the assumed changing point are homogeneous (H_0). This test chooses the changing point that can maximize the statistic, and test if the H_0 will be accepted or rejected. In this thesis, the Pettitt test is applied to the annual mean SSC and streamflow using MATLAB (Dey, 2023).

4.3 Trapping efficiency calculation

Trapping efficiency describes the proportion of the suspended sediment that could be captured by the reservoir. This study calculated the average annual trapping efficiency

and the monthly variation for 4 main reservoirs (Son La, Hoa Binh, Tuyen Quang, Thac Ba) in Vietnam. According to the research of Vörösmarty et al. (2003), the sediment trapping efficiency is a function of the residence time of the river water. The residence time τ at the location of the reservoir is calculated as follow:

$$\tau = \frac{V}{Q} \tag{1}$$

where V is the storage of the reservoir, Q is the release of the reservoir.

Then, the sediment trapping efficiency TE_0 is calculated using τ as follow:

$$TE_0 = 1 - \frac{0.05}{\sqrt{\tau}} \tag{2}$$

When the discharge under the pre-disturbance condition is available, the original TE_0 could be modified:

$$TE = 1 + \left(\frac{Q_{post}}{Q_{pre}}\right)(TE_0 - 1) \tag{3}$$

where TE is the modified trapping efficiency, Q_{post} and Q_{pre} are the post- and pre-reservoir streamflow, respectively.

4.4 Sediment flux modelling

This thesis used TOPKAPI-ETH model to simulate the basin-scale suspended sediment flux. TOPKAPI-ETH model is a physically-based distributed hydrological model. It includes all the main hydrological processes such as infiltration, soil moisture limited evapotranspiration, saturation excess runoff, etc. This model simulates the sediment flux with overland flow erosion along hillslopes erosion and sediment transport along channel components. It accounts for infrastructures such as reservoirs and water diversions/abstractions and their operations. Sediment storage behind reservoirs or other water impoundment infrastructures is implemented in the model through the sediment trapping efficiency.

4.4.1 Soil erosion

In the soil erosion module of TOPKAPI-ETH model, the sediment production rate at

the cell level equals the local sediment-transport capacity T_c (Prosser and Rustomji, 2000) as follows:

$$T_c = \alpha q^{\beta} S^{\gamma} \quad (4)$$

where α [kg $s^{0.4}$ $m^{-4.8}$] is an input map that represents the land surface condition, q is the overland flow, S is the slope gradient, β and γ are transport exponents from Prosser and Rustomji (2000). The input α map is calculated on a factor C representing the land cover, a factor K representing the soil erodibility and a calibration parameter α_1 [kg $s^{-1.8}$ $m^{-2.6}$]:

$$a(x, y) = \alpha_1 * C(x, y) * K(x, y) \quad (5)$$

where x and y represent the coordinates of the cell.

The crop management index $C(x, y)$ accounts for how different land covers reduce the soil loss compared to those losses occurring in bare fallow areas (ESDAC, 2023). The C value (unitless) represents the proportion of the original soil loss that would occur with a certain land cover type. In this thesis, the corresponding C values for different land covers were assigned according to literature (Table 4).

Table 4 The crop management index (C-Factor value) for different land cover types.

Land cover	C value	References
Rainfed cropland	0.5	Yang et al. (2003)
Irrigated cropland		
Mosaic cropland	0.267	Bakker et al. (2008), Yang et al. (2003), Panagos et al. (2015),
Mosaic natural vegetation		
Closed and closed to open broadleaved evergreen or deciduous forest	0.003	Panagos et al. (2015)
Closed to open needle leaved evergreen forest		
Mosaic tree and shrub, mosaic herbaceous, and sparse vegetation	0.075	Bakker et al. (2008), Panagos et al. (2015)
Shrubland (evergreen, deciduous)	0.055	Bakker et al. (2008)
Grassland	0.08	Yang et al. (2003), Borrelli et al. (2017)
Tree cover flooded saline water, and shrub or herbaceous cover flooded	0.05	Bakker et al. (2008), Panagos et al. (2015)
Urban	0	de Vente et al. (2009)
Water		

The soil erodibility factor $K(x,y)$ is defined as the mean annual soil loss per unit of rainfall erosivity for a standard condition of the bare soil (recently tilled-up-and-down slope without conservation practice) (Wischmeier and Smith, 1978). For this study, the topsoil soil properties for a depth of 0 – 5 cm, 5 – 15 cm, 15 – 30 cm were averaged over 0 – 30 cm for K-factor calculation. K-factor was calculated according to Torri et al. (2007) and Sharpley and Williams (1990), respectively.

$$K_{Torri} = 0.0293\left(0.65 - D_G + 0.24{D_G}^2\right) \tag{6}$$

$$\exp\left(-0.0021\frac{OM}{CLA} - 0.00037\left(\frac{OM}{CLA}\right)^2 - 4.02\,CLA + 1.72\,CLA^2\right)$$

where K_{Torri} is the K-factor according to Torri's method, OM is the mass percentage of the organic material, CLA is the mass percentage of the clay, D_G is the geometric mean particle size, which is calculated as follow:

$$D_G = \sum_{i=1}^{3} f_i * \log_{10}\sqrt{d_{max} + d_{min}} \tag{7}$$

where f_i is the mass fraction of the particle size class, d_{max} is the maximum diameter in i-th class, d_{min} is the minimum diameter in i-th class. In this thesis, particle size classes include clay (d_{max} = 0.002 mm, d_{min} = 0.00005 mm), silt (d_{max} = 0.05 mm, d_{min} = 0.002 mm), and sand (d_{max} = 2 mm, d_{min} = 0.05 mm) according to ISRIC World Soil documentation. The d_{min} for clay was set to 0.00005 mm according to Shirazi et al. (1988).

The K-factor of for Sharpley and Williams's method was calculated as follow:

$$K_{Sharpley} = \left(0.2 + 0.3 * \exp\left(-0.026 * SAN\left(1 - \frac{SIL}{100}\right)\right)\right) * \left(\frac{SIL}{CLA + SIL}\right)^{0.3} \tag{8}$$
$$* \left(1.0 - \frac{0.25C}{C + \exp(3.72 - 2.95C)}\right)$$
$$* \left(1.0 - \frac{0.7SN1}{SN1 + \exp\left(-5.51 + 22.9SN1\right)}\right)$$

where SAN, SIL, CLA and C are the sand, silt, clay, and organic carbon content of the soil (%), respectively. $SN1 = 1 - SAN/100$.

The K-factor map presents no-value for some cells with channel or delta due to the lack of soil properties. In order to avoid that these cells are excluded from the modelling, all of the no-value cells were replaced with the averaged a value ($a = \alpha_1 * C * K$).

4.4.2 Suspended sediment transport

In the channel suspended sediment transport module, the sediment flux of each cell is given by the sum of four sediment waves: inflow from the upstream cell, outflow to the downstream cell (neglecting the diffusion process), resuspension, and deposition. The horizontal flux along the flow direction is solved analytically in the model as a first-order ordinary differential equation. The vertical sediment flux E is assumed as the difference between the deposition qs_d and the resuspension rate qs_e:

$$E = qs_d + qs_e \tag{9}$$

The deposition rate qs_d is a function of the settling velocity wf_{st} and the concentration near the bed SSC_d (eq. 10). And the concentration SSC_d is calculated according to Lin (1984) as in eq. 11.

$$qs_d = wf_{st} * SSC_d \tag{10}$$

$$SSC_d = \left(3.25 + 0.55 \ln\left(\frac{wf_{st}}{ku_*}\right)\right) * SSC \tag{11}$$

The resuspension rate qs_e derives from an empirical relationship that also concerns the settling velocity wf_{st} (Bernett and Norin, 1977) as follow:

$$qs_e = wf_{st} * \beta * SSC_e \tag{12}$$

where β is a calibrated parameter, and SSC_e is the reference concentration after Van Rijn et al., (2001).

The settling velocity wf_{st} of the suspended sediment is related to the median diameter d_{st} as follows:

$$wf_{st} = \begin{cases} \dfrac{(G-1)gd_{st}}{18v} & if\ 65\ \mu m < \ d_{st} \leq 100\ \mu m \\ \dfrac{10v}{d_{st}}\left(\sqrt{1+\dfrac{0.01(G-1)gd_{st}^3}{v^2}}-1\right) & if\ 100\ \mu m < \ d_{st} < 1000\ \mu m \\ 1.1\sqrt{(G-1)gd_{st}} & if\ 1000\ \mu m \leq \ d_{st} \end{cases} \quad (13)$$

where G is the specific gravity (= 2.65), v is kinematic viscosity coefficient of water (= 10^{-6} m^2/s), g is the acceleration of gravity (= 9.8 m/s^2).

For the RRB, the median diameters of the surface sediments are 0.35, 0.16, 0.175 mm in Da, Thao, and Lo rivers, respectively (Ministry of Agriculture and Rural Development, 2009). In the estuaries and coastal zones, the particle size of the superficial sediments ranges from 5 to 195 μm (Duc et al., 2007). In this study, the diameter of the surface sediment was set as 0.25 mm, and the corresponding wf_{st} is supposed to be 0.06 m/s. However, the deposition and resuspension processes are not fully implemented in the current version of the model. Therefore, these processes were not included in this work and the settling velocity wf_{st} was set equal 0.

4.4.3 Reservoir operation

In TOPKAPI-ETH model, reservoirs are considered to influence the sediment transport in two ways: by changing the discharge, and thus the transport capacity of the flows, and by altering the sediment supply because of the sediment trapping. To activate the reservoir component of the model, additional information is required as follows.

First, the technical characteristics of the reservoirs, such as the location, the water level-surface area function, the water level-maximum release function, the water level-volume function, the minimum and maximum water release, and the maximum storage capacity were extracted from a technical report of a previous project conducted in the catchment by the Politecnico di Milano (IMRR, 2015).

Among other options (e.g., natural lakes), reservoirs can be operated in coordination on the basis of specific operating policies, i.e., parameterized functions that on the basis of the water level in the reservoirs and the technical characteristics of the reservoirs, identify release decisions for each reservoir. Policies used in this work are

obtained by the research team of Prof. Andrea Castelletti at Politecnico di Milano through a state-of-the-art multi-objective optimization approach accounting for three main objectives: hydropower generation, water supply for irrigation and flood protection of the capital city of Hanoi.

The trapping efficiencies of the reservoirs were manually input into the module. Firstly, the mean annual water level and discharge were calculated using the daily observed data. The corresponding mean annual storage could be computed on the basis of the mean annual water level according to the report of IMRR project (2015). Then the trapping efficiency of each reservoir was obtained using the method in 4.3.

4.5 Calibration and validation

The model was calibrated by changing the parameter α_1 in the soil erosion module. In order to match the observed and simulated SSC under the natural condition (without the impact of the reservoir construction). The undisturbed period for all stations were firstly extracted. Among all of the stations, Lai Chau station has the longest observation period (2005 - 2010) that is hardly influenced by reservoir constructions. It is located in the middle of the RRB and belongs to the Da River, which is the main sediment source of the Red River (Figure 5). The calibration mainly focused on matching the simulated daily SSC values of Lai Chau station to observed values. Ham Yen station, which is located at Lo River (one of the main tributaries of Red River), was selected as the validation station. The calibration and validation periods are both from 2005 to 2010.

To validate the model performance, the simulations of mean monthly values and extreme values were both evaluated. For the mean monthly SSC, Nash–Sutcliffe efficiency (NSE), root mean square error (RMSE), and correlation coefficient (R) were calculated for the calibration and validation periods as follows:

$$NSE = 1 - \frac{\sum_{t=1}^{T}(SSC_o^t - SSC_m^t)^2}{\sum_{t=1}^{T}(SSC_o^t - \overline{SSC_0})^2} \quad (14)$$

where $\overline{SSC_o}$ is the mean of observed SSC values, SSC_o^t and SSC_m^t are the observed and the modelled SSC at time t, respectively.

$$RMSE = \sqrt{\frac{\sum_{t=1}^{N}(SSC_o^t - SSC_m^t)^2}{N}} \quad (15)$$

where N is the number of the observed months, $SSC_o^t$and SSC_m^t are the observed and modelled SSC at time t, respectively.

$$R = \frac{\sum(SSC_m^t - \overline{SSC_m})(SSC_o^t - \overline{SSC_o})}{\sqrt{\sum(SSC_m^t - \overline{SSC_m})^2 \sum(SSC_o^t - \overline{SSC_o})^2}} \quad (16)$$

where SSC_m^t and SSC_o^t are the observed and modelled SSC at time t, respectively; $\overline{SSC_m}$ and $\overline{SSC_o}$ are the mean of simulated and observed SSC values, respectively.

To assess the model performance for simulating extreme events, the contribution of high SSC events on the total annual sediment load at Lai Chau was firstly evaluated. The threshold for extreme events was set equal to the 95th percentile of the dataset. The sediment load (daily SSC × daily discharge (Q)) was firstly calculated at the daily scale for observed and simulated data, respectively. Then the observed and simulated sediment load were summed up and compared at the annual scale.

Furthermore, to investigate if high SSC events are triggered by high Q or precipitation (P) and if the model could capture this characteristic, the corresponding discharge at the same location and the precipitation of the contributing sub-basin were extracted. The SSC, Q and P of high SSC events were plotted to explore their relationships.

4.6 Sensitivity analysis

This thesis mainly evaluated the model's sensitivity regarding the following three aspects:

The first one is the sensitivity to different K-factor calculation methods. K-factor map is related to soil properties and influences the soil erosion simulation. There are two methods for K-factor calculation that were developed by Torri et al. (1997) and Sharpley and Williams (1990), respectively. This thesis compared the simulation results using the above-mentioned two methods, and investigate if the simulated SSC is sensitive to different K-factor calculation methods.

The second uncertainty is from the calibrated parameter α_1 that determines the soil erodibility. In the TOPKAPI-ETH model, the value of α_1 is universal throughout the entire basin. However, in reality, this parameter is different in space reflecting different environmental conditions associated to erosion and sediment transport (e.g., sediment supply). Since the RRB is a large basin and the environment is not homogeneous, it is worth to investigate how does the model respond to the changing α_1 value. In this study, the calibrated α_1 was increased and decreased by 10% and 20% to test the model's responses.

Besides, the median diameter of the surface sediment also presents spatial variability (Ministry of Agriculture and Rural Development, 2009). To test the sensitivity of the model to this variability, the input median diameter of the surface sediment was also increased and decreased by 10% and 20%.

4.7 Simulating the impact of anthropogenic activities

In past decades, the RRB has experienced land use changes and reservoir constructions. In order to reconstruct the impact of these anthropogenic activities and investigate the model's responses to these changes, several scenarios were applied in the model simulation (Table 5).

Firstly, extreme landuse change scenarios (scenarios 1, 2 in Table 5) were firstly considered to test the maximum decrease or increase of the simulated sediment transport. Then different land use types were changed proportionally to investigate the model responses. Besides, land use changes were made at different locations to test if the model is sensible to the spatial distribution of land use changes.

Table 5 Descriptions of anthropogenic activities' scenarios.

No.	Descriptions	
1	Land Use Changes	Change all of the land use to forest
2		Change all of the land use to cropland
3		Forest + 10% randomly
4		Forest + 20% randomly
5		Forest + 1 pixel around the current forest (+ about 20%)

6		Cropland + 1 pixel along the main stream (+ about 10%)
7		Cropland + 2 pixels along the main stream (+ about 20%)
8		Cropland + 2 pixels around the current cropland (+ about 10%)
9		Cropland + 3 pixels around the current cropland (+ about 20%)
10		Urban + 1 pixel along the main stream
11		Urban + 2 pixels along the main stream
12		Urban + 3 pixels around the current urban
13		Urban + 5 pixels around the current urban
14	Reservoir Construction	Designed reservoir trapping efficiency (TE)
15		TE - 10%
16		TE - 20%

*All the changes were made based on the land cover map in the year 2015. The main stream refers to the 4th and 5th order rivers.

The impact of the reservoirs on sediment transport was simulated using the reservoir module of the model. The sediment transport was firstly simulated without the reservoir module, which reproduces the sediment transport regime under the natural condition. Then the sediment transport was simulated with the reservoir module, and a decrease of the sediment transport could be expected. The decrease of the simulated sediment transport would be compared to the observed value and used to explain the impact of the reservoir constructions. Besides, the actual storage could be smaller than the designed amount considering the deposition of the sediment in the reality. Therefore, the trapping efficiency was reduced by 10% and 20% to investigate the influence of the decreasing trapping effect of the reservoir (scenarios 14 – 16 in Table 5).

4.8 Future scenarios

4.8.1 Land use

The future land use of RRB was extracted from global land use projection of Chen et al. (2022). This projection presents the land use for 2015 – 2100 with 1-km resolution. The projection adopted IPCC coupling socioeconomic and climate change scenarios. Chen et al. (2022) adopted the International Geosphere Biosphere Programme (IGBP) land use classification system. The classification was transformed to the ESA-CCI classification to match the land use categories of the previous simulation in this thesis. In this thesis, the projection for the year 2050 was used for simulation. The land uses

(Figure 7) under four SSP-RCP scenarios (O'Neill et al., 2016) were considered:

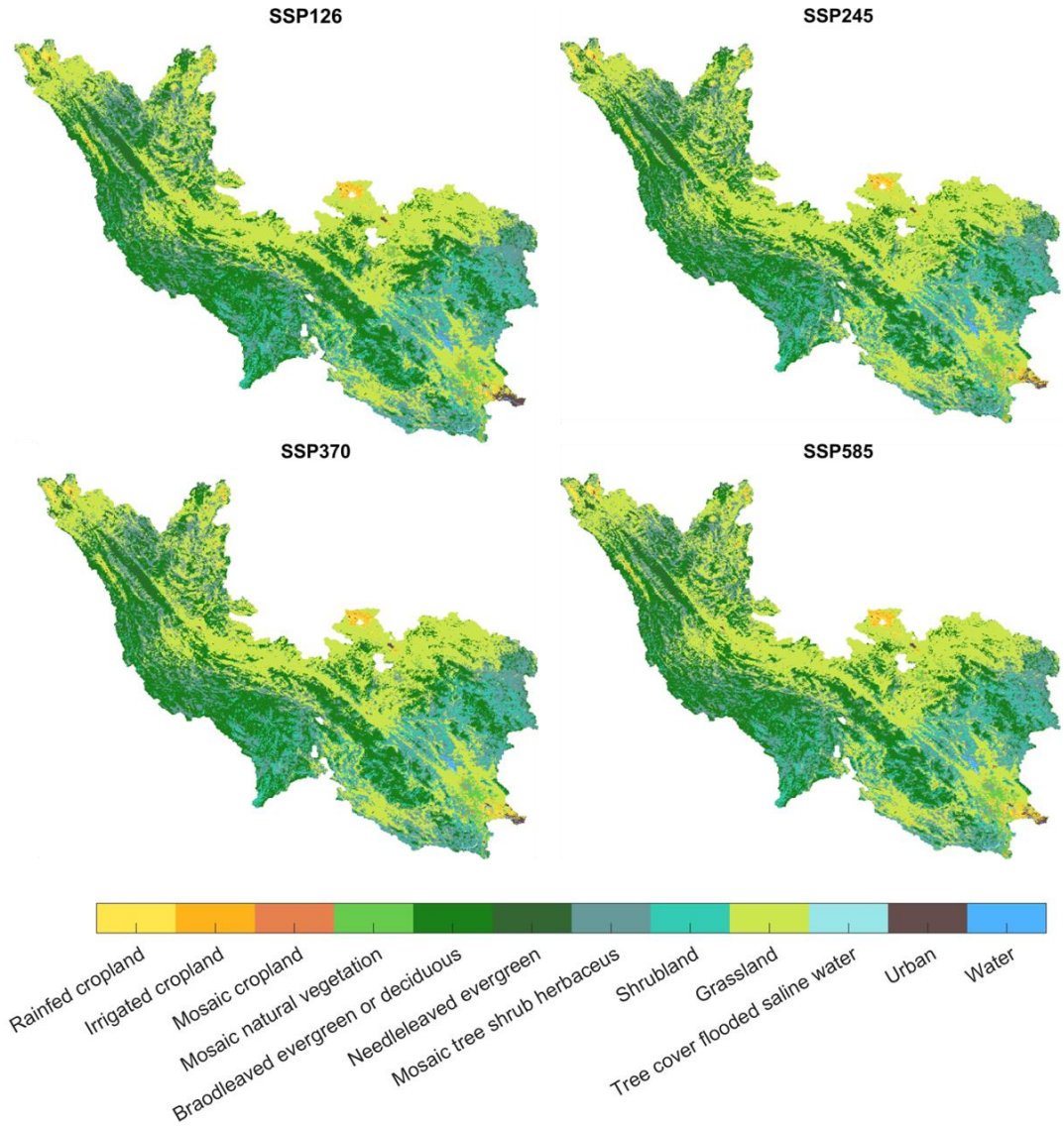

Figure 7 Land use predictions for the year 2050 under different SSP-RCP scenarios.

1. SSP126: Green pathway. It assumes that the climate protection measures are being taken. The radiative forcing would be 2.6 W/m² by the year 2100. The areas of forest and urban are the largest under this scenario compared to the other three scenarios.

2. SSP245: Middle of the road. It assumes that the climate protection measures are being taken, but the environmental systems are facing a certain degradation. The radiative forcing would be 4.5 W/m² by the year 2100. This scenario has the largest area of grassland compared to the other three scenarios.

3. SSP370: Regional rivalry. It assumes an increasing inequality and a decreasing investment on education and technology. Some regions would suffer drastic environmental damage. The radiative forcing would be 7.0 W/m² by the year 2100. This scenario has the smallest area of cropland and urban compared to the other three scenarios. Many cropland that is located at high elevation is replaced by grassland or forest.

4. SSP585: Fossil-fueled development. It assumes that the global economy increases rapidly basing on an intensified exploitation of fossil fuel resources. The radiative forcing would be 8.5 W/m² by the year 2100. The area of cropland is the largest under this scenario compared to other three.

4.8.2 Operating policies of the reservoirs

The future operating policies of the four main reservoirs in the basin could be optimized to satisfy different requirements. In this thesis, four operation policies with different priorities were considered.

1. P1: Minimize the flood risk (namely mean daily water excess) in Hanoi.
2. P2: Maximize the hydropower production (namely mean daily energy production of the four reservoirs).
3. P3: Maximize the available water amount for irrigation.
4. P4: A compromise policy for the above-mentioned requirements.

The values of the parameters of these four operating policies were obtained through an Evolutionary Multi-Objective Direct Policy Search (EMODPS) approach (Giuliani, et al., 2016) under future climate and future water demand projections. The EMODPS first parameterizes the operating policy within a given family of functions, then it explores the parameter space seeking the best parameterization of the operating policies with respect to the objectives of the problem (hydropower production, water suppl y for agriculture, and flood protection). Such an optimization is performed using multi-objective evolutionary algorithms (MOEAs), which explore the tradeoffs across the selected objectives (Maier et al., 2014).

5. Time series analysis

5.1 Streamflow

The Mann-Kendall test conducted on the observed mean annual streamflow revealed that four stations (out of fourteen) had a significant decreasing trend during their respective observed periods (Figure 8). All four stations are situated along the main stream of the Red River, with Hanoi and Son Tay located close to the delta, Hoa Binh along the Da River, and Lao Cai along the Thao River.

These four stations were also found to have a significant changing point during their observation periods, while other stations did not exhibit any statistically significant changing points in the Pettit test. The changing points for these four stations occurred between 2004 and 2010. The average annual mean streamflow has decreased by about 20% to 40% after the changing points. Of particular interest is that the year of the changing points did not align with the start of the commission of respective reservoirs, but rather with the period of reservoir construction. For instance, the construction of Son La reservoir began in 2005 and concluded in 2012 (Table 1), and the observed changing point in streamflow occurred in 2009.

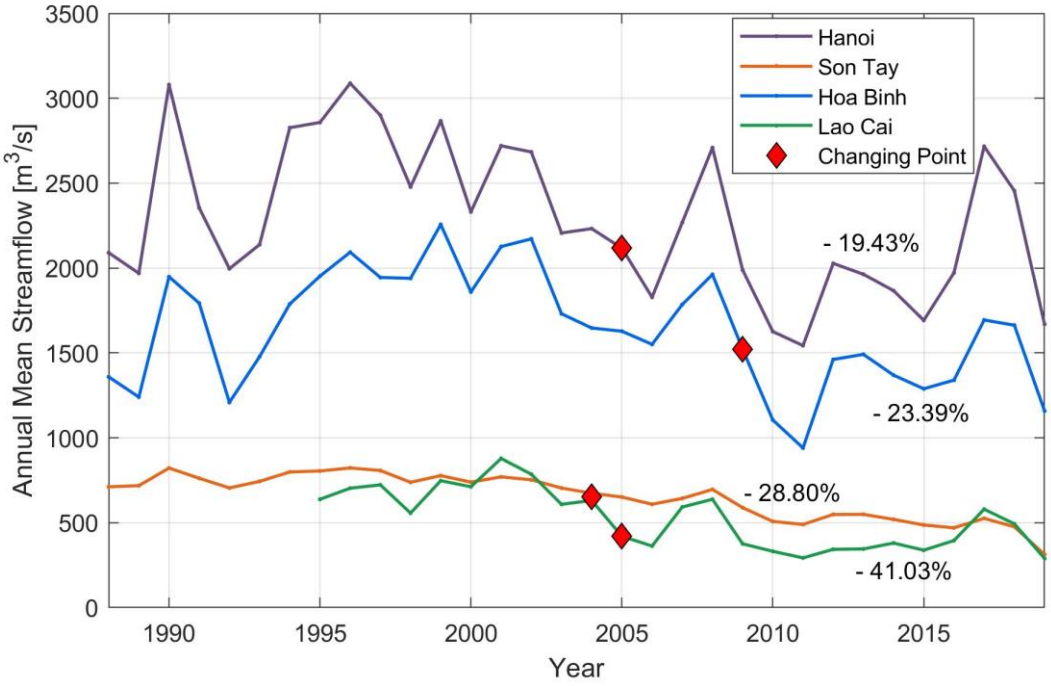

Figure 8 Annual mean streamflow and the year of changing point for Hanoi, SonTay, Hoa Binh and Lao Cai station.

Table 6 provides the Mann-Kendall's outputs for the mean monthly discharges of the 14 stations in the basin. The significant increasing trend mainly concentrates in winter months, particularly in January. Over 50% of the stations show a significant increasing trend in January. Conversely, the significant decreasing trend was found to be concentrated in the wet season when the discharge reaches its peak in a year (Figure 3). This suggests that during the time of the highest flow, a substantial number of stations exhibited a decreasing trend.

Table 6 Mann-Kendall's test outputs for the monthly mean streamflow

Station	Annual	Jan.	Feb.	Mar.	Apr.	May	June	July	Aug.	Sept.	Oct.	Nov.	Dec.
Bao Yen													
Chiem Hoa													
Genh Ga													
Gia Bay													
Hanoi													
Ham Yen													
Hoa Binh													
Lai Chau													
Lao Cai													
Son Tay													
Ta Bu													
Thanh Son													
Vu Quang													
Yen Bai													

Figure 9 further supports that the decline in discharge is more pronounced during the wet season compared to the dry season. All the four stations in Figure 8 show a significant decreasing trend in mean annual streamflow. Such a decrease is particularly evident during the wet season. In the case of the Hanoi station, the highest mean monthly discharge reached nearly 10,000 m^3/s but has decreased by almost half to less than 6,000 m^3/s. In contrast, for the dry season, the ranges of monthly mean streamflow variation before and after the changing points only present a slight difference. After the changing point, there has been a noticeable flattening of seasonal variation in streamflow, especially for Hanoi and Hoa Binh station.

These findings suggest two important factors: First, the significant changing points during reservoir constructions reveals a possible link between the construction and operation of reservoirs and the alteration of streamflow in the Red River Basin (RRB). Second, the decrease in discharge during the wet season indicates the potential influence of reservoir operation on the streamflow temporal pattern in the basin.

Besides the possible link between reservoirs construction and decreasing streamflow, the reduction in mean annual streamflow could also be related to climate, i.e., reduction in precipitation. The evaporation due to water impoundment behind reservoirs could also be a possibility that results in a decreasing streamflow.

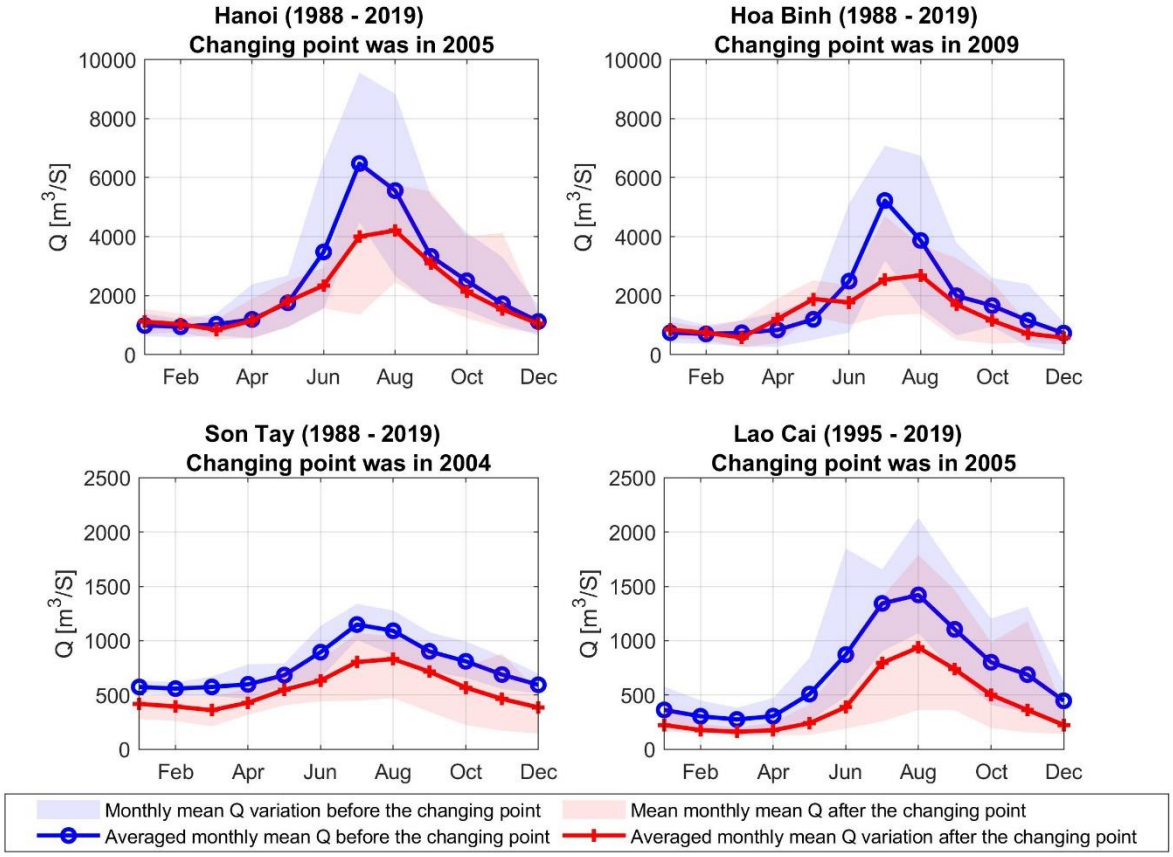

Figure 9 Monthly mean streamflow before and after the changing points.

5.2 Suspended sediment concentration

The Mann-Kendall test conducted on the annual mean SSC shows that no station had a significant increasing SSC during the observed period. Six stations (out of 14) had a significant decreasing trend (Figure 10), and they are distributed along different tributes. The timing of the decreasing trend in annual mean SSC was mainly from 2001 to 2010, a period marked by intensive reservoir construction in the basin (Table 1).

While most stations showed a significant decreasing trend in observed mean annual SSC, only two of them, namely Thuong Cat and Lai Chau, displayed a significant changing point during the observation period. At Thuong Cat station, the changing point occurred in 2002, leading to a remarkable decrease of approximately 50% in the

annual mean SSC after the changing point. Similarly, Yen Bai station experienced a changing point in 2008, resulting in a significant reduction in the mean annual SSC (decreased by 62.77%). The decrease in annual mean SSC for other stations exhibited a more gradual trend rather than a sudden change.

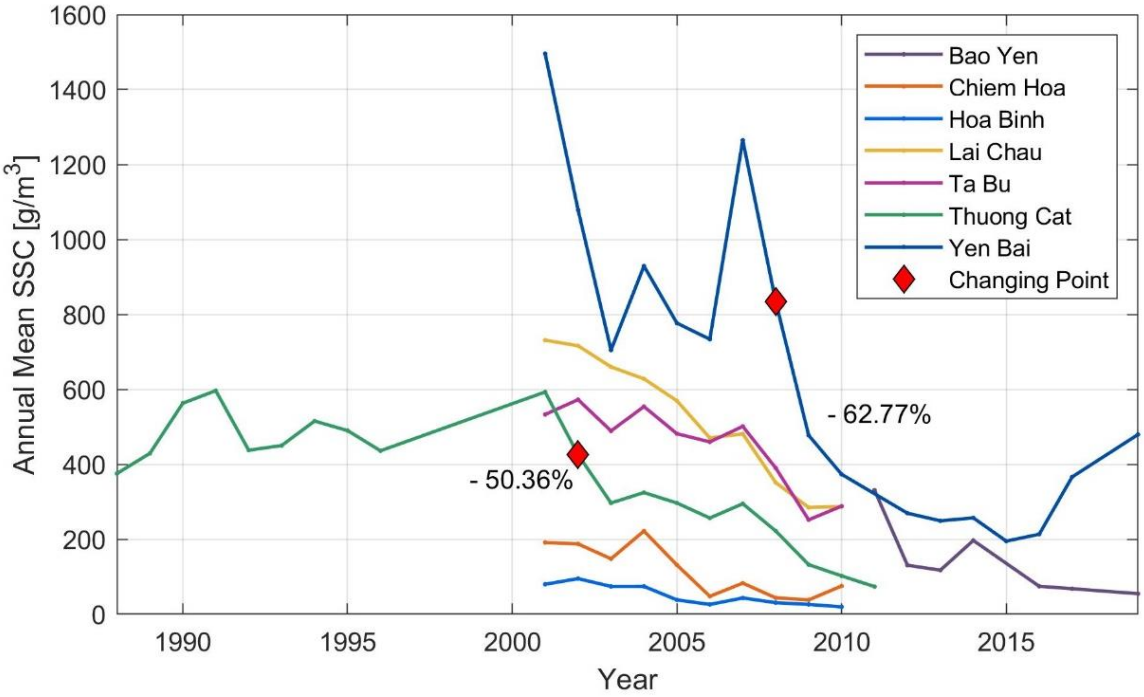

Figure 10 Annual mean SSC for stations with significant decreasing trends and the timing of the changing points.

Table 7 provides the trend analysis results for the observed mean monthly SSC. Unlike the trend observed for streamflow (Table 6), none of the stations show a significant increasing trend for either the mean annual or monthly SSC. Instead, a consistent decreasing trend in mean monthly SSC is detected throughout the entire year. The decrease in mean monthly SSC mainly concentrated in the wet season, which aligns with the period when the monthly mean streamflow also exhibits a noticeable decreasing trend (as shown in Table 6).

However, for the individual station, the months with a significant decreasing trend in SSC do not always coincide with those displaying a significant decreasing trend in streamflow. This observation suggests that the decline in SSC is likely influenced by other factors in the basin, apart from changes in streamflow.

Table 7 Mann-Kendall's test outputs for the monthly mean suspended sediment concentration (SSC).

Station	Annual	Jan.	Feb.	Mar.	Apr.	May	June	July	Aug.	Sept.	Oct.	Nov.	Dec.
Bao Yen													
Chiem Hoa													
Genh Ga													
Gia Bay													
Hanoi													
Ham Yen													
Hoa Binh													
Lai Chau													
Lao Cai													
Son Tay													
Ta Bu													
Thanh Son													
Thuong Cat													
Vu Quang													
Yen Bai													

Figure 11 provides a comparison of the monthly mean SSC variation before and after the changing point for the two stations with significant changing points. Similar to the streamflow trends shown in Figure 8, the decrease in mean monthly SSC is particularly prominent during summer, when the peak SSC typically occurs. For instance, at Yen Bai station, the monthly mean SSC in August decreased from about 2500 g/m^3 to less than 1000 g/m^3 after the changing point.

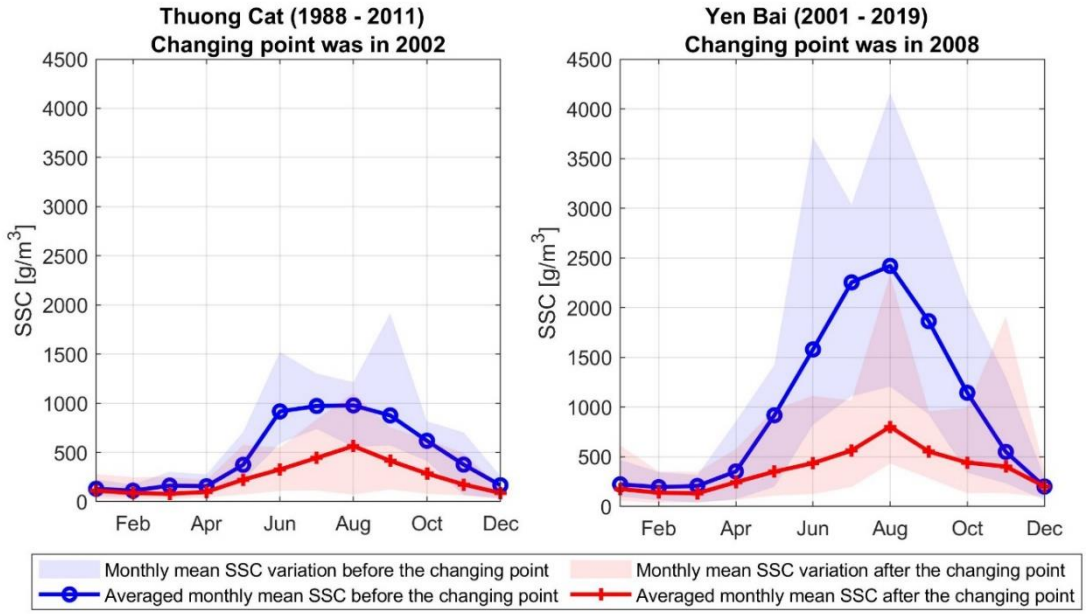

Figure 11 Monthly mean suspended sediment concentration (SSC) before and after changing points.

Besides, the timing of the peak monthly SSC also changed after the changing point. At Thuong Cat station, the mean monthly SSC values for June, July, and August were similar before the changing point. However, after the changing point, the peak mean monthly SSC became more evident in August. The shift in the timing of peak SSC is as noticeable as the amount of the decrease of SSC.

6. Basin-scale sediment dynamics simulation

6.1 Model performance evaluation

After model calibration using trail-and-error method, the calibrated parameter α_1 is 0.3 for Torri et al. (1997) 's method and 0.05 for Sharpley and Williams (1990) 's method. The input $a(x,y)$ map ($a(x,y) = \alpha_1 * C(x,y) * K(x,y)$), C-Factor and K-factor maps are attached in the appendix.

In this section, the model performance in simulating suspended sediment concentration (SSC) is evaluated for calibration and validation stations, respectively. Additionally, since SSC is correlated with streamflow (Q) and precipitation (P), the second section further assessed how well could the model capture the SSC – Q – P relationship of RRB in high SSC events.

6.1.1 Model calibration and validation

Figure 12 and 13 present a comparison of the simulated and observed SSC at the calibration and validation stations, respectively. The observed SSC shows a large intra-annual variation. At the calibration station (Figure 12), the monthly mean SSC could reach over 1500 g/m^3 in wet seasons, while is only about 200 g/m^3 in dry seasons. The model presents a good performance in capturing the observed seasonal variation of SSC at Lai Chau, though there are some occasional discrepancies in the timing of the peak flow compared to the observed data. During the dry season, the model tends to slightly overestimate the SSC values. Nevertheless, it's worth noting that Lai Chau station is subject to the influence of some foreign reservoirs, which may impact the accuracy of the model's predictions. Despite these challenges, the model generally reproduces the observed SSC values and variations at the Lai Chau station quite well, with the majority of the results aligning closely with the observed data.

The model assumes that the validation station (Ham Yen in Figure 13) is supposed to have similar SSC values as the calibration station (Lai Chau in Figure 12). However, the monthly mean SSC at Ham Yen is generally overestimated in the model, especially in the wet season. Similar to the situation of Lai Chau station, there are also several

small reservoirs that are located upstream of Ham Yen station, but it appears that reservoirs have had a stronger impact on Ham Yen than Lai Chau. Besides, the calibrated α_1 value at Lai Chau may not totally fit into the situation at Ham Yen. The overestimation also reveals the importance for accounting for the spatial variability of the calibrated parameter.

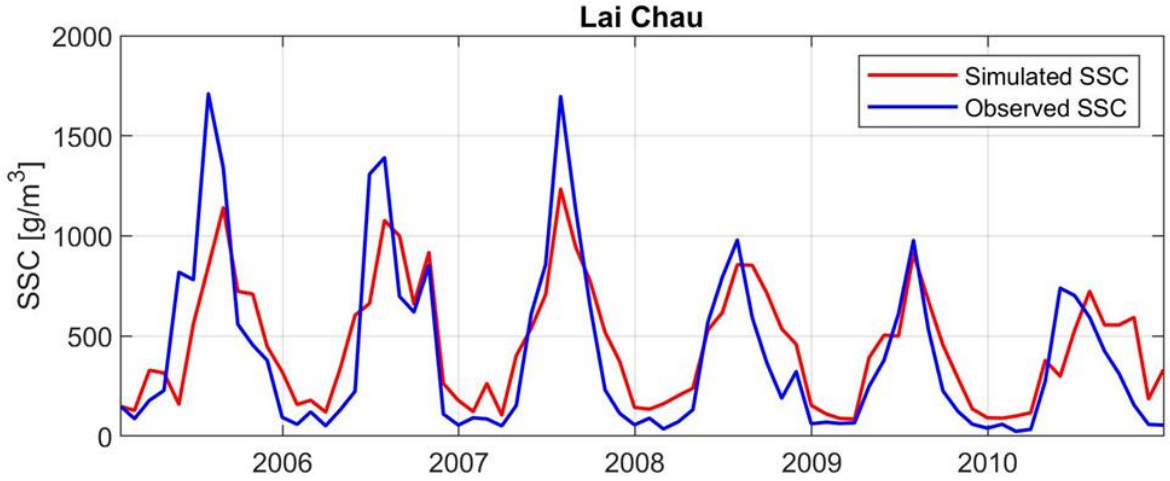

Figure 12 The simulated and observed monthly mean SSC at the calibration station (Lai Chau). The input alpha map was obtained using Torri et al. (1997)'s method.

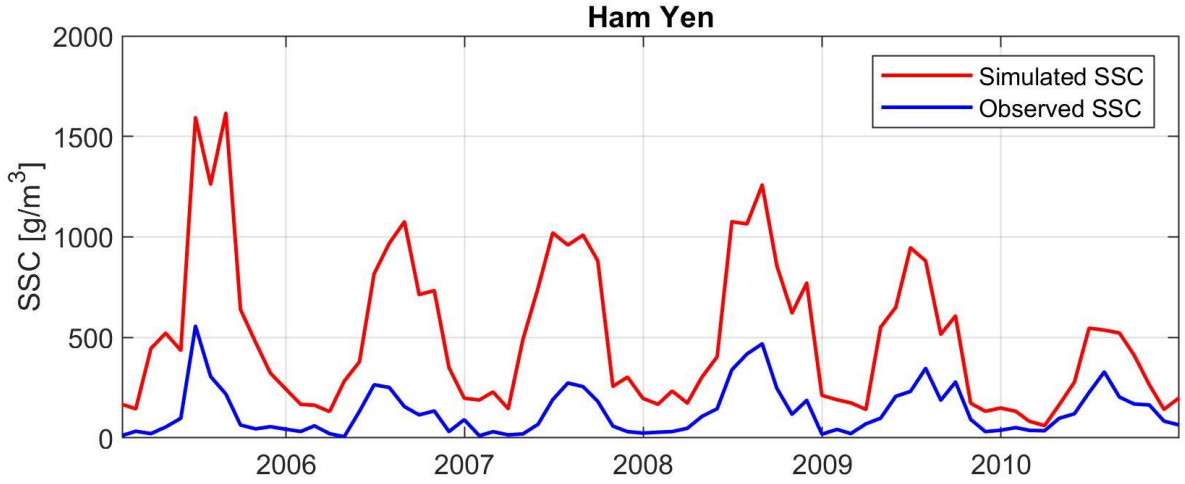

Figure 13 The simulated and observed monthly mean SSC at the validation station (Ham Yen). The input alpha map was obtained using Torri et al. (1997)'s method.

Table 8 estimated the model performance quantitively at the calibration and the validation stations. The R^2 at both Lai Chau and Ham Yen is over 0.65, which indicates the model's capacity in capturing the temporal variation at monthly scale. The NSE and RMSE at Lai Chau is 0.67 and 237.92 g/m^3, respectively. As for Ham Yen station, the NSE is negative and RMSE is higher than that at the calibration station. This could be attributed to the overestimation of SSC as shown in Figure 13.

Table 8 Goodness of fit for the calibration (Lai Chau) and the validation (Ham Yen) station.

Station	Method for K-factor calculation	NSE	RMSE	R^2
Lai Chau (2005 - 2010)	Torri et al. (1997)	0.67	237.92	0.70
	Sharpley and William (1990)	0.66	242.42	0.70
Ham Yen (2005 - 2010)	Torri et al. (1997)	-14.37	464.98	0.67
	Sharpley and William (1990)	-19.68	539.32	0.65

6.1.2 Model performance in simulating high SSC events

The threshold for identifying high SSC events was set equal to the 95th percentile of the daily SSC from 2005 to 2010. For the observed data at Lai Chau, the threshold is equal to 1579.5 g/m^3. Model simulations present a value of the 95th percentile of daily SSC equal to 1423.0 g/m^3 which is similar to the observed one, and reflects the model's capability in simulating SSC during extreme events.

Figure 14 shows the sediment load at Lai Chau from 2005 to 2010, alongside the contribution of high SSC events each year. In the first three years, the observed annual sediment load ranged from 3.0 to 5.0 × 10^7 t per year. For the last three years, the observed annual sediment load decreased to around 1.0 to 3.0 × 10^7 t per year. Remarkably, the simulated annual sediment load falls into the similar range as the observed values and also presented a decline in the sediment load from 2008 to 2010.

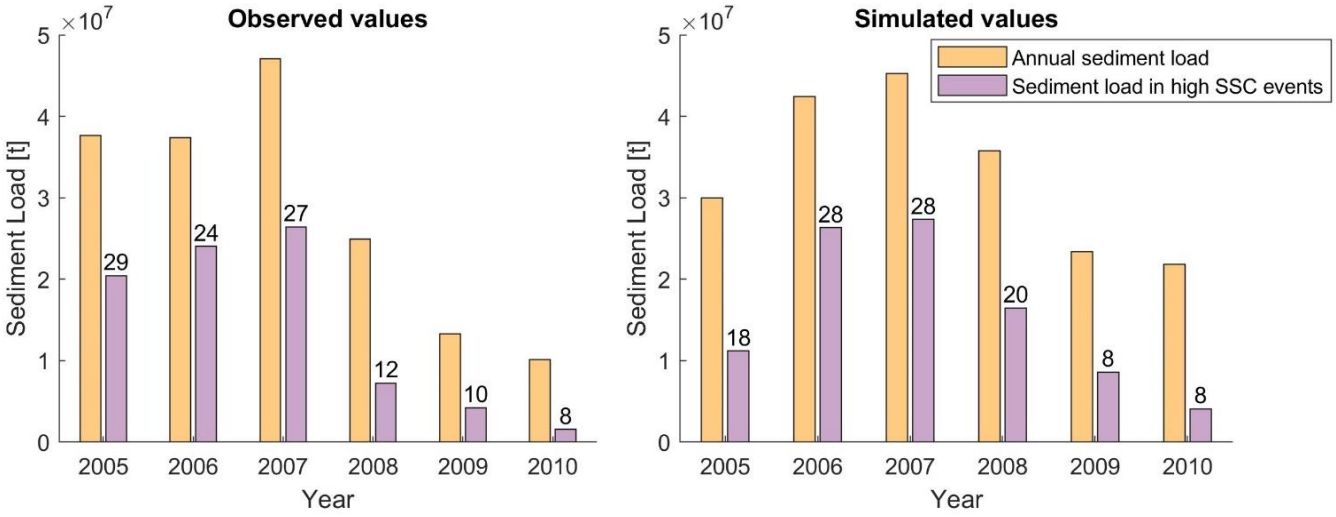

Figure 14 Annual sediment load at Lai Chau station and the sediment load in high SSC events. The numbers of high SSC days in each year were presented above purple bars.

The model also well simulated both the total sediment load of high SSC events and the days of high SSC events in each year (Figure 14). It is worth noting that nearly half of the annual sediment load can be attributed to rare and high SSC events. When the amounts of high SSC days decreased from above 20 to around 10 in the last three years, there was a corresponding decrease in the annual sediment load. The model effectively captured these changes as well.

The SSC, Q, and the corresponding precipitation (P) in high SSC events of Lai Chau station are shown in Figure 15. For the observed data, high SSC values do not always correspond to high Q. The daily precipitation in high SSC events was generally lower than 30 mm. In contrast, the SSC, Q and precipitation show high consistency in high SSC events for the simulated data. Higher simulated SSC values generally align with higher simulated Q, and the corresponding precipitation tends to be higher as well (generally higher than 30 mm). A possible explanation is that intense rainfall events generate events such as landslides that contribute large amount of sediment into the channels/rivers. The model does not include such events, but only erosion due to overland flow. Therefore, the correlation between rainfall and SSC showed in the observations is not reflected in the simulations.

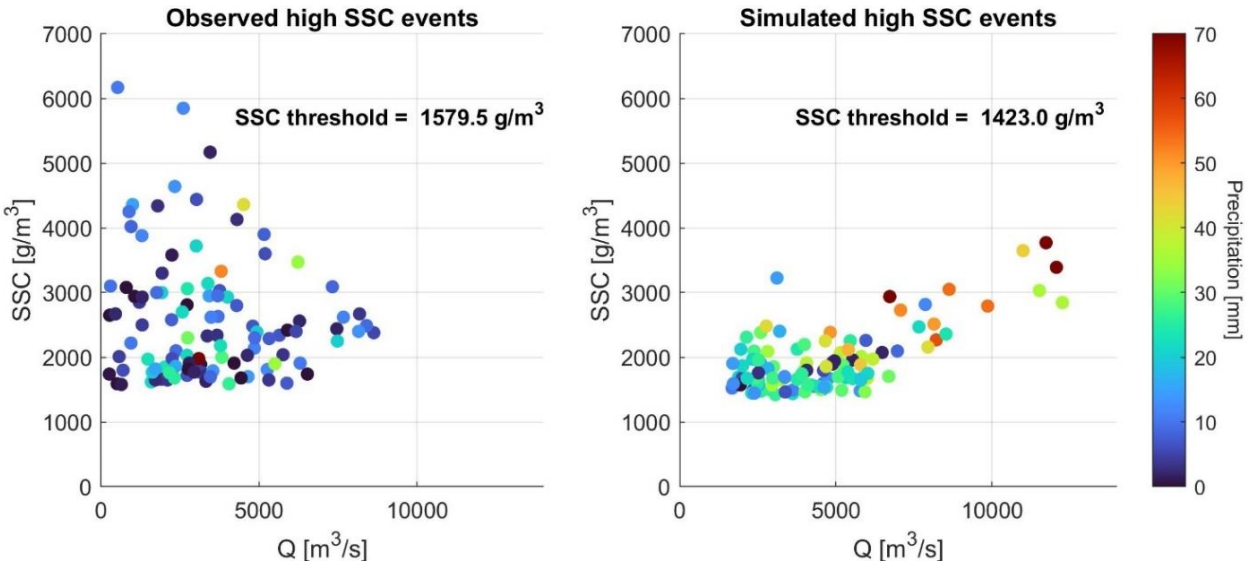

Figure 15 Scatter plots of suspended sediment concentration (SSC), streamflow (Q), and the corresponding precipitation (P) in high SSC events at Lai Chau station.

In general, the model can properly simulate the annual sediment load, the intra-annual

variation of SSC, the magnitude of extreme SSC events, and the contribution of high SSC events to the total sediment load. Therefore, it could be employed to simulate and analyze the potential impact of anthropogenic activities, such as land use change and reservoirs.

6.2 Sensitivity analysis

In this section, model responses to variations in K-factor calculation methods, particle size of the sediment, and α_1 value that is employed in generating land surface conditions were evaluated.

Figure 16 shows that mean monthly simulated SSC values have comparable fluctuations when using soil erodibility maps that were calculated by different methods. In wet seasons, the simulated SSC at Lai Chau station exhibits higher value using Torri et al' s method and is closer to the observed values compared to that using Sharpley and William's method. However, in most months (e.g., in the year 2009 and 2010), the difference in the simulated SSC using these two methods could be negligible.

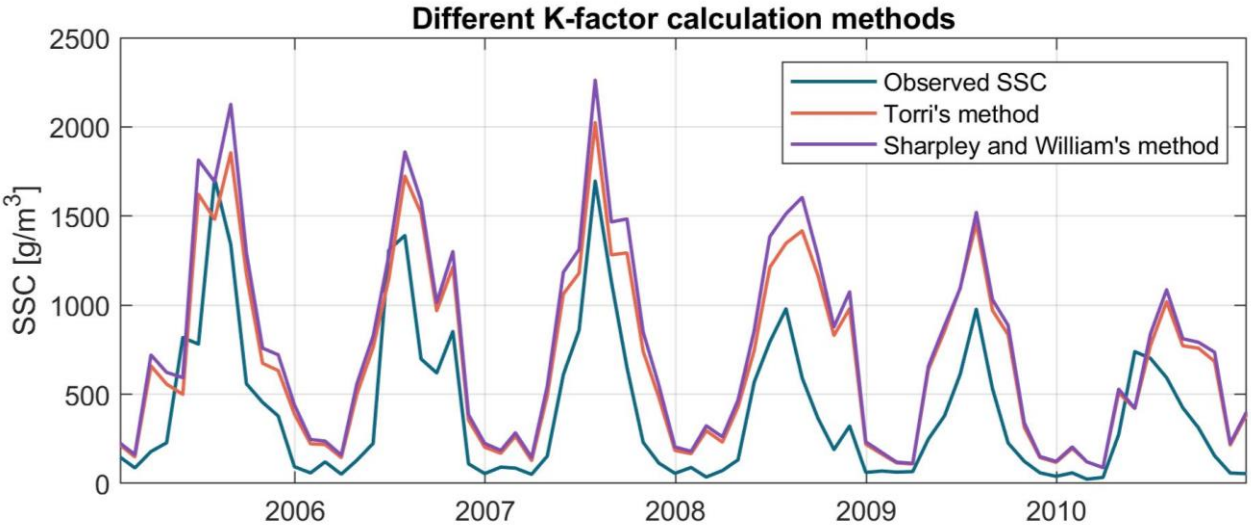

Figure 16 Mean monthly simulated SSC at Lai Chau station from 2005 to 2010 using two methods (namely Torri et al. (1997) and Sharpley and William (1990)) to calculate the K-factor.

Changes of the sediment diameter (± 10%) did not lead to any change in the simulated SSC. The simulated daily SSC maintained the same when the sediment diameter was increased and decreased by 0.025 mm. This indicates that the model is not very sensitive to changes of the sediment diameter and a change of 0.025 mm in sediment

diameter appears to be too minute to result in variation in the sediment transport.

Figure 17 shows the model's sensitivity to the parameter α_1. For both methods of K-factor calculation, the model tends to be more sensitive to the decrease of α_1 value compared to an increase. For example, in August of 2008, the mean monthly simulated SSC decreases by more than 20% when the α_1 value decreases by 20%, while the mean monthly simulated SSC only increases by about 5% when the α_1 value increases by 20%. This non-linear behavior could be associated with the non-linearity and threshold-based nature of the sediment transport equation.

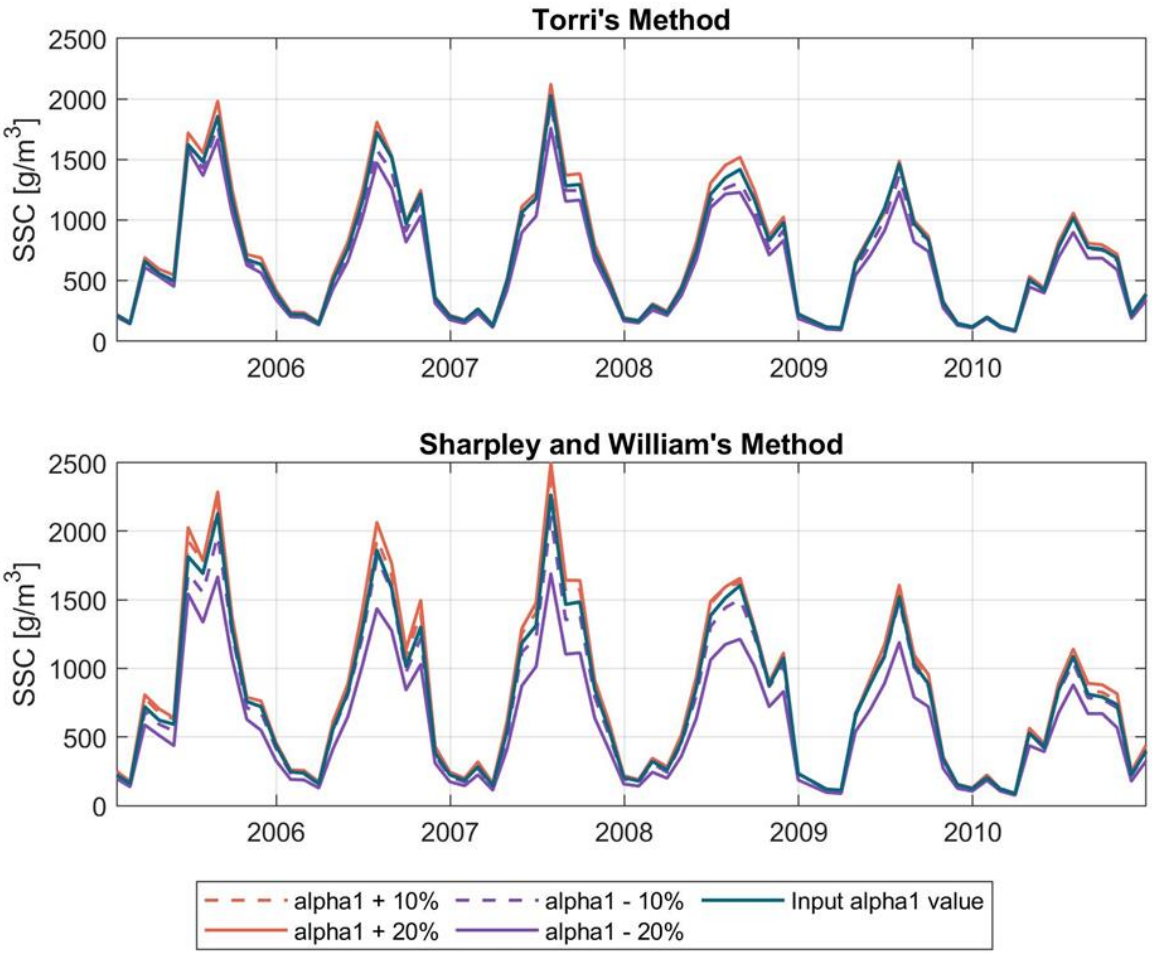

Figure 17 Monthly mean simulated SSC at Lai Chau from 2005 to 2010 with different alpha1 values. Input alph1 value is 0.3 and 0.05 for Torri et al. 's and Sharpley and Williams 's method, respectively.

6.3 Simulated basin-scale sediment regime

The mean annual cumulative erosion mass of RRB was estimated to be 4.35×10^8 t. The southwestern and the northeastern part of the basin presents a generally higher cumulative erosion mass (Figure 18). The annual cumulative mass of these regions is

generally higher than 10^6 kg/km^2. The northern part where the red river originated and the delta region shows a relative lower cumulative erosion mass compared to other regions. The annual cumulative mass is about 10^5 kg/km^2 in these regions.

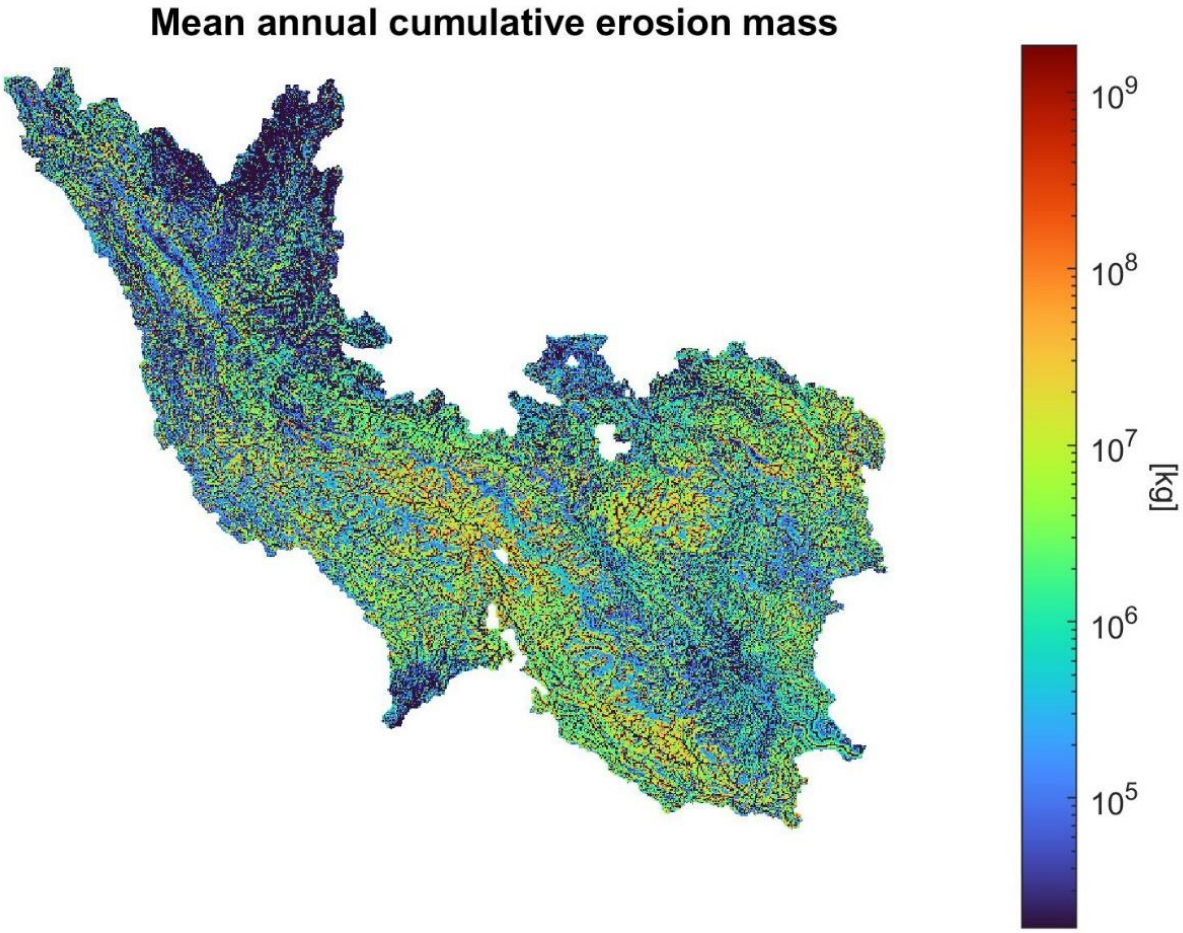

Figure 18 Mean annual cumulative erosion mass of the red river basin (2005 - 2010).

Figure 19 shows the mean cumulative erosion mass of each month. The lowest mean monthly cumulative erosion mass occurs in January. It starts to increase from April. Such an increase is not homogeneous in the basin. For example, in May, the increase of cumulative erosion mass in the north is not as evident as other regions. The cumulative erosion mass starts to decrease from September. It decreases to about lower than 10^5 kg/km^2 in November. The timing of seasonal fluctuations of cumulative erosion mass is generally universal in space, which corresponds to the observed temporal variation of SSC at individual stations across the basin, and is related to the seasonality of rainfall and streamflow.

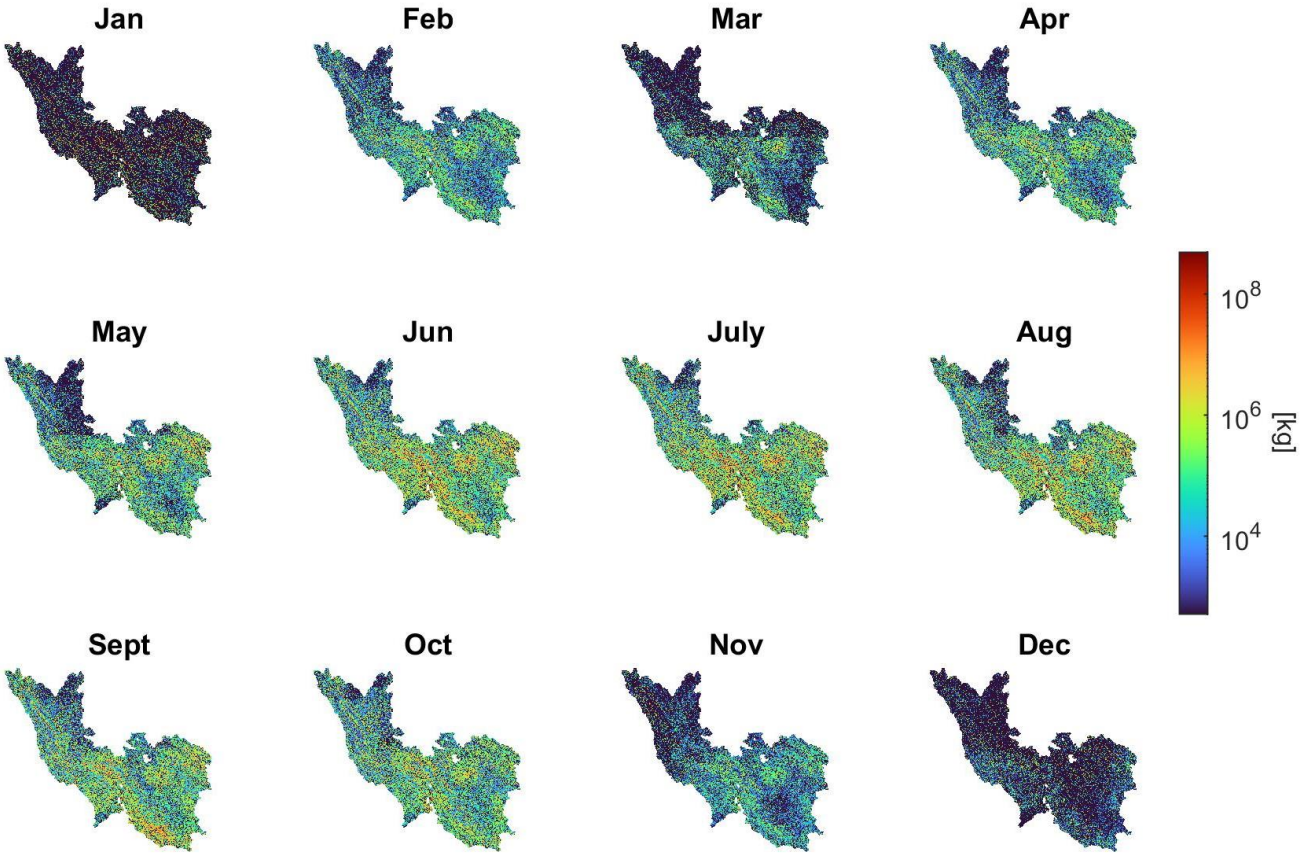

Figure 19 Mean monthly cumulative erosion mass of the red river basin (2005 - 2010)

Figure 20 shows the spatial variation of the simulated SSC of red river network. The extreme high (> 10^4 g/m^3) and low (< 10 g/m^3) annual mean SSC mostly occur in the first and the second order streams. The SSC tends to be stable when small tributes flow into main streams (4th and 5th order rivers). The annual mean SSC of main streams ranges from 500 to 1000 g/m^3. Thao river (the middle one) possesses the highest annual mean SSC among the three main tributes of red river system, then follows with Da river that flows through the western part of the basin. Lo River (locating at the northeastern part) has the lowest annual SSC among three main tributes. When the river passes through regions with high cumulative erosion mass, an increase of SSC could be observed in Figure 20 (e.g., the middle part of Da river, where the cumulative erosion mass in Figure 18 is extremely high).

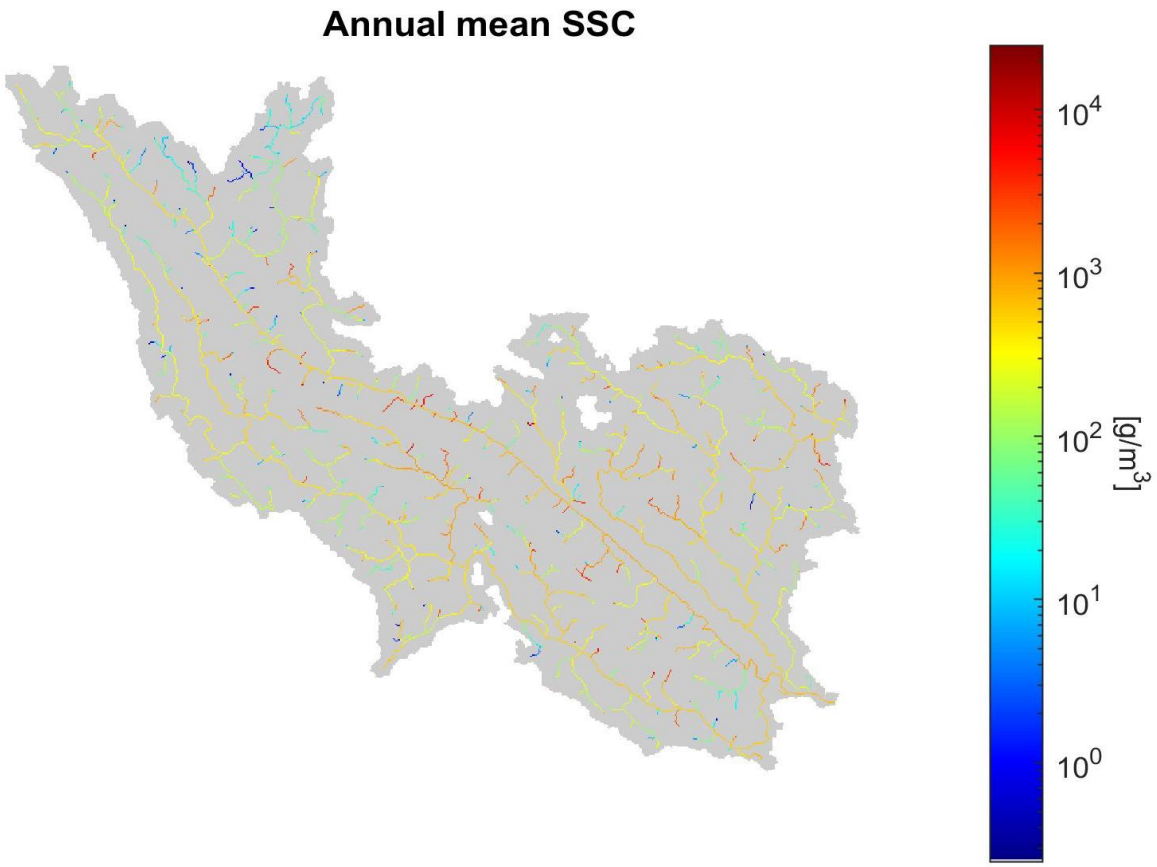

Figure 20 Averaged annual mean SSC (2005 - 2010) of red river basin.

7. Scenario analysis of the basin-scale sediment dynamic

7.1 Land use changes scenarios

This section presents the model's responses to different land use changes scenarios (without reservoirs). Firstly, the sediment flux at Hanoi station (which situates close to the basin outlet) under different scenarios was analyzed. Furthermore, the changes in intra-annual variability of the sediment load and the spatial variation of the soil erosion were investigated in the second and the third parts of this section, respectively.

7.1.1 Sediment flux at Hanoi

Figure 21, 22 and 23 show the annual mean Q and SSC at Hanoi station under different land use changes scenarios. In scenarios involving the increase of forest (Figure 21), the increase of forest area does not induce any shifts of the simulated interannual variability of Q or SSC. The simulated Q remains stable with the increase of forest, even when the entire basin is hypothetically covered by forest (Figure 21). However, the annual mean simulated SSC decreases from over 500 g/m^3 to lower than 100 g/m^3 under the "All Forest" scenarios. This suggests the forest's significant role in reducing sediment production. Interestingly, when the area of forest was randomly increased, the annual mean simulated SSC did not decrease as expected.

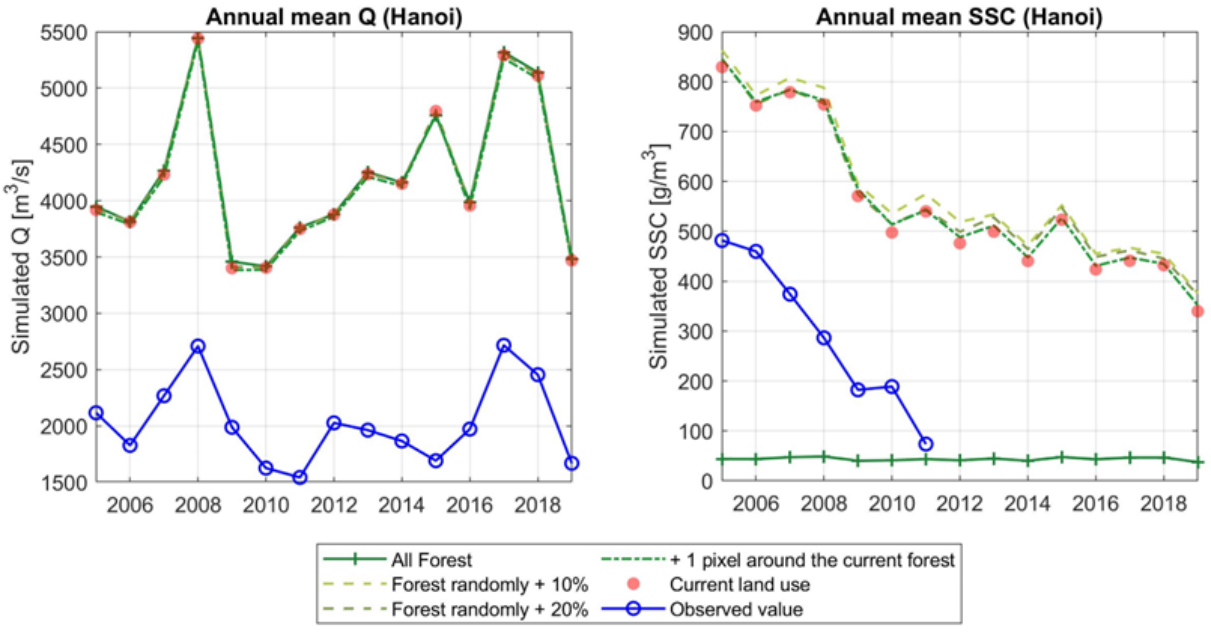

Figure 21 Annual mean Q and SSC at Hanoi station from 2005 to 2019 under different forest expansion scenarios.

Figure 22 shows that the increase of the cropland could lead to the decrease of annual mean Q and increase the annual mean SSC at Hanoi station. Under the “All Cropland” scenario, the annual mean simulated Q decreases by about 12%. Meanwhile, the annual mean simulated SSC increases from lower than 1000 g/m^3 to over 3000 g/m^3 (which is not plotted in Figure 22 to maintain the comparability with other scenarios in Figure 21 and 23). Similar to forest expansion scenarios, the increase of cropland results in a more evident change in annual mean SSC compared to Q. In addition, the annual mean simulated SSC at Hanoi appears to be more sensitive to the location of land use changes instead of the proportion. When the cropland is increased alongside the main stream, the increase of annual mean SSC is generally 50% larger in comparison to the scenario where cropland expansion occurs around the existing cropland, though the proportions of cropland expansion are approximately 20% for both scenarios.

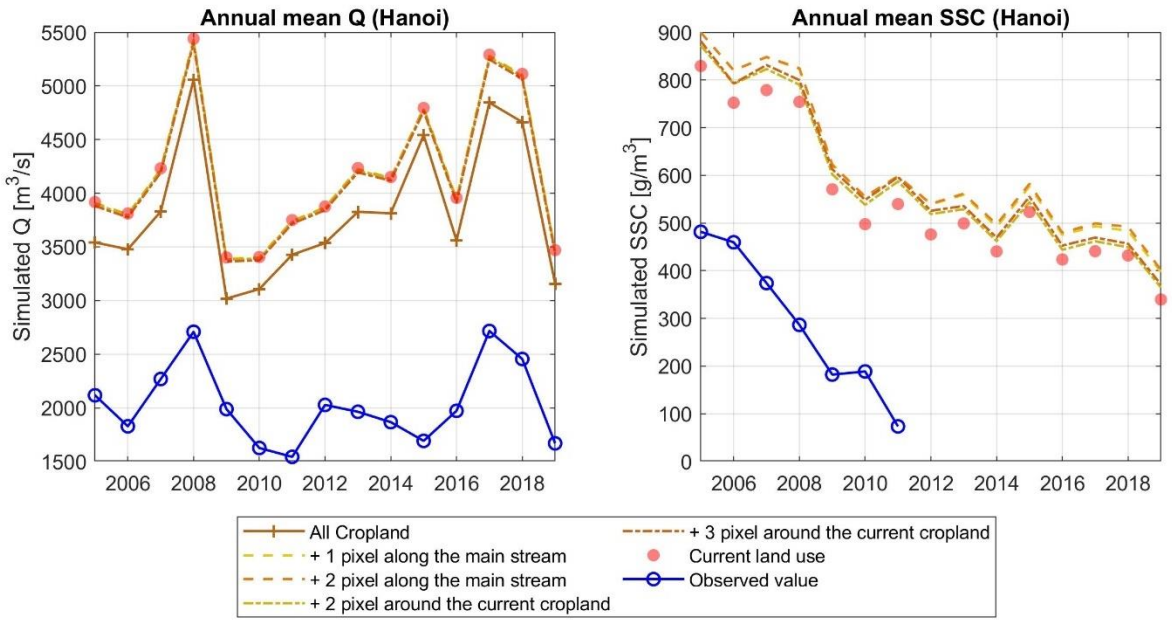

Figure 22 Annual mean Q and SSC at Hanoi station from 2005 – 2019 under different cropland expansion scenario.

Figure 23 presents the simulated Q and SSC under various urban expansion scenarios. The annual mean simulated Q maintains stable with the increase of urban. Interestingly, when examining the alterations in the annual average simulated SSC, the changes exhibit contrasting directions as urban expansion occurs at different locations. When urban expansion takes place around the current urban, the annual mean SSC tends

to increase in comparation to the current land use. Conversely, the annual mean simulated SSC tends to decrease when the urban expansion occurs alongside the main stream.

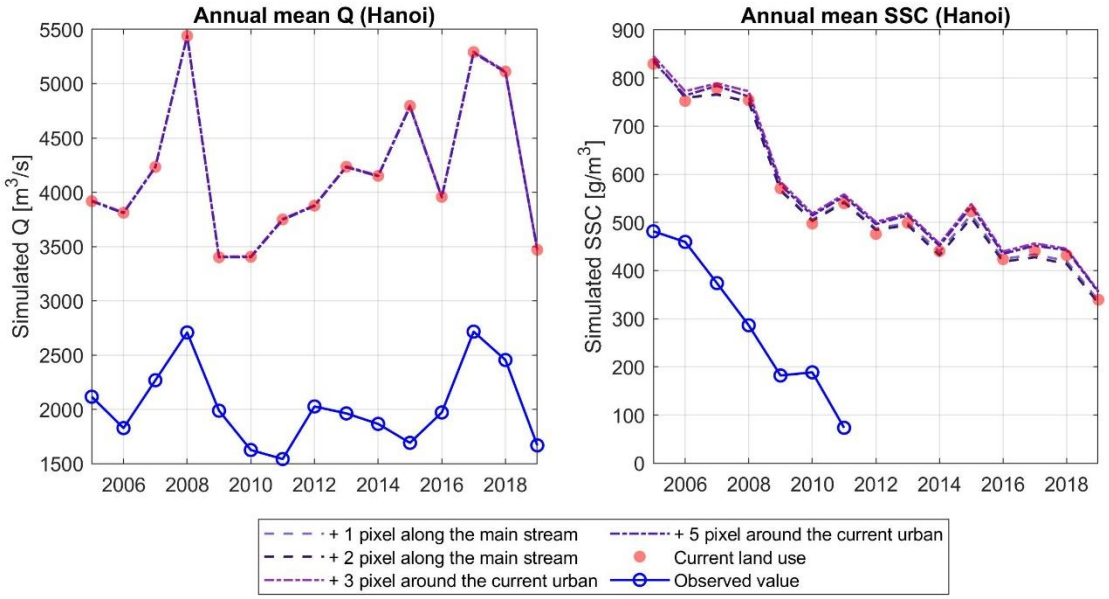

Figure 23 Annual mean Q and SSC at Hanoi station from 2005 – 2019 under different cropland expansion scenarios.

Across different land use scenarios, despite the similarity between the interannual variability of the simulated data and the observed data, the values for simulated Q and SSC are generally higher than observed values at Hanoi. From 2005 to 2019, the actual land use changes (as outlined in section 3.4) were not as extensive as those subjected to the scenario analysis. This implies the presence of other influencing factors that contribute to basin-scale sediment flux beyond land use changes.

In addition, land use changes always exert opposing impacts on Q and SSC. For instance, the expansion of cropland could lead to a simultaneous reduction in discharge while increasing soil erosion (Figure 21). However, the sediment load is influenced by both Q and SSC. Consequently, in order to capture the comprehensive impact of varying Q and SSC across different scenarios, the average annual sediment load at Hanoi station was computed as in Figure 24.

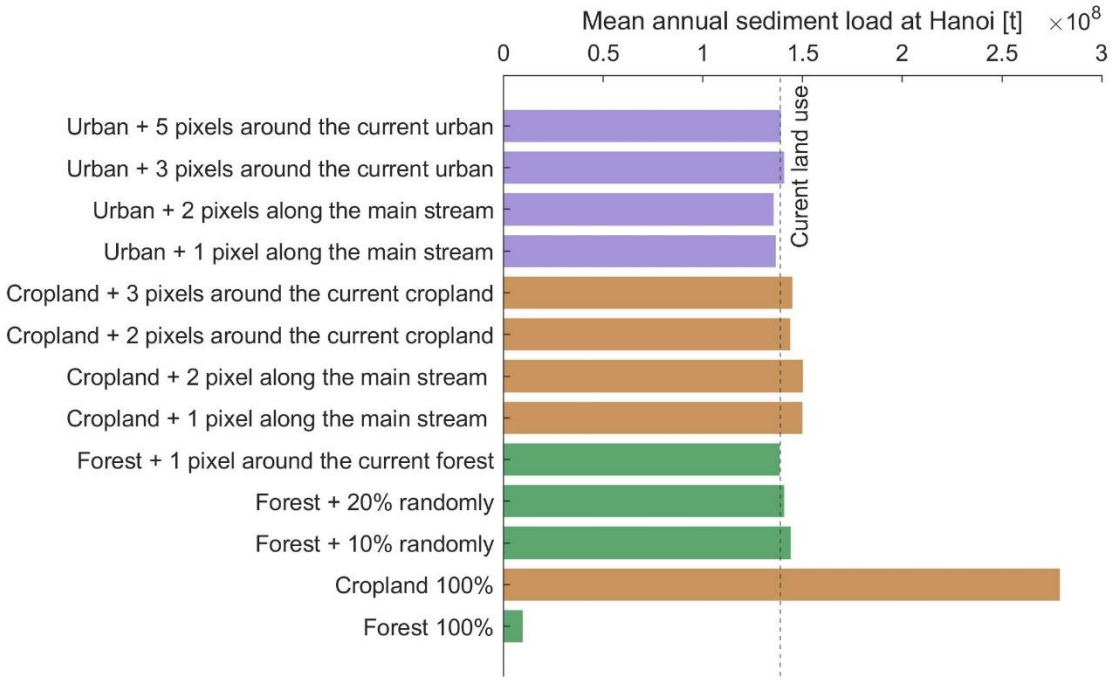

Figure 24 Mean annual sediment load at Hanoi station under different land use changes scenarios.

Changes in the annual sediment load at Hanoi station are not as evident as that in SSC as shown in Figure 24. In some scenarios, such as when the forest is increased by 20% (randomly or adjacent to the existing forest), the changes in the annual sediment load are less than 0.001% and difficult to be detected. Nevertheless, a consistent trait existing in SSC changes (Figure 20, 21 and 22) is also apparent in the annual sediment load changes. Across various scenarios, the simulated sediment load exhibits higher sensitivity to the location rather than the proportion of land use changes.

7.1.2 Intra-annual variability of sediment load

Figure 25 depicts the intra-annual fluctuations in sediment load across various scenarios, highlighting the model's different responses during the wet season (May to October) and the dry season (November to April). For example, when the forest is increased by 20% randomly (scenario A) or around the existing forest (scenario B), the mean monthly sediment load of scenario B is 3% lower than that of scenario A during the wet season. In contrast, during the dry season, the monthly mean sediment load of scenario B is 0.05% higher than scenario A. This phenomenon is also observed when only the proportion of land use is altered. For instance, when the cropland is expanded by 2 pixels (scenario C) and 3 pixels (scenario D) around the current

cropland, respectively, the mean monthly sediment load of scenario D surpasses that of scenario C by 0.3% in April. Conversely, in January, it is around 0.2% lower than scenario C.

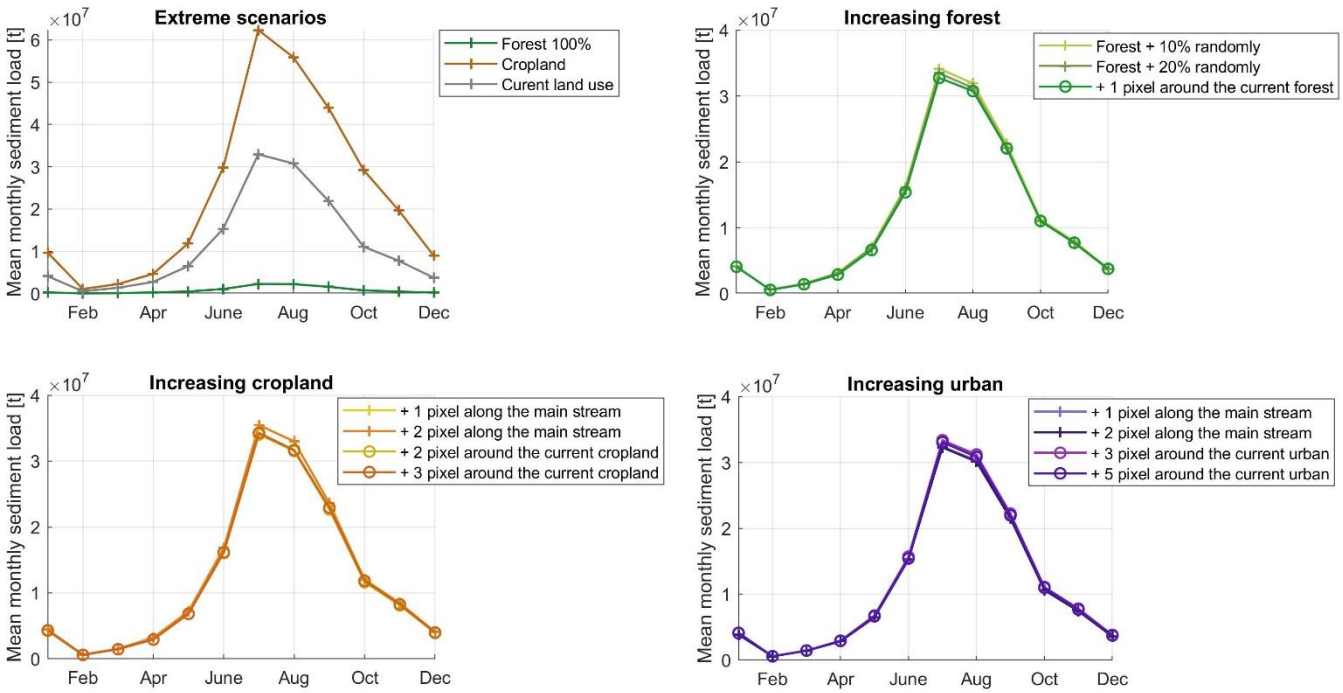

Figure 25 Mean monthly sediment load for different land use changes scenarios.

The above-mentioned analysis indicates that changes in land use can induce varying and even contradictory effects across different months. This could also be one of the reasons behind the absence of distinct variations in annual sediment load among different land use change scenarios (Figure 24), as the alterations in intra-annual sediment load variability tend to offset each other to some extent.

7.1.3 Spatial pattern of changes in erosion

In order to explore how the location of land use changes influences erosion processes, this section compared the simulated cumulative erosion mass under various land use change scenarios with that using the current land use.

When the entire basin is covered by forest, approximately 80% and 20% of pixels experiencing land use changes presents a decrease and increase in the cumulative erosion mass, respectively (Figure 26). Regarding pixels without land use changes, only about 30% of them show no changes in annual cumulative erosion. Meanwhile,

about 30% of these pixels displays an increase in erosion, while another 30% shows a decrease in erosion. This indicates that the erosion processes have also changed even for locations without land use changes.

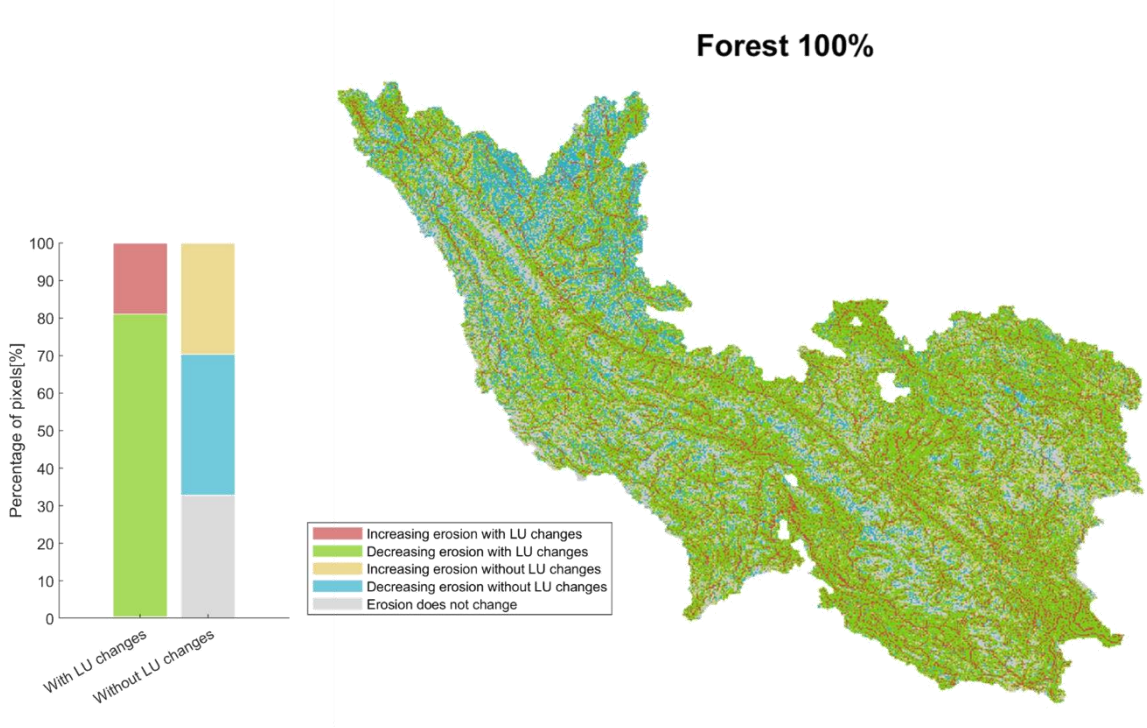

Figure 26 Changes in mean annual cumulative erosion mass (2005 - 2010) when the entire basin is covered with forest. LU = Land use.

For another extreme scenario that the entire basin is covered by cropland, about 80% of the pixels with land use changes presents an increasing annual cumulative erosion mass as expected (Figure 27), while the rest pixels present a decreasing annual cumulative erosion mass.

Regarding the cropland that has already existed (18.7 % of the entire basin), the cumulative erosion mass of about 70% of these areas is influenced by land use changes at other locations. Among these affected pixels, those experiencing a reduction in cumulative erosion mass are mainly concentrated in the delta region (Figure 27). This phenomenon could potentially be attributed to the decrease in the simulated streamflow at the delta (Figure 22), which probably results in a reduced sediment transport capacity in this region.

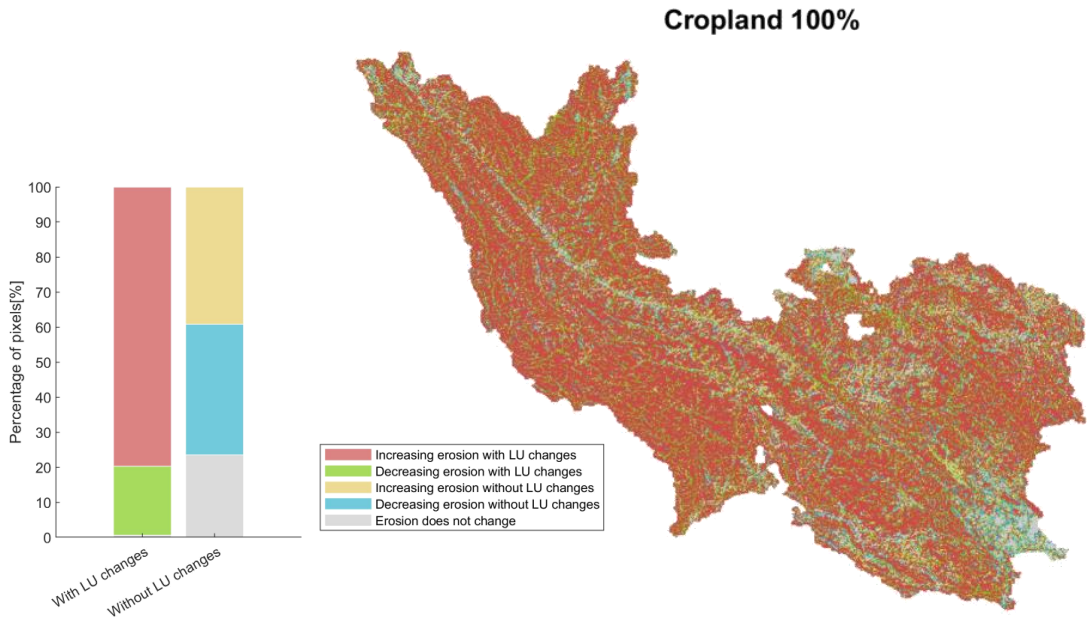

Figure 27 Changes in mean annual cumulative erosion mass (2005 - 2010) when the entire basin is covered by cropland. LU = Land use.

Figure 26 & 27 show the spatial variation of changes in mean annual cumulative erosion of extreme scenarios, where more than 70% of the basin has experienced land use changes. Therefore, it is expectable that the hydrology would be greatly altered and further influence the area without land use changes. However, in reality, land use changes mostly occur with a limited proportion. The following analysis demonstrates how does the erosion change in space when the basin experiences a small portion of land use change (< 10%).

Figure 28 shows the changes in the spatial pattern of cumulative erosion mass under two forest expansion scenarios. When the forest is increased by 20% randomly, only about 45% of pixels with land use changes present a changing annual cumulative erosion mass. About 50% of these pixels appear to have an increasing trend. For locations without land use changes, the cumulative erosion mass of about 40% of them (more than 30% of RRB) appears to be influenced by the increase of forest. The proportion of pixels that present an increasing and decreasing cumulative erosion mass are almost the same under this scenario, which could be one of the reasons for the unobvious changes in mean annual sediment load at Hanoi (Figure 24).

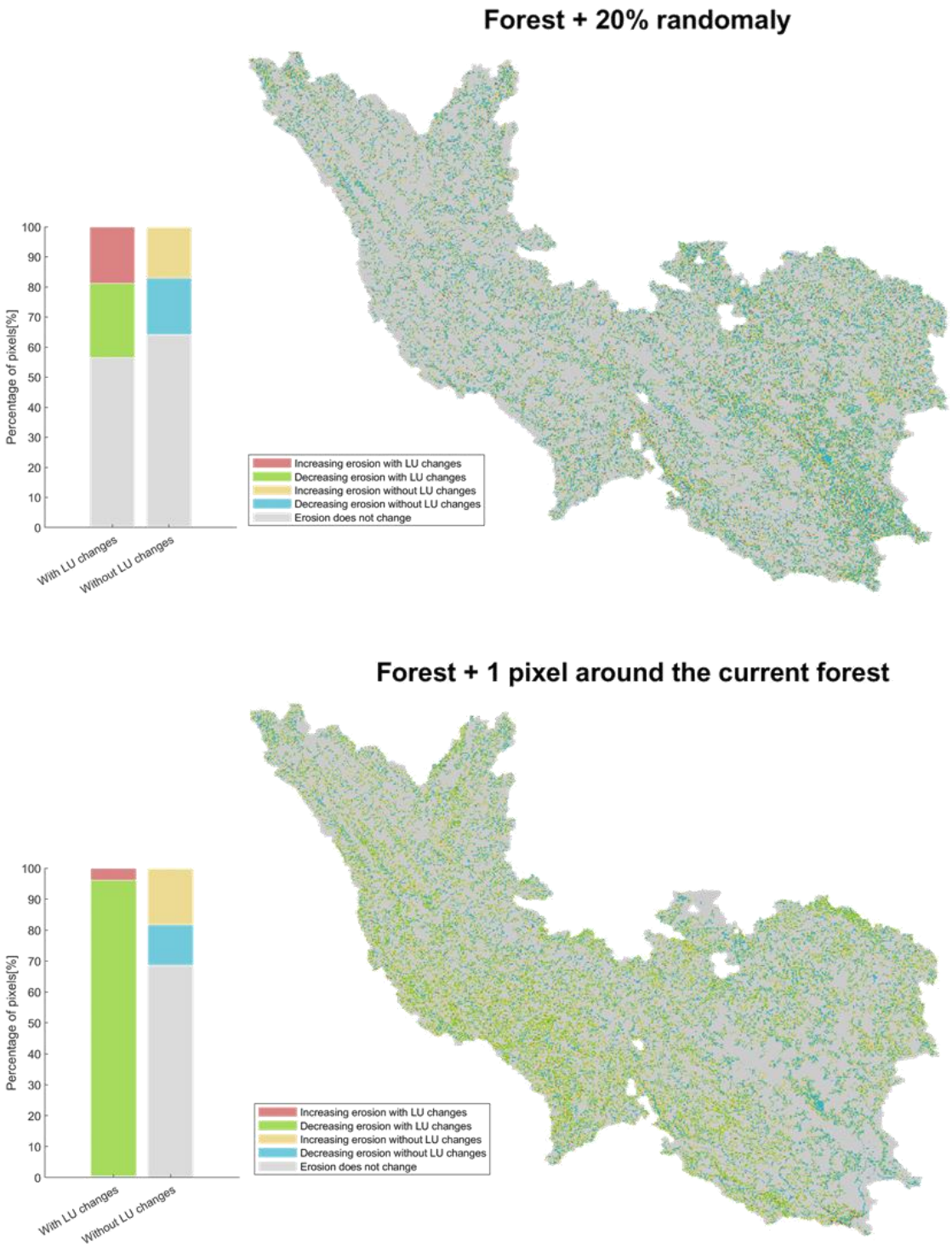

Figure 28 Changes in the mean annual cumulative erosion mass under different forest expansion scenarios. LU = Land use.

When the area of forest is expanded around the current forest, more than 90% of the pixels with land use changes present a decreasing cumulative erosion (Figure 28). Nevertheless, for the locations without land use changes (about 90% of RRB), the proportion of pixels with an increasing cumulative erosion mass is larger than those with a decreasing cumulative erosion mass. The opposite responses for locations with

and without land use changes compensate the changes in cumulative erosion mass at different locations, which demonstrates that the simulated mean annual sediment load at Hanoi does not change when the forest is increased by 1 pixel around the current forest (Figure 24).

Figure 29 shows the alterations in the spatial distribution of cumulative erosion mass for two cropland expansion scenarios. For both scenarios, more than 85% of pixels with land use changes present an increasing cumulative erosion mass. However, for locations without land use changes, a larger area (about 30% of the entire basin) would be impacted when the cropland expands around the current cropland. When the cropland is increased along the main stream, the increased eroded sediment could be directly transported to the stream and the influenced area is relative limited. This results in a direct increasing sediment supply to the stream (Figure 24). In comparation, when the cropland expands around the current cropland, the induced decreasing erosion of downstream pixels due to decreasing streamflow (Figure 22) compensates the increasing erosion of pixels that experienced land use changes. This explains that the annual sediment load at Hanoi is higher when the new cropland is concentrated along the main stream (Figure 24).

The impact of urban expansion on the annual cumulative erosion mass is relatively limited in space compared to other scenarios (Figure 30). Less than 5% of the pixels without land use change is impacted by the increasing area of urban. Regarding locations with land use changes, more than 80% of them present a decreasing cumulative erosion mass due to the lack of available sediment to be transported to the stream. However, when the urban expands around the current urban, the increasing erosion for pixels without land use changes could compensate the decreasing erosion mass of the new urban. When the eroded sediment is delivered to the main stream, it is possible that the sediment load is even higher than that of the current land use. In contrary, when the urban land is increased along the main stream, the reduced erosion mass could directly decrease the sediment transport into the stream and further reduce the sediment load.

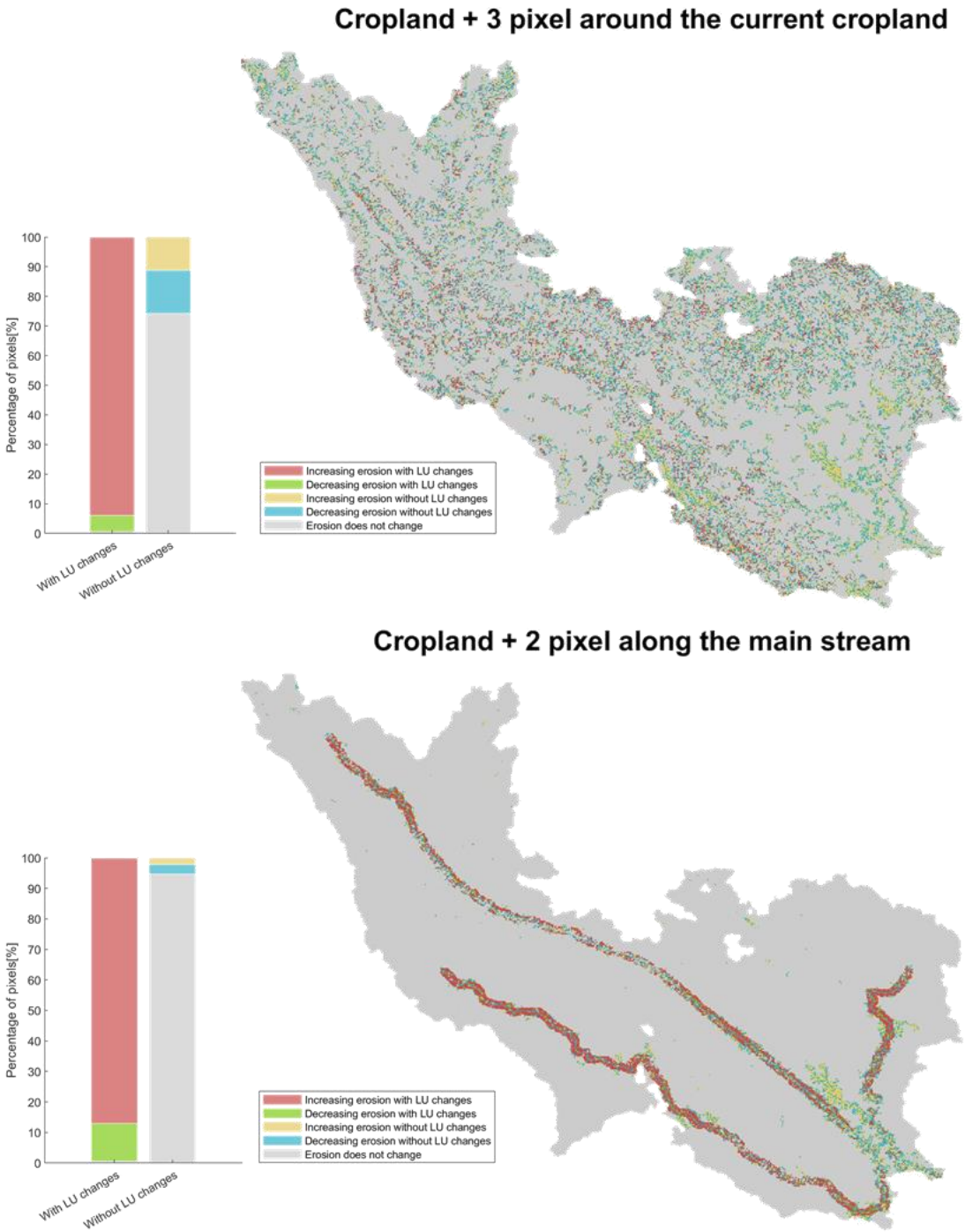

Figure 29 Changes in the mean annual cumulative erosion mass under different cropland expansion scenarios. LU = Land use.

The above-mentioned analysis further illustrates that different locations of land use changes could influence the spatial pattern of the basin-scale erosion to different extents. Land use changes at one cell can influence not only its own erosion dynamics, but also the erosion of neighboring cells and even cells that are situated far from the land use changes. These phenomena reveal the complicated interactions among land

use, soil erosion, sediment transport, and hydrology. They underscore the significance of considering not only the area but also the specific locations of land use changes when evaluating the resultant effects on sediment transportation. It also highlights the need of a spatially distributed analysis or modelling.

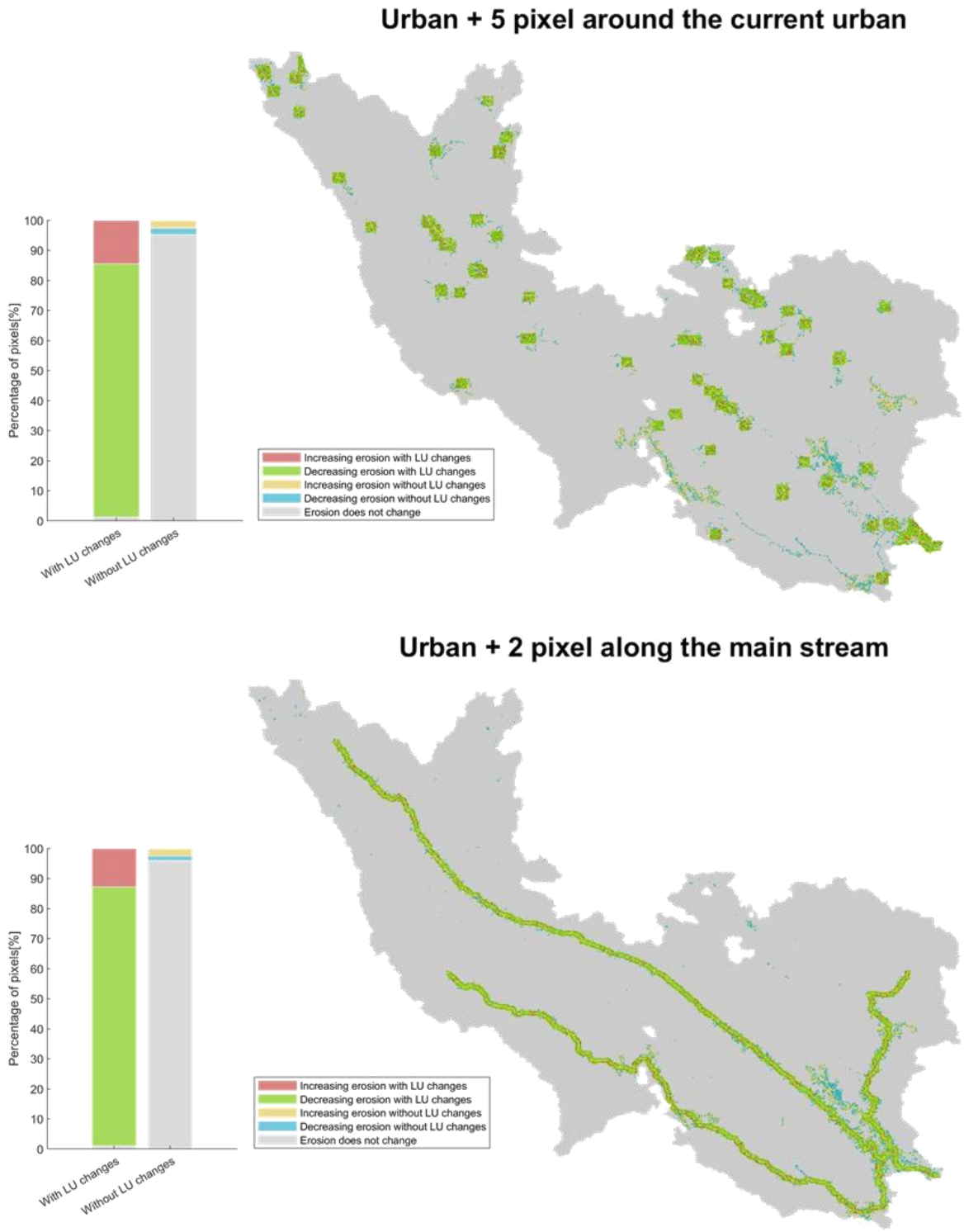

Figure 30 Changes in the mean annual cumulative erosion mass under different urban expansion scenarios. LU = Land use.

7.2 Reservoir operations

7.2.1 Trapping effect of the reservoir

The mean annual trapping efficiency (TE) of the four main reservoirs within RRB is shown in Table 9. All four reservoirs have a TE that is higher than 85%. Son La reservoir (locating at the main stream of Da river) has the largest storage (40.02 km^3) and the highest TE of 95.04%. Hoa Binh reservoir is also located at the main stream of Da river with a TE of 88%. Thac Ba and Tuyen Quang reservoirs are located along the Lo River subbasin (Figure 2), and have a TE of 94.40% and 87.38%, respectively.

Table 9 Annul mean trapping efficiency (TE) of the four main reservoirs within red river basin.

Reservoir	Water level (m)	Storage (km^3)	Release (km^3/year)	Inflow (km^3/year)	Residence Time (Year)	TE (Original)	TE
Son La	203.78	40.02	43.00	44.92	0.93	94.82%	95.04%
Hoa Binh	106.76	7.77	53.43	58.38	0.15	86.89%	88.00%
Thac Ba	53.40	1.82	3.43	4.21	0.53	93.14%	94.40%
Tuyen Quang	110.52	1.53	11.30	12.26	0.14	86.42%	87.48%

*The trapping efficiency was calculated using the observed data from 2011 to 2019.

Figure 31 shows the intra-annual variability of the trapping efficiency (TE) of the four main reservoirs within the Red River Basin. The monthly TE of the four reservoirs all range from about 75% to 95%. The simulated TE presents the lowest value in the wet season. This corresponds to the low residence time during this period, when the streamflow is the highest in a year. The seasonal variation of the observed TE is different from the simulated pattern, since the reservoir operation in the reality do not always follow the previously designed “best” operation policy. Son La and Hoa Binh stations show the lowest observed TE in spring, and the lowest simulated TE in summer. The simulated TE of Thac Ba and Tuyen Quang stations show the lowest value in February, and start to increase in summer. These two stations both present the highest observed and simulated TE in November and December.

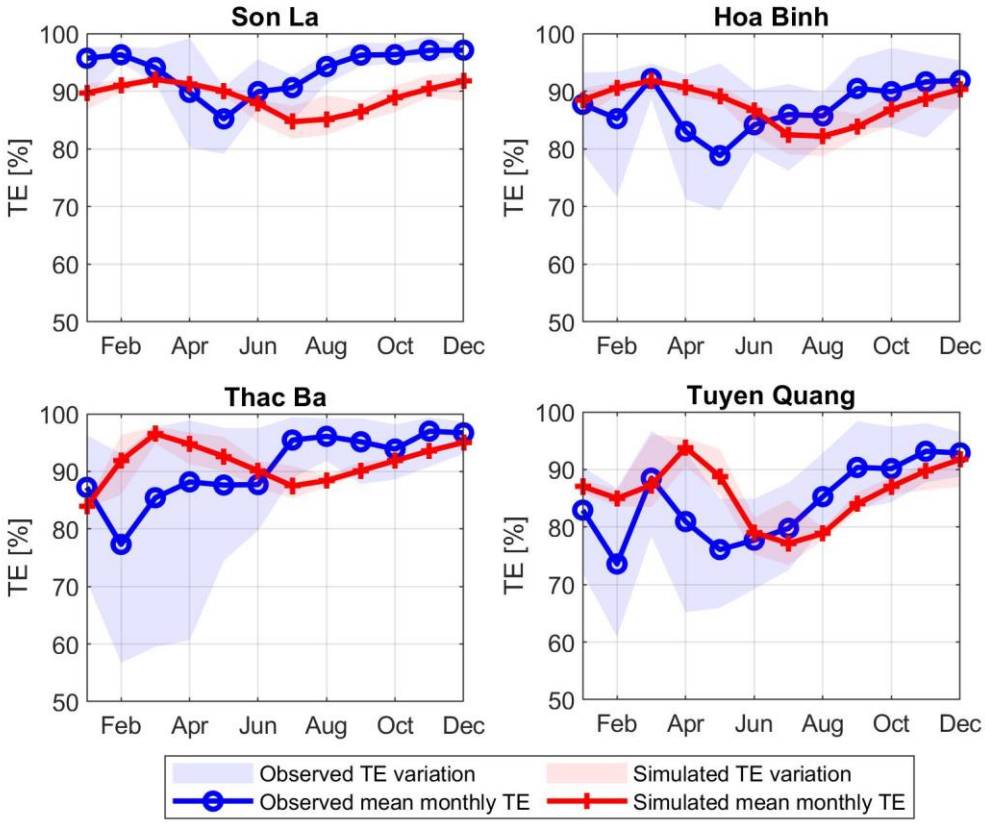

Figure 31 Monthly mean observed and simulated trapping efficiency (TE) for the four main reservoirs.

Figure 32 shows the simulated streamflow at four stations that are located downstream of the four main reservoirs. In scenarios involving reservoir operations, the simulated discharge shows lower peak flow and higher low flow compared to that without reservoirs. Nevertheless, the simulated streamflow does not present large differences in the intra-annual variation under the reservoir operation scenarios.

In the contrary, the simulated SSC presents an obvious decrease under the influence of reservoir operation (Figure 33), especially for Ta Bu and Hoa Binh stations that are located downstream of the largest reservoir, Son La. At Hoa Binh station, the simulated SSC under reservoir operation scenario is much more comparable to the observed values compared to that without reservoir. However, for Chiem Hoa and Vu Quang stations, the simulated SSC under reservoir operation scenario is still higher than the observed values. This corresponds to the overestimation of SSC at the northeastern of the basin (e.g., Ham Yen station in Figure 13), which indicates that the sediment transport in this region potentially experiences influence from other factors that are not included in this model.

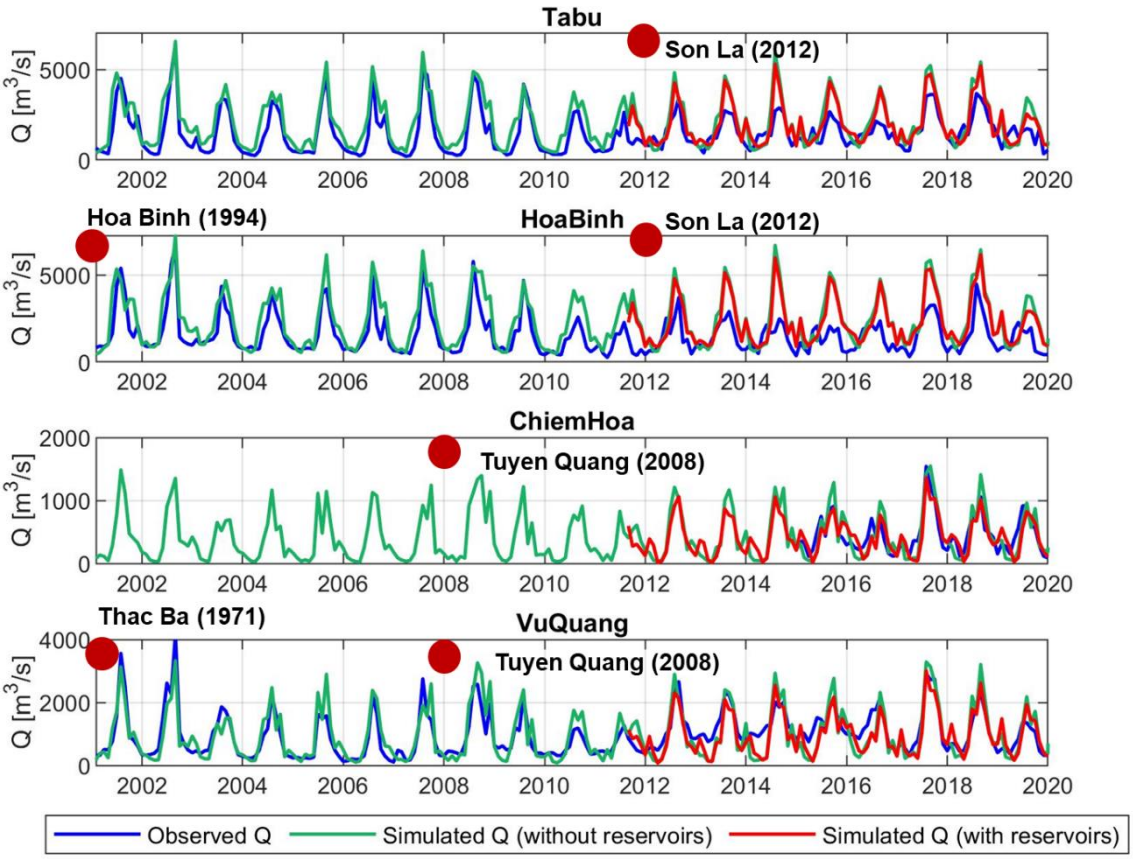

Figure 32 Simulated monthly mean streamflow (Q) under the reservoir operation scenario for four stations locating downstream of four main reservoirs.

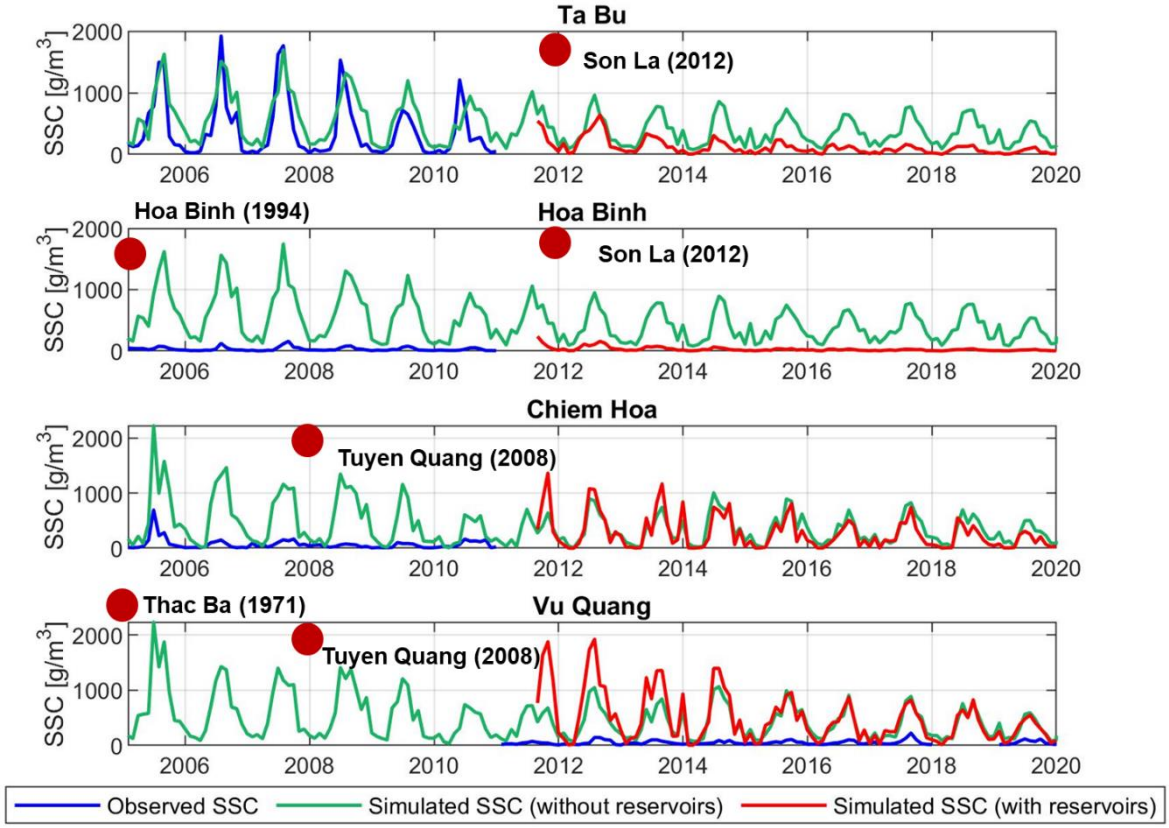

Figure 33 Simulated monthly mean suspended sediment concentration (SSC) under the reservoir operation scenario for four stations locating downstream of the four main reservoirs.

7.2.2 Influence on the sediment load at Hanoi

Figure 34 shows the impact of reservoir operation on the simulated sediment load at Hanoi. The simulated sediment load experiences a reduction ranging from 0.25 to 1 × 10^8 t per year (about 25% - 50%) when the model incorporate the reservoir operations. Such a decrease is higher than that under the land use changes scenarios (Figure 24), and is comparable to the decrease of observed SSC near the outlet (Figure 10). When the trapping efficiency (TE) of reservoirs is decreased by 10% or 20%, the annual sediment load shows a corresponding increase of around 10% or 20%. However, the simulated sediment load under reservoir operation scenarios is still higher than observed values. This indicates that the sediment load would be probably influenced by other factors that are not included in the model by far.

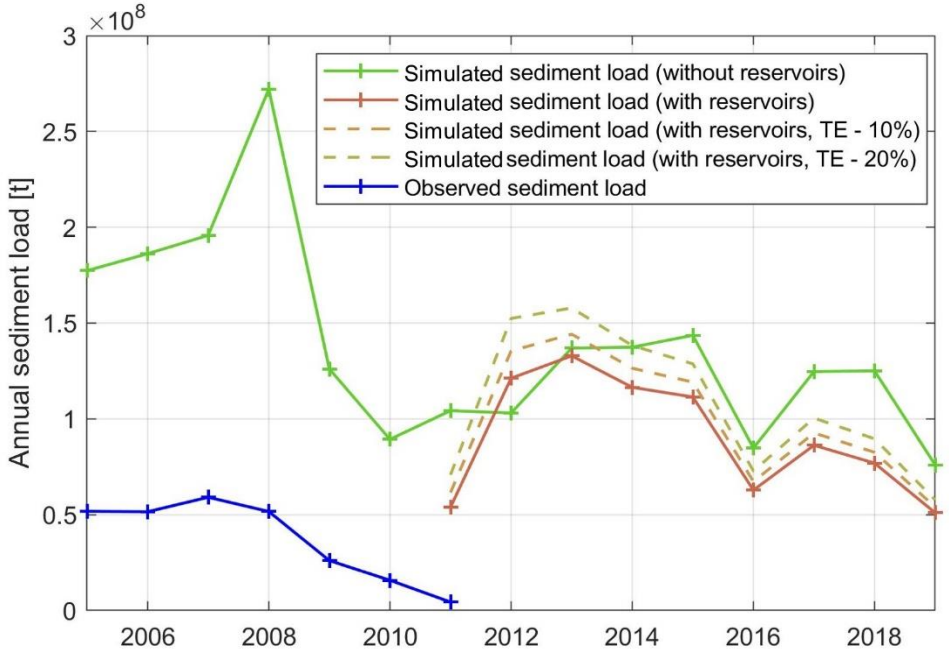

Figure 34 Annual sediment load at Hanoi from 2005 to 2019. TE = Trapping efficiency.

The intra-annual variability of the sediment load is also influenced by reservoir operations (Figure 35). Firstly, the sediment load variation of each month has decreased under the reservoir operation scenario. In the first plot of Figure 35, the sediment load in August ranges from approximately 0.2 to 1.5 × 10^8 t, whereas under reservoir operation scenario, this range narrows to about 0.1 to 0.3 × 10^8 t.

The sediment load also shows a general decrease in scenarios involving reservoir operations, especially during the wet season. For example, in August, the monthly sediment load experiences a reduction from approximately 3.5 × 10^8 t to about 2.2 × 10^8 t (about 40%) at Hanoi. Furthermore, reservoir operations also exert an influence on the timing of peak sediment load. Formerly occurring in July without reservoirs, the peak sediment load has shifted to August under the reservoir operation scenario.

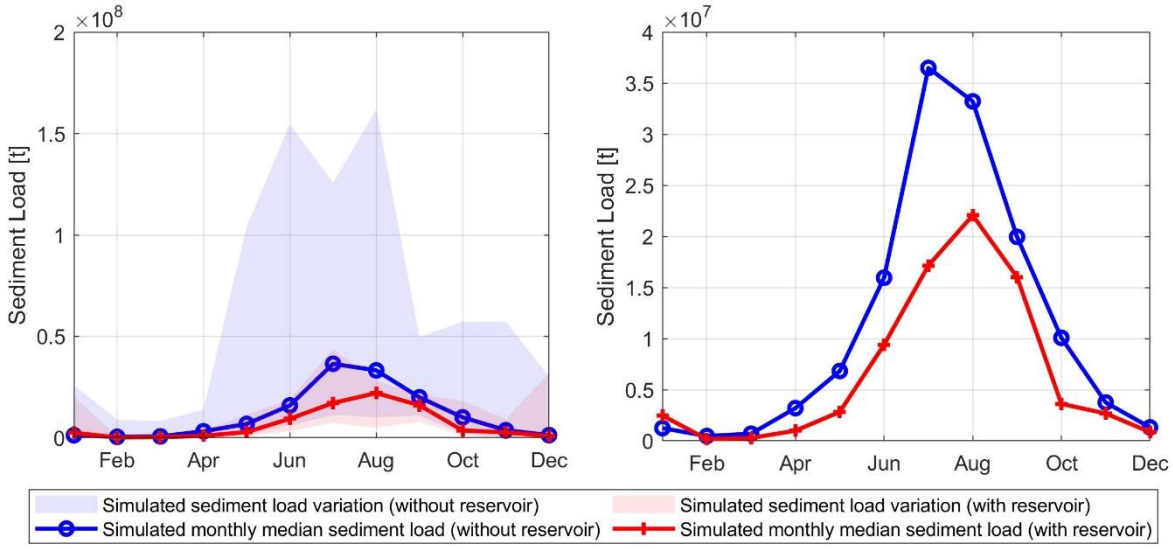

Figure 35 Simulated monthly sediment load at Hanoi (2005 - 2019) under scenarios with and without reservoir.

8. Future changes in the sediment regime

8.1 Future land use changes scenarios

The simulated cumulative erosion mass decrease for all the four land use changes scenarios driven by the different SSPs (Figure 36), compared to the current value (Figure 18). The decreasing erosion is particularly evident in the western and central regions of the basin, where the mosaic cropland and vegetation are expected to transform to grassland and forest in 2050 (Figure 5 & 7).

The spatial distribution of cumulative erosion mass exhibits a similar pattern across the various scenarios. The highest annual cumulative erosion is generally located in the southwestern and northeastern regions. Among the depicted scenarios in Figure 36, scenario SSP126 shows the largest reduction in cumulative erosion mass. The averaged reduction is 2.62×10^8 t/year, which is higher than 50% of the current annual cumulative erosion mass. Scenario SSP245 shows the smallest reduction in cumulative erosion mass with the value of 2.28×10^8 t. Scenarios SSP370 and SSP585 present a reduction of cumulative erosion mass of 2.55 and 2.43×10^{11} t, respectively.

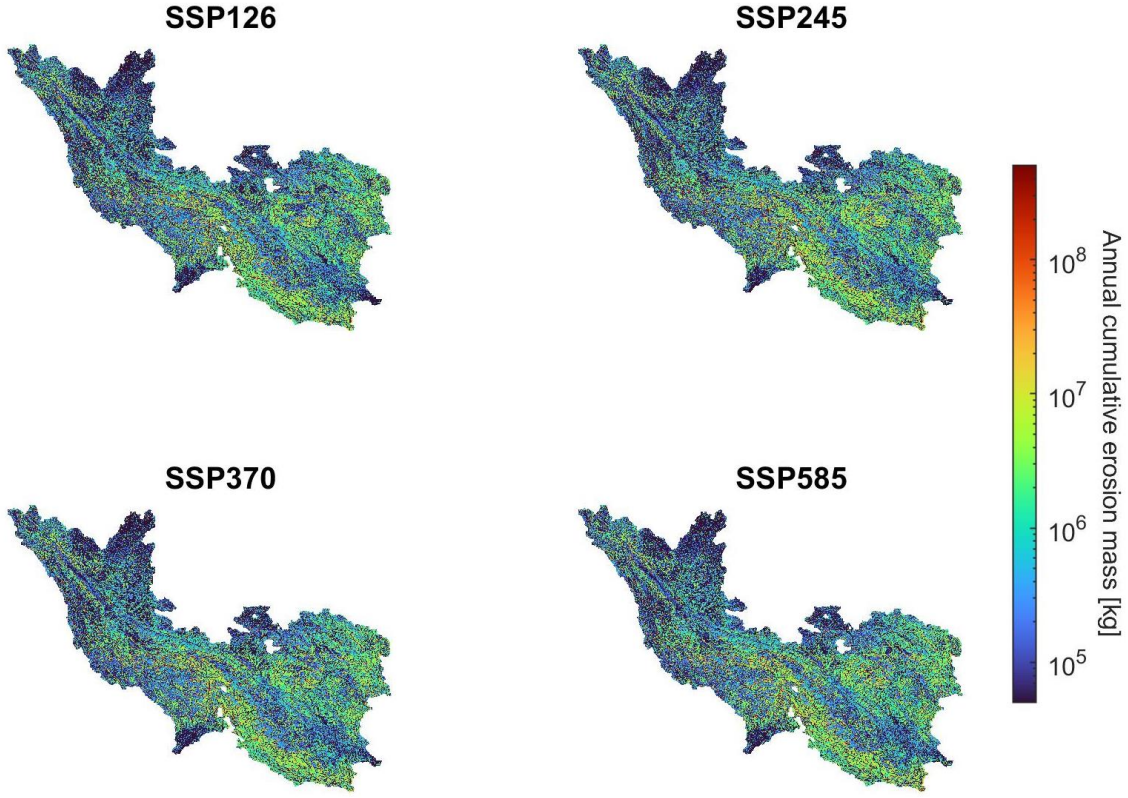

Figure 36 Annual cumulative erosion mass under different SSP scenarios. The input meteorological data was from 2005 to 2010.

The mean annual sediment load at Hanoi present lower values in comparison to the present land use configuration for all the four SSP scenarios. The simulated sediment load in the SSP126 scenario exhibits the lowest annual sediment load among the four scenarios, followed by the SSP370, SSP585, and SSP245 scenarios. This ranking corresponds to the simulated cumulative erosion mass that is shown in Figure 37.

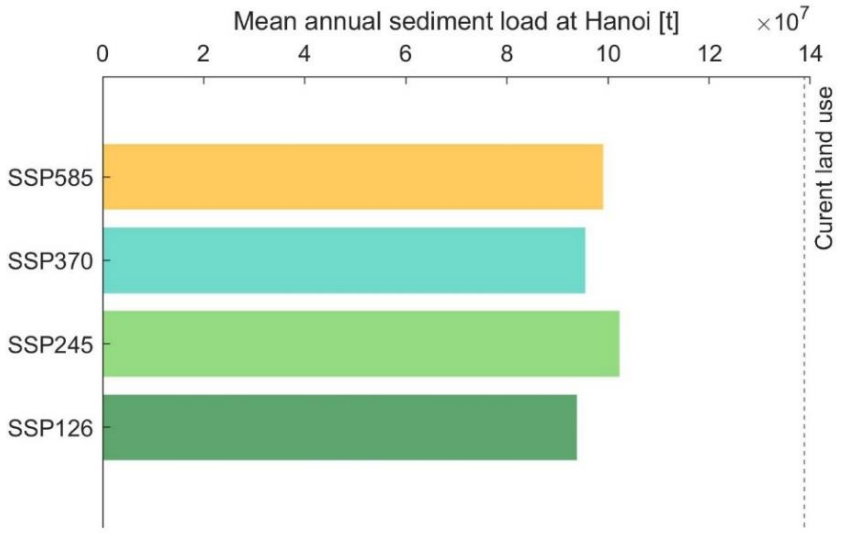

Figure 37 Simulated mean annual sediment load (2005 - 2019) at Hanoi using the land use maps of 2050 under different SSP scenarios.

It is interesting to note that while the annual sediment load reduction at Hanoi in 2050 is generally less than 30% across all scenarios, the decline in cumulative erosion mass exceeds 50% compared to the present state. This indicates that the relationship between cumulative erosion and the resulting sediment load can be influenced by complex interactions and processes within the basin's hydrological system. The decrease in erosion does not always result in the same amount of reduction in the sediment load.

Figure 38 shows the simulated monthly suspended sediment load (SSL) at Hanoi using land use maps of 2050 under different SSP scenarios. In comparison to the simulated results using the current land use map, both the median monthly sediment load and its variability exhibit a reduction in the future scenario, particularly during the wet season. The intra-annual variations for the four scenarios are similar to each other. The simulated sediment load under SSP126 scenario presents the smallest peak sediment

load, which corresponds to the previous results about the annual cumulative erosion mass (Figure 36) and the mean annual suspended sediment load (Figure 37).

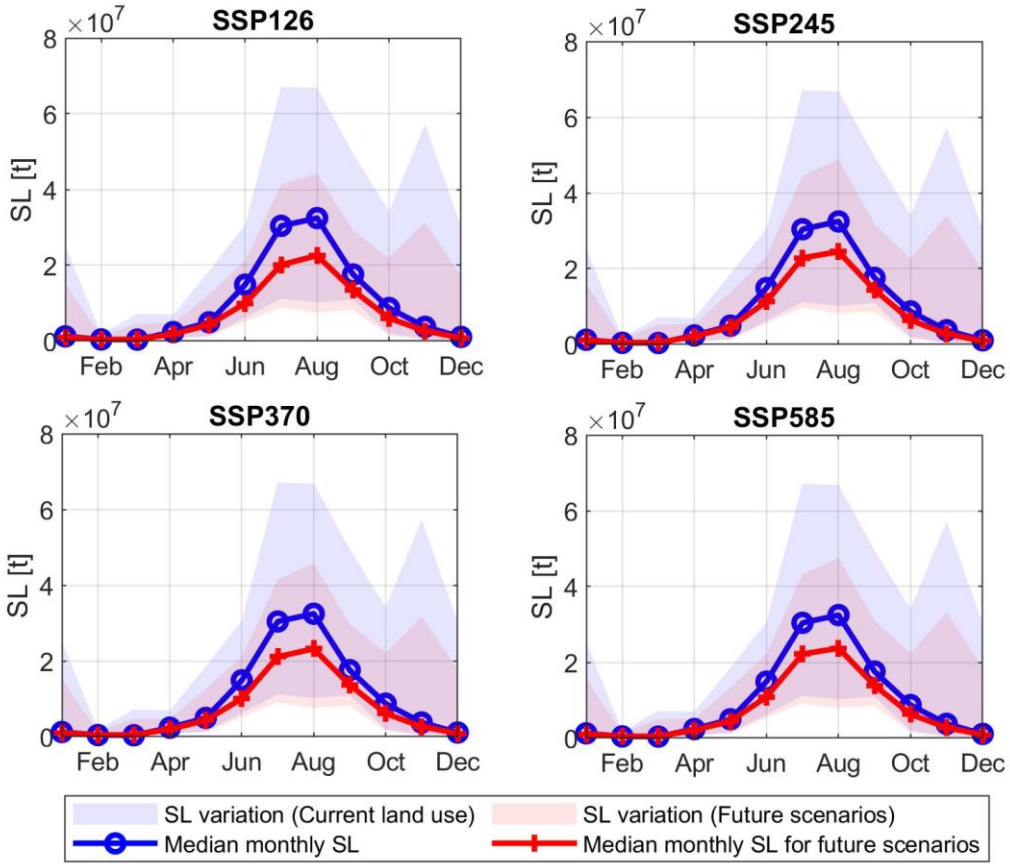

Figure 38 Simulated monthly suspended sediment load (SL) at Hanoi using future land use maps under different SSP scenarios.

8.2 Future reservoir operation policies

The influences of different reservoir operations scenarios are depicted in Figure 39. Hanoi station experiences a reduction in mean annual sediment load from approximately 14 × 10^7 t to 9 × 10^7 t under the influence of reservoir operations. Under the natural river system, the Da River is supposed to serve as a primary source of sediment for the basin, with an annual sediment load exceeding 6 × 10^7 t. However, the sediment contribution from the Da River decreases to around 0.2 × 10^7 t (> 95%) due to the presence of two large reservoirs: Son La and Hoa Binh. Conversely, the Thao River, which initially exhibited the lowest sediment load among the three main tributaries, transforms into the main sediment source of the basin under reservoir

operation scenarios.

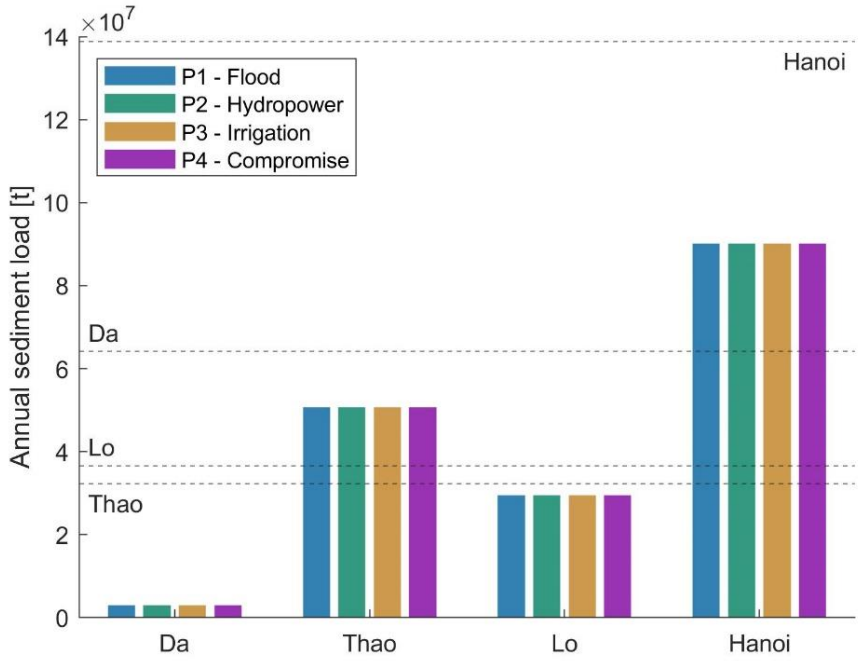

Figure 39 Mean annual sediment load (2011 - 2019) under different reservoir operation scenarios. Subbasin Da, Thao, and Lo is represented by the simulation at Hoa Binh, Yen Bai and Vu Quang station, respectively.

Different reservoir operation policies do not appear to exert different influences on the annual sediment load, as expected. The simulated sediment load for stations in Figure 39 remain nearly consistent across different reservoir operation policies. The similar phenomenon is also observed in the simulated monthly sediment load as shown in Figure 40. The simulated median monthly sediment load and the variability in the monthly sediment load remain consistent across different reservoir operation scenarios. For all operation policies in Figure 40, the decrease of the monthly sediment load is more evident than that under the future land use changes scenarios (Figure 38), though about 40% cropland is anticipated to transform to forest grassland in 2050. This indicates that the presence of reservoirs has a more significant influence on sediment load rather than different operation policies.

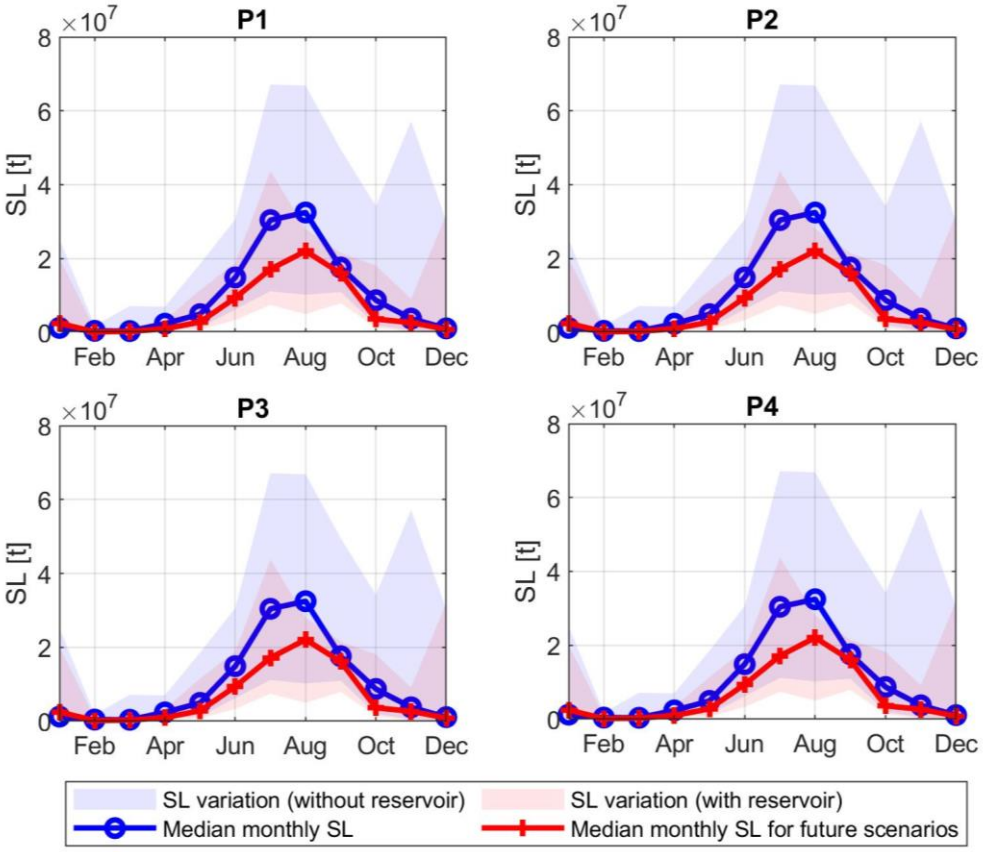

Figure 40 The monthly sediment load at Hanoi (2011 - 2019) under different reservoir operation scenarios.

9. Discussion

9.1 Impacts of land use changes

The scenario analysis in section 7.1 shows the that land use changes could influence both the erosion spatial pattern and the intra-annual variation of the sediment load. These make the potential impacts of land use changes of great uncertainty, though the sediment load does not present a tremendous change under different land use changes scenarios.

Firstly, land use changes alter the hydrology and soil erodibility simultaneously. The changes in streamflow and soil erodibility always present the opposing directions (Figure 21 & 22). Since sediment transport is related to both overland flow and soil erodibility, the combined impact of changing hydrology and soil erodibility could change the temporal and spatial pattern of the previous sediment transport. For example, the increase of cropland could result in an increased sediment load in summer due to the enhanced soil erodibility, while a decreased sediment load in winter due to the reduced streamflow (Figure 25). Besides, land use changes at one cell also influence the erosion of neighboring cells. For example, when forest is expanded around the current forest (Figure 28), the erosion of the neighboring cells is increased due to an increasing streamflow. Though the annual sediment load does not have an evident change (Figure 24), the sediment transport pattern in space is not negligible (Figure 28).

Concerning the sediment regime, the model reveals that the sediment load at Hanoi is more sensitive to the location instead of the proportion of land use changes within the basin. For example, when the forest is increased randomly in space, the annual sediment load even increases at Hanoi with only less than 50% of the new forest presenting a decreasing erosion. While when the forest is expanded around the current forest, more than 95% of new forest shows a decreasing cumulative erosion mass. Ouyang et al. (2010) also found that the sediment transportation is more related to the patch edge of a certain type of land use instead of the patch area. The increase of patch edge could potentially increase the sediment transportation from the edge cells. This indicates that when the basin experiences degradation, for instance under

scenario SSP245 in Figure 7, the increasing patch edge could exaggerate the increase in erosion and sediment transport (Figure 37).

The above-mentioned possible consequences of land use bring a high uncertainty for evaluating the impact of land use changes on sediment transport. Furthermore, the change in sediment regime could alter the river and costal landscape. Since the cropland of the RRB is mainly located in the delta region and near the river, shifts in the river network would bring high uncertainty to the cropping and irrigation activities of these regions. Therefore, the change in the spatial pattern of sediment transport is supposed to be considered in land use and water resource management work.

9.2 Impacts of reservoir constructions

In comparison to the effects of land use changes, the sediment-trapping effect of reservoirs exerts a more explicit and direct impact on sediment load at Hanoi. Though the changes in streamflow due to reservoir operations is limited (Figure 32), the reduction of the sediment load is more than 50% for large reservoir (e.g., Son La station in Figure 33). These findings resonate with the research conducted by Li et al. in 2020, which investigated sediment load and discharge across basins globally. Typically, reservoirs lead to substantial reductions in sediment load at the outlet of the basin, while discharge rates generally remain stable.

The scenarios analysis about reservoir operations could explain the observed reduction of SSC from 2000 to 2010, when the reservoirs within the RRB were intensively constructed. Also, it is interesting to mention that though many reservoirs were constructed along the Da River and Lo River, large reservoir is not found at Thao River within Vietnamese territory. One possible reason for that could be that about a half of the Thao River is located in Chinese territory, where two large reservoirs have already been constructed since 2005 (Figure 2). The presence of these two reservoirs has already resulted in a decrease of about 50% of SSC at Yen Bai (Figure 6 & 10). The construction of additional reservoirs in Thao River system would exert a more substantial downstream impact on sediment transportation, and also of great uncertainty due to the unknown upstream streamflow and sediment transport.

As expected, different reservoir operation policies do not exert distinct impact on the reduction of sediment load (Figure 39). The reservoir itself and its storage volume is more evident influencing factors for the sediment transportation. For example, the largest reduction of simulated sediment load is observed at Hoa Binh station (Figure 39), located downstream of the two largest reservoirs in Vietnam (Table 1), Son La and Hoa Binh. Thinh et al. (2018) also found that the Son La reservoir results in a 98% decrease of sediment load of Da river cascade system. Such a reduction of sediment transport could result in river bed degradation of the downstream, which would probably change the channel network and decrease the water level of the river. These changes could further impact the extraction of the water and bring uncertainties for the downstream water supply. Since sediment load does no present large differences under various reservoir operation policies, other measures (e.g., artificial sediment flushing at the reservoir bottom) are probably required to take to maintain the downstream geomorphology and mitigate the impact of reservoirs.

The case of the RRB serves as a valuable reference for comprehending the influence of reservoirs on the downstream regions, particularly for transboundary basins. Once the reservoir is commissioned, its impact on the downstream sediment transportation is immediate and irreversible, regardless of the reservoir operation policies. Therefore, the construction of reservoirs and the cooperated water resource management deserve more considerations.

9.3 Challenges and limitations of the current model

The model in this thesis successfully reconstructed the SSC, Q and sediment load time series, and present an advantage in integrating human activities into the natural hydrology processes. However, there are also some challenges and limitations in the modelling processes that need to be mentioned.

The first one is the uncertainty from the data. Though the observed daily Q and SSC data at multiple stations are available for past three decades (Table 2), the information about the measurement equipment replacement, possible measurement errors remain unknown. Therefore, this study chose to trust the observed data in the modelling

process regardless the measurement uncertainties always exist in the reality.

Besides the reliability of the data, the temporal scale of data may also influence describing the sediment transport processes. For example, though the annual sediment load in high SSC events was well captured by the model (Figure 14), the SSC-Q-P relationship for high SSC events that is depicted by the model is different from the observed data (Figure 15). This is probably because that the heavy rainfall and the consequent increase in Q and SSC always happen in the sub-daily scale. Therefore, the daily-scale data and simulation are too coarse to accurately replicate such sub-daily processes. Nevertheless, the model is capable to capture the SSC, Q and sediment variations on monthly and annual scale, while simultaneously maintaining a satisfactory computational efficiency (about 1 hour for a simulating the sediment regime for 1 year).

Due to the limitation in available data and computation power, this model does not manage to elaborate all processes that are related to sediment transport. For example, when assessing the impact of land use changes on sediment transport, this model does not consider the changes in the subsurface processes, e.g., the changes in infiltration rate, soil properties, etc. However, in natural environments, land use changes modify soil properties and structure through factors such as the fallen leaves and alterations in root systems, thereby influencing the subsurface hydrological and sediment transport processes. Therefore, the impacts of land use changes on sediment dynamics could potentially be more pronounced than the simulated results in this thesis.

Regarding erosion processes, the model primarily focuses on overland flow, which constitutes the primary sediment source for the RRB. In reality, sediment detachment can occur through sediment pickup from landslides by hillslope overland flow, from the toe of landslides via river flow, and from incised areas (Battista et al., 2020). However, data regarding past landslides in the RRB is not available, and predicting the trend of future landslide events with various human activities is also challenging. Therefore, this thesis centers on the overland flow erosion process and its potential alterations

under diverse land use change scenarios.

As for the human activities that could influence the sediment regime of the basin, it is worth to note that not all influencing factor are included in the modelling. For example, when considering the land use changes, factors like alterations in crop type and intensity are not fully elaborated. Also, the reservoir operation scenarios did not incorporate the upstream reservoirs of neighboring countries, e.g., Nan Sha and Ma Du Shan reservoirs that are located in China (Table 1, Figure 2). These factors might lead to the overestimation of sediment load at Hanoi under reservoir operations scenarios (Figure 34). Beside the land use changes and reservoir operations, other factors could also influence the sediment regime of the, e.g., sediment mining and irrigation. These human activities also contribute to the complexity of the reconstruction of the SSC time series and make this task more challenging.

10. Conclusion

The observed streamflow (Q) and suspended sediment concentration (SSC) show a significant decreasing trend in the red river basin (RRB) in past two decades (2000 - 2020). The timing of the significant changing points for both Q and SSC corresponds to the reservoir construction period (2005 - 2010) in the RRB. The decrease of Q and SSC is particularly evident in the wet season. However, the significant decreasing Q and SSC did not always occur at the same time. The decrease in SSC (over 50%) is more evident than that of Q (about 20 to 40%).

For the station that is generally under the natural condition, the model well reproduced its SSC variation with a Nash-Sutcliffe Efficiency (NSE) of 0.65. The model is not sensitivity to the changes in K-factor calculation method and calibrated parameter that are related to soil erodibility, or the input particle size of sediment. The model proficiently captured SSC values and sediment load during high SSC events. According to the observed data, over 50% of the annual sediment load could be attributed to the large amount of sediment load in less 30 days when the daily SSC is extremely high (>95th percentile). The model's capacity in simulating high SSC events ensured its accuracy in evaluating the annual sediment load. However, the SSC-Q-P relationships are different for observed and simulated data. The simulated data presents a high consistency in SSC, Q, and P, while such a relationship among these three variables was not found for the observed data.

Land use changes could exert opposing impacts on the discharge and the SSC simultaneously, although changes in SSC tend to be more pronounced than changes in discharge. Since the sediment load is determined by both SSC and discharge, the comprehensive impacts of land use changes on sediment load are of great uncertainty. One reason for that is the inconsistency of alternations in different seasons. For example, the cropland expansion could result in increasing sediment load in wet seasons and decreasing sediment load in dry seasons. Another reason is the changes in the soil erosion pattern. Land use change at one cell can not only influence its own erosion, but also other locations due to the various interactions and processes in

hydrology and sediment transport within the basin. The locations instead of proportion of land use changes present a stronger impact on the simulated sediment load. This indicates the importance of considering the location of land use changes in reconstructing the interaction between human activities and the natural system, which also reflects the advantage of a physically-based distributed model.

The impact of reservoirs on the sediment load is more evident than that of land use changes. For the four main reservoir within the RRB, their annual mean trapping efficiencies are all about 90%. With the presence of these four reservoirs, the reduction of annual sediment load at Hanoi could reach 25% to 50%. The most evident reduction in sediment is found in summer when the sediment load is the highest in a year, though the trapping efficiency in this season is the lowest due to the flood protection requirement. Besides the amount of sediment load, reservoir operations could also shift the timing of the peak sediment load in a year.

In future scenarios, the proportion of cropland is expected to decrease from about 18 % to 11%. The transition from cropland to forest or grassland would result in about 50% of reduction (2.5×10^8 t) in the mean annual cumulative erosion mass, and about 30% of reduction (2.0×10^7 t) in the mean annual sediment load at Hanoi. Scenario SSP126 (green pathway) and SSP245 (land degradation) presents the largest and the smallest reduction of sediment load in the future, respectively. Regarding different future reservoir operation policies, the sediment load does not present evident difference across different reservoir operation scenarios. The presence of reservoirs themselves (particularly for those with large storage volume like Son La) will greatly reduce the sediment load and shift the sediment delivery from tributes to the delta region, regardless the operating policy that would be chosen in the future.

References

Amsler, M. L., & Drago, E. C. (2009). A review of the suspended sediment budget at the confluence of the Parana and Paraguay Rivers. Hydrological Processes, 23(22), 3230-3235. doi:10.1002/hyp.7390

Arnold, J. G., Srinivasan, R., Muttiah, R. S., & Williams, J. R. (1998). Large area hydrologic modelling and assessment: Part I. Model development. Journal of the American Water Resources Association, 34(1), 73-89.

Bakker, M. M., Govers, G., van Doom, A., Quetier, F., Chouvardas, D., & Rounsevell, M. (2008). The response of soil erosion and sediment export to land-use change in four areas of Europe: The importance of landscape pattern. Geomorphology, 98(3-4), 213-226. doi:10.1016/j.geomorph.2006.12.027

Battista, G., Schlunegger, F., Burlando, P., & Molnar, P. (2020). Modelling localized sources of sediment in mountain catchments for provenance studies. Earth Surface Processes and Landforms, 45(14), 3475-3487. doi:10.1002/esp.4979

Bennett, J. P. and Nordin, C. F. (1977). Simulation of sediment transport and armouring. Hydrological Sciences Bulletin, 22(4):555–569.

Borrelli, P., Robinson, D.A., Fleischer, L.R., Lugato, E., Ballabio, C., Alewell, C., Meusburger, K., Modugno, S., Schütt, B., Ferro, V., Bagarello, V., Oost, K.V., Montanarella, L. and Panagos, P. (2017). An assessment of the global impact of 21st century land use change on soil erosion. Nature Communications, 8(1), 2013. doi:10.1038/s41467-017-02142-7

Bui, L. K., Awange, J., & Vu, D. T. (2022). Precipitation and Soil Moisture Spatio-Temporal Variability and Extremes over Vietnam (1981-2019): Understanding Their Links to Rice Yield. Sensors (Basel, Switzerland), 22(5), 1906. https://doi.org/10.3390/s22051906

CEIC (2021). Vietnam Population Density: By Provinces. https://www.ceicdata.com/en/vietnam/population-density-by-provinces

Chen, G., Li, X., & Liu, X. (2022). Global land projection based on plant functional types with a 1-km resolution under socio-climatic scenarios. Scientific Data, 9(1), 125. doi:10.1038/s41597-022-01208-6

Dang, T. H., Coynel, A., Orange, D., Blanc, G., Etcheber, H., & Le, L. A. (2010). Long-term monitoring (1960–2008) of the river-sediment transport in the Red River Watershed (Vietnam): Temporal variability and dam-reservoir impact. Science of the Total Environment, 408(20), 4654-4664. https://doi.org/10.1016/j.scitotenv.2010.07.007

Dao The Tuan, Molle François (2000). The Chao Phraya delta in perspective: a comparison with the Red River and Mekong deltas, Vietnam. In The Chao Phraya delt: historical development, dynamics and challenges of Thailand's rice bowl. Bangkok: Kasetsart University, p. 399-421. The Chao Phraya Delta: Historical Development, Dynamics and Challenges of Thailand's Rice Bowl: International Conference, Bangkok (THA), 2000/12/12-15.

de Vente, J., & Poesen, J. (2005). Predicting soil erosion and sediment yield at the basin scale: Scale issues and semi-quantitative models. Earth-Science Reviews, 71(1-2), 95-125. doi:10.1016/j.earscirev.2005.02.002

de Vente, J., Poesen, J., Govers, G., & Boix-Fayos, C. (2009). The implications of data selection for regional erosion and sediment yield modelling. Earth Surface Processes and Landforms, 34(15), 1994-2007. doi:10.1002/esp.1884

Dendy, F. E., & Bolton, G. C. (1976). Sediment yield-runoff-drainage area relationships in the United States. Journal of Soil and Water Conservation, 31, 264-266.

Dey Pankaj (2023). Pettitt Change point test for univariate time series data (https://www.mathworks.com/matlabcentral/fileexchange/60973-pettitt-change-point-test-for-univariate-time-series-data), MATLAB Central File Exchange. Retrieved June 8, 2023.

Duc, D. M., Nhuan, M. T., Ngoi, C. V., Nghi, T., Tien, D. M., van Weering, T. C. E., & van den Bergh, G. D. (2007). Sediment distribution and transport at the nearshore zone of the Red River delta, Northern Vietnam. Journal of Asian Earth Sciences, 29(4), 558-565. https://doi.org/10.1016/j.jseaes.2006.03.007

ESA (2022). MRLC maps series from 1992 onwards (v207 and v2.1.1). https://climate.esa.int/fr/projects/land-cover/data/#mrlc-maps-series-from-1992-onwards-(v207-and-v2.1.1)

European Soil Data Centre (ESDAC) (2023, July, 1). Cover Management Factor. https://esdac.jrc.ec.europa.eu/themes/cover-management-factor. Retrieved July 1, 2023.

Ewen, J., Parkin, G., & O'Connell, P. E. (2000). SHETRAN: distributed river basin flow and transport modelling system. Journal of Hydrologic Engineering, 5(3), 250-258.

Fatichi, S., Rimkus, S., Burlando, P., Bordoy, R., & Molnar, P. (2015). High-resolution distributed analysis of climate and anthropogenic changes on the hydrology of an Alpine catchment. Journal of Hydrology, 525, 362–382. https://doi.org/10.1016/j.jhydrol.2015.03.036

Fatichi, S., Vivoni, E.R., Ogden, F.L., Ivanov, V.Y., Mirus, B., Gochis, D., Downer, C.W., Camporese, M., Davison, J.H., Ebel, B.A., Jones, N., Kim, J., Mascaro, G., Niswonger, R., Restrepo, P., Rigon, R., Shen, C., Sulis, M. and Tarboton, D (2016). An overview of current applications, challenges, and future trends in distributed process-based models in hydrology. Journal of Hydrology, 537, 45-60. doi:10.1016/j.jhydrol.2016.03.026

Fatichi Simone (2023). Mann-Kendall Test (https://www.mathworks.com/matlabcentral/fileexchange/25531-mann-kendall-test), MATLAB Central File Exchange. Retrieved June 8, 2023.

Flanagan, D. C., Ascough II, J. C., Nearing, M. A., & Laflen, J. M. (2001). The water erosion prediction project (WEPP) model. In R. S. Harmon & W. W. Doe III (Eds.), Landscape Erosion and Evolution Modelling (pp. 145-199). New York: Kluwer Academic.

Fournier, F. (1960). Climat et érosion: la relation entre l'érosion du sol par l'eau et les précipitations atmosphériques. Presses Universitaires de France.

Garcia-Ruiz, J. M. (2010). The effects of land uses on soil erosion in Spain: A review. CATENA, 81(1), 1-11. doi:10.1016/j.catena.2010.01.001

Giuliani, M., Castelletti, A., Pianosi, F., Mason, E., & Reed, P. M. (2016). Curses, Tradeoffs, and Scalable Management: Advancing Evolutionary Multiobjective Direct Policy Search to Improve Water

Reservoir Operations. Journal of Water Resources Planning and Management, 142(2). doi:10.1061/(asce)wr.1943-5452.0000570

Hiep, N. H., Luong, N. D., Ni, C. F., Hieu, B. T., Huong, N. L., & Du Duong, B. (2023). Factors influencing the spatial and temporal variations of surface runoff coefficient in the Red River basin of Vietnam. Environmental Earth Sciences, 82(2). doi:10.1007/s12665-022-10726-w

Kendall, M.G. (1975). Rank Correlation Methods, 4th edition, Charles Griffin, London.

Kmusser, 2009. Red hong river map. Retrieved from: https://en.wikipedia.org/wiki/File:Red_hong_rivermap.png , last access: 21.05.2023.

IMRR Project (2015). Integrated and sustainable management of Red-Thai Binh Rivers System in a changing climate, Politecnico di Milano.

Le, T. P. Q., Garnier, J., Gilles, B., Sylvain, T., & Van Minh, C. (2007). The changing flow regime and sediment load of the Red River, Viet Nam. Journal of Hydrology, 334(1-2), 199-214. doi:10.1016/j.jhydrol.2006.10.02

Lehner, B., Verdin, K., Jarvis, A. (2008). New global hydrography derived from spaceborne elevation data. Eos, Transactions, American Geophysical Union, 89(10): 93–94. https://doi.org/10.1029/2008eo100001

Li, H. Y., Tan, Z., Ma, H., Zhu, Z., Abeshu, G. W., Zhu, S., Cohen, S., Zhou, T., Xu, D., & Leung, L. R. (2022). A new large-scale suspended sediment model and its application over the United States. Hydrology and Earth System Sciences, 26(3), 665-688.

Lin, B. (1984). Current Study of Unsteady Transport of Sediment in China. Tokyo-kyot edition.

Mann, H.B. (1945). Non-parametric tests against trend, Econometrica 13:163-171.

Maier, H.R., Kapelan, Z., Kasprzyk, J., Kollat, J., Matott, L.S., Cunha, M.C., Dandy, G.C., Gibbs, M.S., Keedwell, E., Marchi, A., Ostfeld, A., Savic, D., Solomatine, D.P., Vrugt, J.A., Zecchin, A.C., Minsker, B.S., Barbour, E.J., Kuczera, G., Pasha, F., Castelletti, A., Giuliani, M. and Reed, P.M. (2014). Evolutionary algorithms and other metaheuristics in water resources: Current status, research challenges and future directions. Environmental Modelling & Software, 62, 271-299. doi:10.1016/j.envsoft.2014.09.013

Meng, X. M., Zhu, Y., Yin, M. S., & Liu, D. F. (2021). The impact of land use and rainfall patterns on the soil loss of the hillslope. Scientific Reports, 11(1). doi:10.1038/s41598-021-95819

Milliman, J., & Farnsworth, K. (2011). River Discharge to the Coastal Ocean: A Global Synthesis. Cambridge: Cambridge University Press. doi:10.1017/CBO9780511781247

Ministry of Agriculture and Rural Development. (2009). Research application on the use of MIKE21 model to assess, predict and prevent river bank erosion (north, central and south Vietnam. Technical report of the project 2006–2008 of the Ministry of Agriculture and Rural Development, Hanoi, Vietnam.

Morgan, R.P.C. (2001). A simple approach to soil loss prediction: a revised Morgan–Morgan–Finney model. Catena, 44, 305–322.

Morgan, R.P.C., Quinton, J.N., Smith, R.E., Govers, G., Poesen, J., Auerswald, K., Chisci, G., Torri, D., & Styczen, M.E. (1998). The European Soil Erosion Model (EUROSEM): a dynamic approach for

predicting sediment transport from fields and small catchments. Earth Surface Processes and Landforms, 23, 527–544.

O'Neill, B.C., Tebaldi, C., van Vuuren, D.P., Eyring, V., Friedlingstein, P., Hurtt, G., Knutti, R., Kriegler, E., Lamarque, J.F., Lowe, J., Meehl, G.A., Moss, R., Riahi, K. and Sanderson, B.M. (2016). The Scenario Model Intercomparison Project (ScenarioMIP) for CMIP6. Geosci. Model Dev., 9(9), 3461-3482. doi:10.5194/gmd-9-3461-2016

Ouyang, W., Skidmore, A. K., Hao, F. H., & Wang, T. J. (2010). Soil erosion dynamics response to landscape pattern. Science of the Total Environment, 408(6), 1358-1366. doi:10.1016/j.scitotenv.2009.10.062

Panagos, P., Borrelli, P., Meusburger, K., Alewell, C., Lugato, E., & Montanarella, L. (2015a). Estimating the soil erosion cover-management factor at the European scale. Land Use Policy, 48, 38-50. doi:10.1016/j.landusepol.2015.05.021

Panagos, P., Borrelli, P., Poesen, J., Ballabio, C., Lugato, E., Meusburger, K., . . . Alewell, C. (2015b). The new assessment of soil loss by water erosion in Europe. Environmental Science & Policy, 54, 438-447. doi:https://doi.org/10.1016/j.envsci.2015.08.012

Phan, D.C., Trung, T.H., Truong, V.T., Sasagawa, T., Vu, T.P.T., Bui, D.T., Hayashi, M., Tadono, T. and Nasahara, K.N. (2021). First comprehensive quantification of annual land use/cover from 1990 to 2020 across mainland Vietnam. Scientific Reports, 11(1). doi:10.1038/s41598-021-89034-5

Pierini, N. A., Vivoni, E. R., Robles-Morua, A., Scott, R. L., & Nearing, M. A. (2014). Using observations and a distributed hydrologic model to explore runoff thresholds linked with mesquite encroachment in the Sonoran Desert. Water Resources Research, 50(10), 8191-8215.

Prosser, I. and Rustomji, P. (2000). Sediment transport capacity relations for overland flow. Progress in Physical Geography, 24(2):79–93.

Quinn, J. D., Reed, P. M., Giuliani, M., & Castelletti, A. (2017). Rival framings: A framework for discovering how problem formulation uncertainties shape risk management trade-offs in water resources systems. 53(8), 7208-7233. https://doi.org/10.1002/2017WR020524

Renard, K. G., Foster, G. R., Weesies, G. A., McCool, D. K., & Yoder, D. C. (1997). Predicting soil erosion by water: a guide to conservation planning with the revised universal soil loss equation (RUSLE). Agriculture Handbook, vol. 703. Washington DC: US Department of Agriculture.

Ritchie, H., Roser, M., and Rosado, P. (2022). Vietnam: Energy Country Profile. Published online at OurWorldInData.org. Retrieved from: https://ourworldindata.org/energy

Shirazi, M. A., Boersma, L., Hart, J. W. (1988). A unifying quantitative analysis of soil texture: improvement of precision and extension of scale. Soil Science Society of America Journal, 52 (1):181–190.

Sharpley, A. and Williams, J. (1990). EPIC: The erosion-productivity impact calculator. U.S. Department of Agriculture Technical Bulletin, (1768):235.

Smith, P., House, J. I., Bustamante, M., Sobocka, J., Harper, R., Pan, G. X., West, P. C., Clark, J. M., Adhya, T., Rumpel, C., Paustian, K., Kuikman, P., Cotrufo, M. F., Elliott, J. A., McDowell, R., Griffiths, R. I., Asakawa, S., Bondeau, A., Jain, A. K., Meersmans, J., & Pugh, T. A. M. (2016). Global change

pressures on soils from land use and management. Global Change Biology, 22(3), 1008-1028.

Szilassi, P., Jordan, G., van Rompaey, A., & Csillag, G. (2006). Impacts of historical land use changes on erosion and agricultural soil properties in the Kali Basin at Lake Balaton, Hungary. CATENA, 68(2), 96-108. https://doi.org/10.1016/j.catena.2006.03.010

Thinh, L. V., Ranzi, R., Rulli, M. C., & Ieee. (2018, Jun 12-15). Modeling soil erosion and sediment load for Red River basin (Vietnam): impact of land use change and reservoirs operation. Paper presented at the IEEE International Conference on Environment and Electrical Engineering (EEEIC) / IEEE Industrial and Commercial Power Systems Europe (ICPS Europe), Univ Palermo, Palermo, ITALY.

Torri, D., Poesen, J., and Borselli, L. (1997). Predictability and uncertainty of the soil erodibility factor using a global dataset. Catena, 31(1-2):1–22.

van Rijn, L. (1993). Principles of Sediment Transport in Rivers, Estuaries and Coastal Seas.

Vörösmarty, C. J., Meybeck, M., Fekete, B., Sharma, K., Green, P., & Syvitski, J. P. M. (2003). Anthropogenic sediment retention: major global impact from registered river impoundments. Global and Planetary Change, 39(1), 169-190. https://doi.org/10.1016/S0921-8181(03)00023-7

Walling, D. E., & Fang, D. (2003). Recent trends in the suspended sediment loads of the world's rivers. Global and Planetary Change, 39(1), 111-126. https://doi.org/10.1016/S0921-8181(03)00020-1

Wischmeier W. H. and Smith D. D (1978). Predicting rainfall erosion losses: a guide to conservation planning. Number 537. Department of Agriculture, Science and Education Administration.

World Data. (2023, June 9). Climate in Red River Basin. https://www.worlddata.info/asia/vietnam/climate-red-river-delta.php. Retrieved June 13, 2023.

Yang, D., Kanae, S., Oki, T., Koike, T., & Musiake, K. (2003). Global potential soil erosion with reference to land use and climate changes. 17(14), 2913-2928. https://doi.org/10.1002/hyp.1441

Yang, H. F., Yang, S. L., Xu, K. H., Milliman, J. D., Wang, H., Yang, Z., Chen, Z., & Zhang, C. Y. (2018). Human impacts on sediment in the Yangtze River: A review and new perspectives. Global and Planetary Change, 162, 8-17. doi:10.1016/j.gloplacha.2018.01.001

Young, R. A., Onstad, C. A., Bosch, D. D., & Anderson, W. P. (1989). AGNPS: a nonpoint-source pollution model for evaluating agricultural watersheds. Journal of Soil and Water Conservation, 44(2), 168-173.

Yuen, K. W., Hanh, T. T., Quynh, V. D., Switzer, A. D., Teng, P., & Lee, J. S. H. (2021). Interacting effects of land-use change and natural hazards on rice agriculture in the Mekong and Red River deltas in Vietnam. Natural Hazards and Earth System Sciences, 21(5), 1473-1493. doi:10.5194/nhess-21-1473-2021

Appendix

Appendix 1: K-factor map, C-factor map, and alpha maps

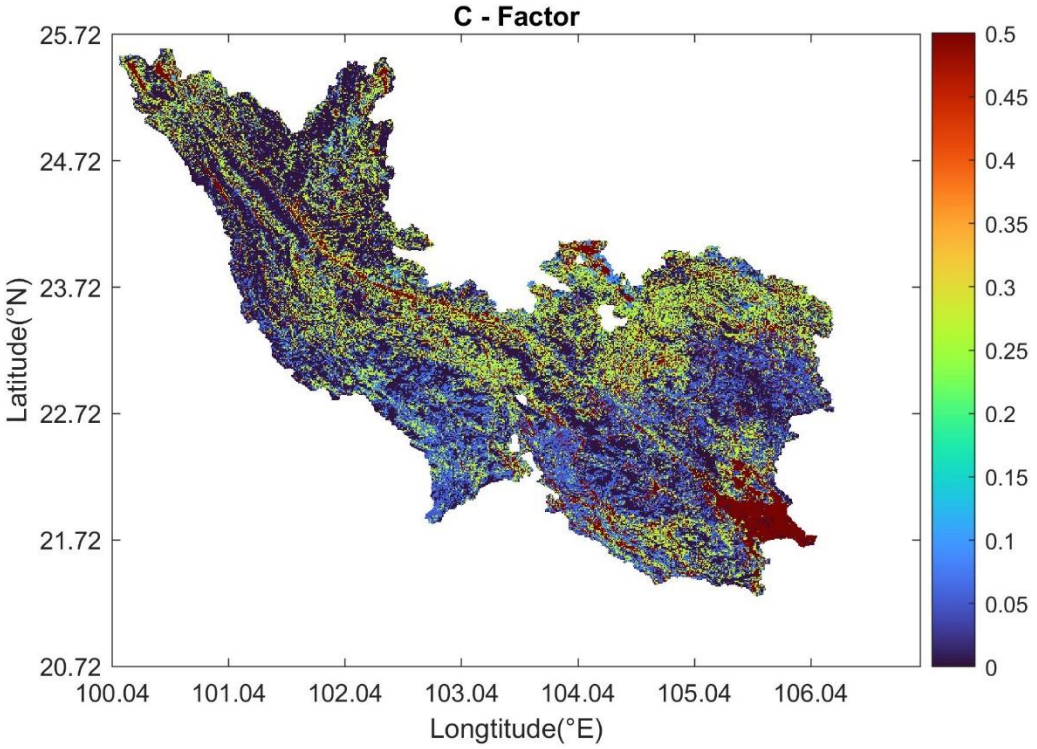

Figure A1-1 C-factor map [-] of the RRB

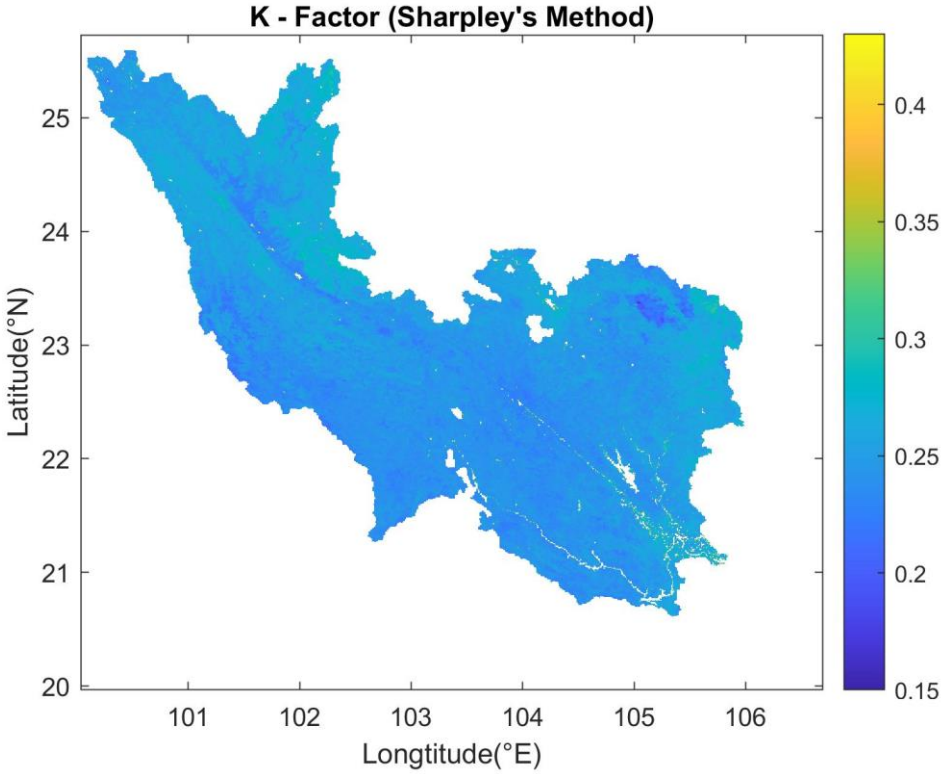

Figure A1-2 K-factor map (Sharpley and William' s method (1990)).

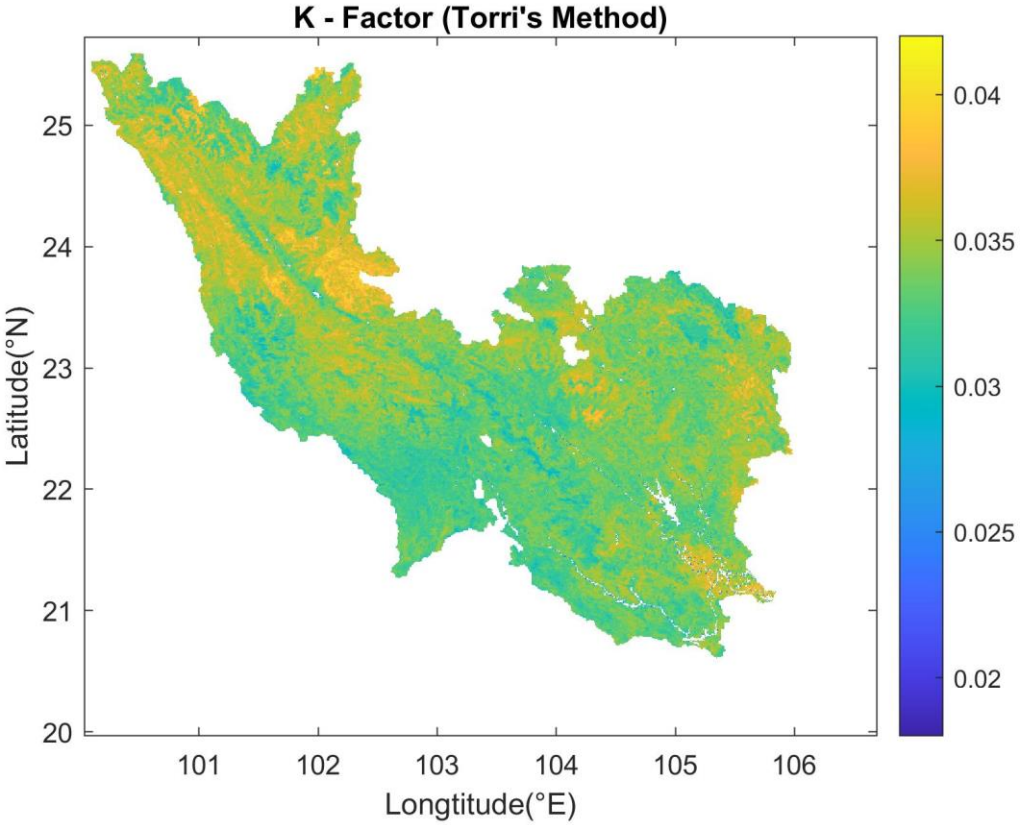

Figure A1-3 K-factor map (Torri et al.' s method (1997)).

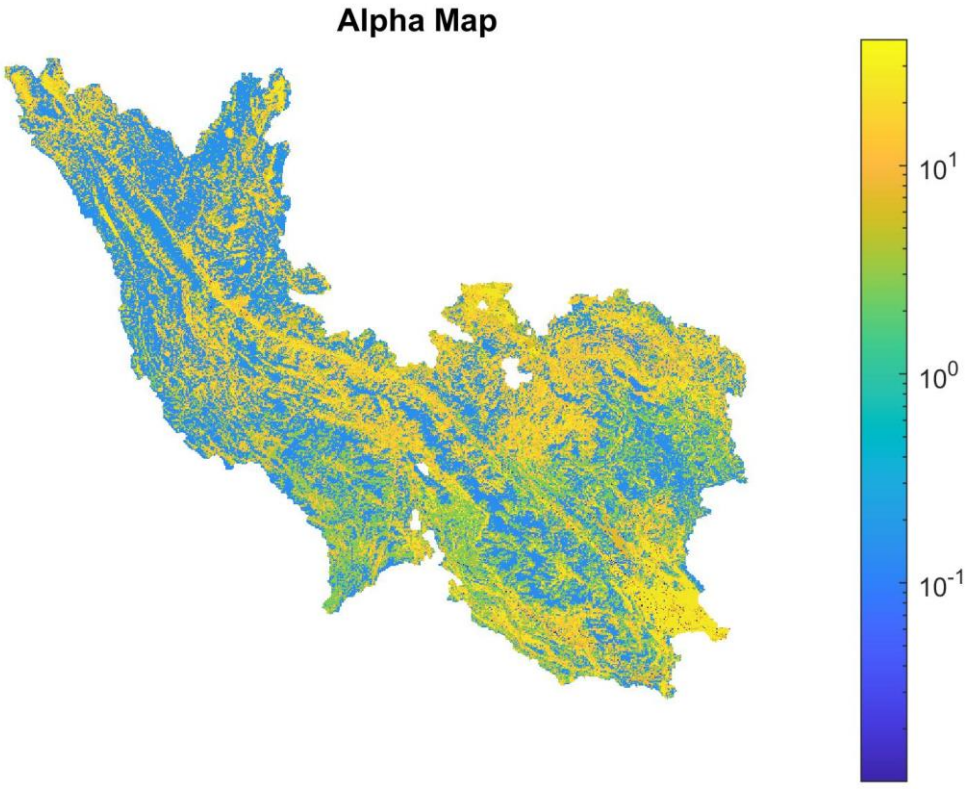

Figure A1-4 Alpha map [kg $s^{-1.8}$ $m^{-2.6}$] using Sharpley and William' s method (1997).

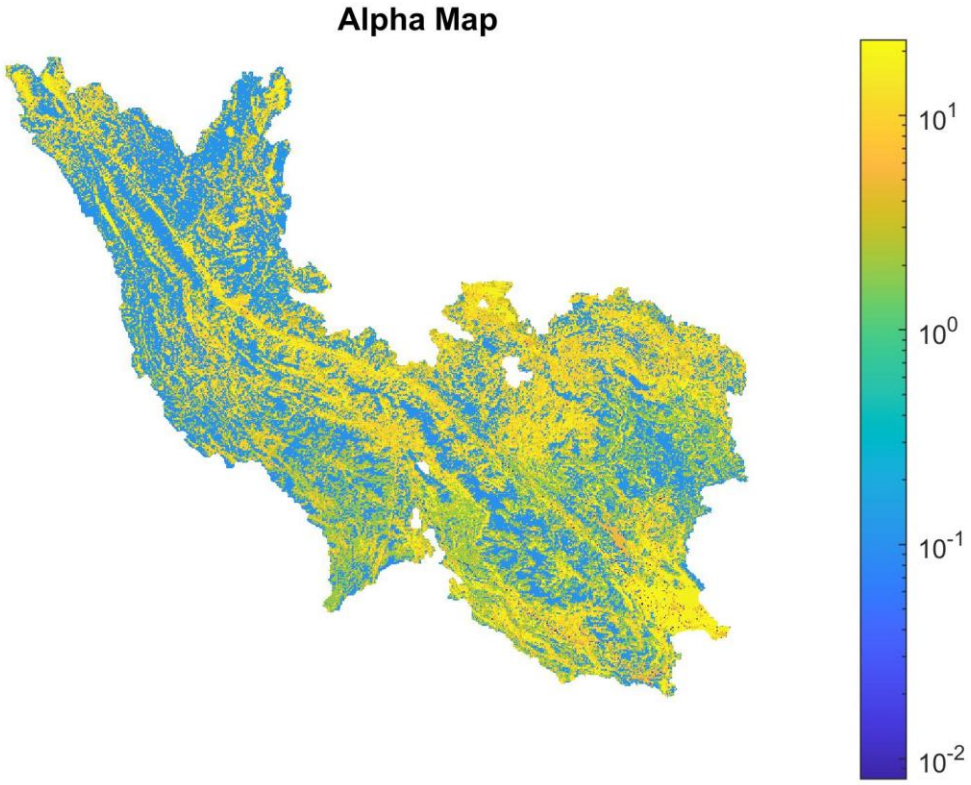

Figure A1-5 Alpha map [kg $s^{-1.8}$ $m^{-2.6}$] using Torri et al.' s method (1997).

Appendix 2: Maps of land use changes in scenarios analysis

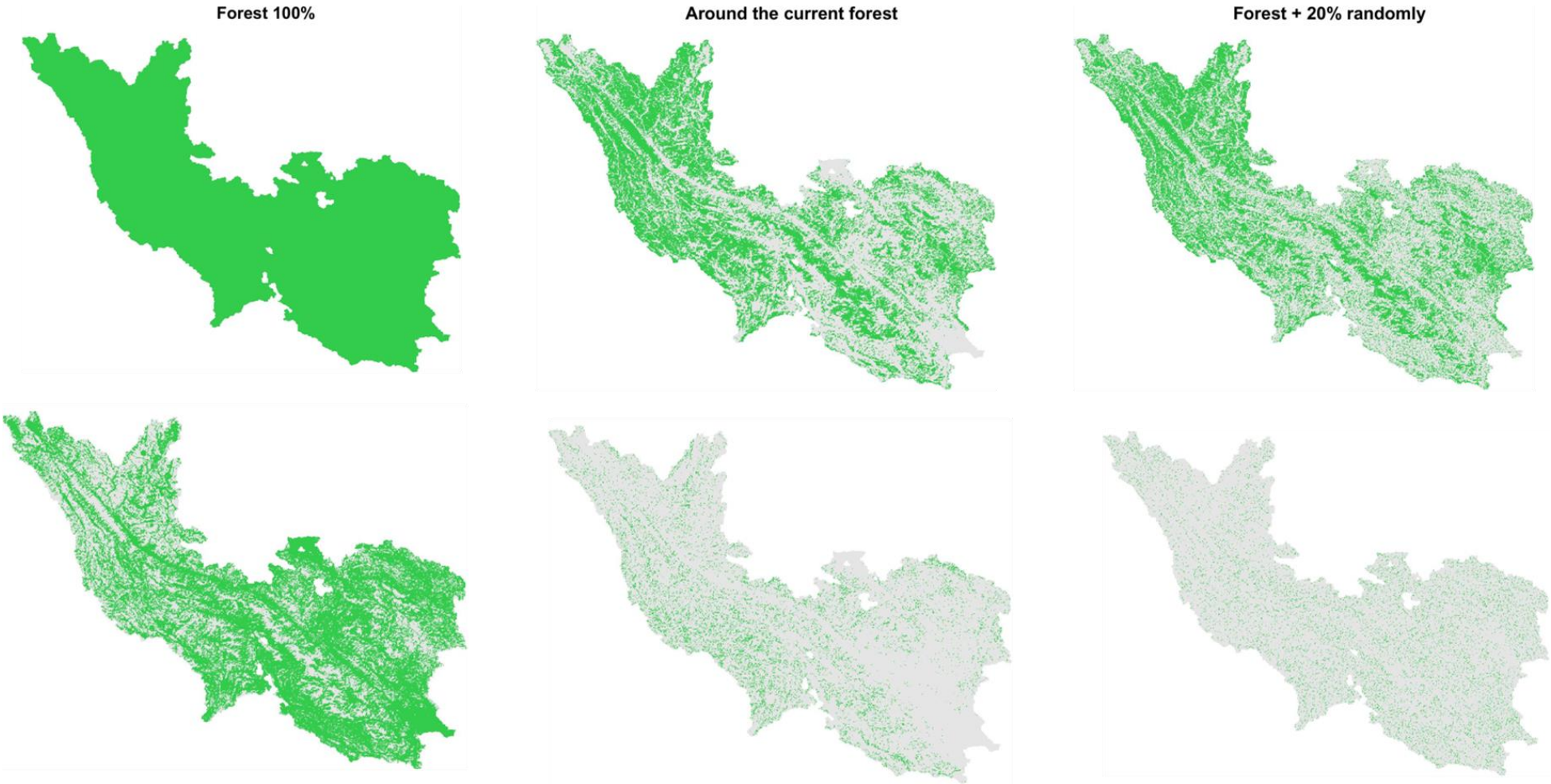

Figure A2-1. Maps of land use changes in forest expanding scenarios. The first row is the land use maps after changes, and the second row shows the locations of land use changes. The increase of forest in the second and the third scenarios are both about 20%.

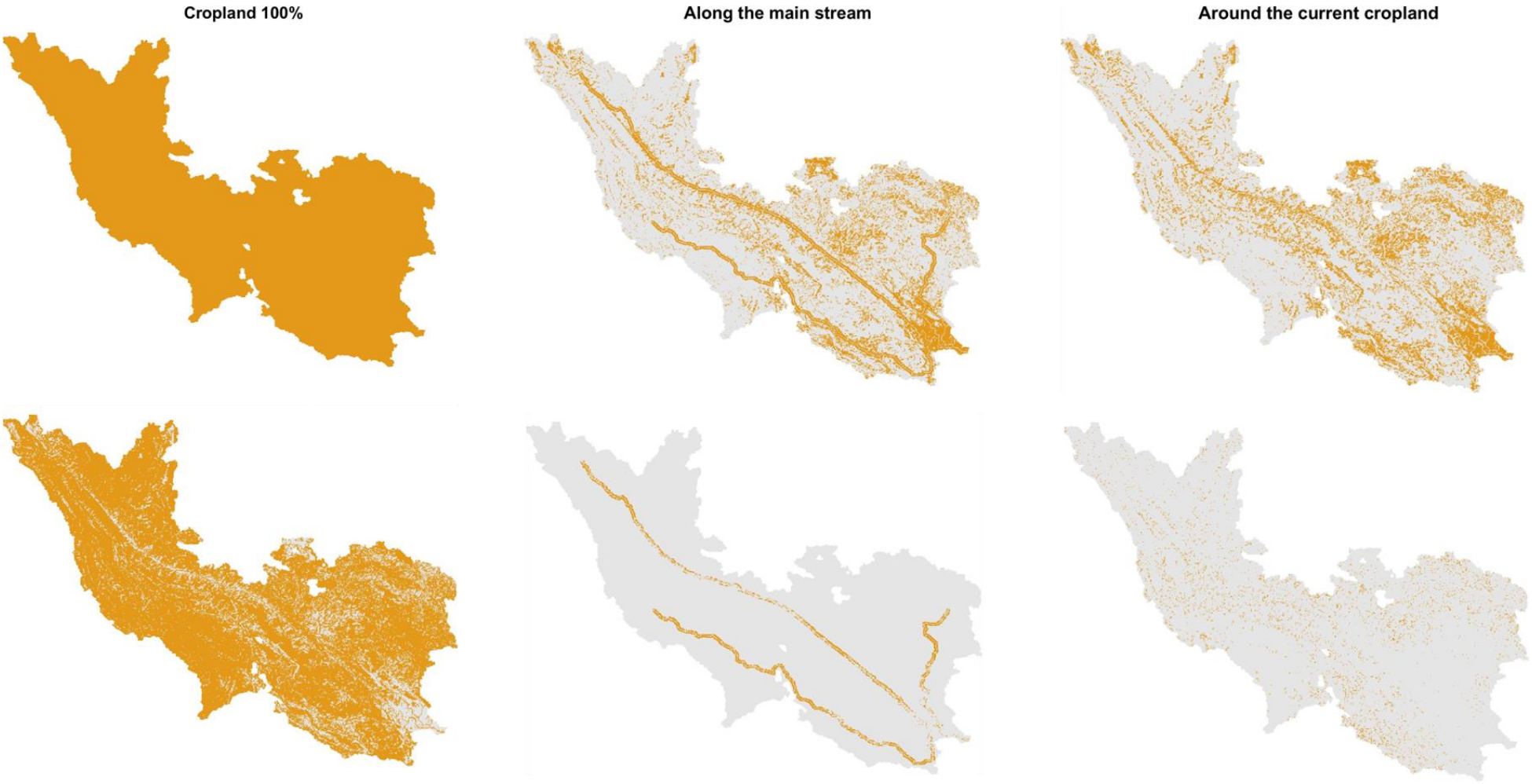

Figure A2-2. Maps of land use changes in cropland expanding scenarios. The first row is the land use maps after changes, and the second row shows the locations of land use changes. The increase of cropland in the second and the third scenarios are both about 20%.

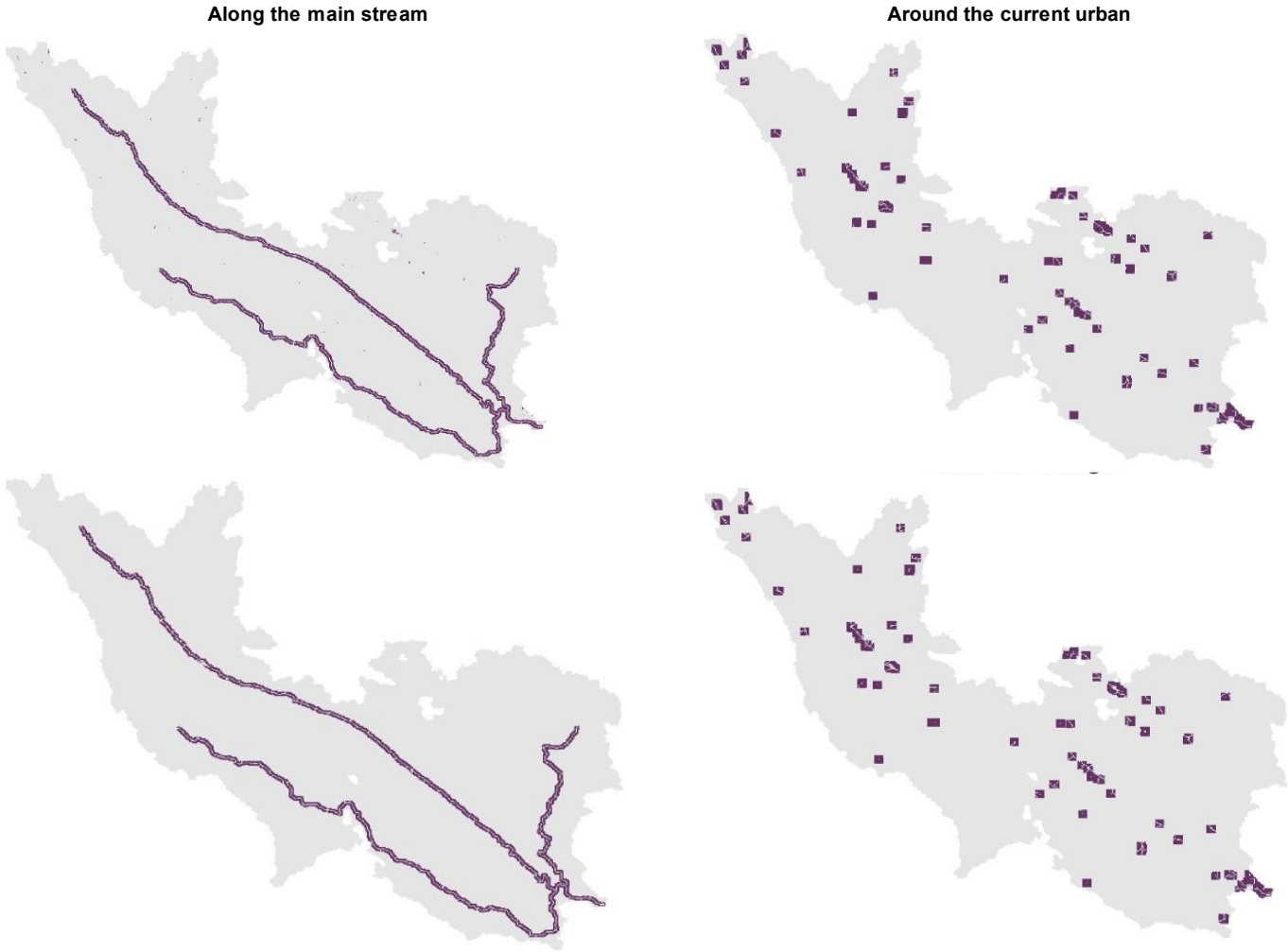

Figure A2-3. Maps of land use changes in urban expanding scenarios. The first row is the land use maps after changes, and the second row shows the locations of land use changes. The proportion of urban in two scenarios both increased from 0.11% to about 5%.

Personal Declaration

I hereby declare that the submitted thesis is the result of my own, independent work. All external sources are explicitly acknowledged in the Thesis.

Date and Signature:

30.09.2023 Yixuan Zhou